

Intuitive Human-Controlled Robotic Arm

By

Cariappa Devaya, Mason Keck, Benjamin Miller, Connor Nail,
Matthew Nolan, Andrea Rio, Efrain Valero-Villavicencio

Final Report Document

*Submitted towards partial fulfillment of the requirements for
Mechanical Engineering Design II – Fall 2021*



School for Engineering of Matter, Transport, and Energy
Arizona State University
Tempe, AZ 85281

Table of Contents

Introduction	3
Problem Formulation	4
Market Example	4
Project Needs	5
Project Goals	5
Objectives	5
Constraints	6
Design Prototype Concepts	7
Andrea Rio	7
Efrain Valero-Villavicencio	9
Cariappa Devaya	10
Benjamin Miller	13
Mason Keck	15
Matthew Nolan	16
Connor Nail	18
Decision Making	20
Design Criteria	20
Numerical Scales	22
Decision Matrix	23
Top Design	24
Engineering Analysis	26
Whole Arm	27
Wrist (Section 1)	29
Lower Arm (Section 2)	34
Upper Arm (Section 3)	37
Shoulder Joint (Section 4)	40
Design Progression	41
Parts Receiving	50
Assembly Overview	52
Control System Update	58
Overview	58
Oculus Headset	59
Desktop Application	59

ROS	60
Real Time Servoing	60
Arduino	61
Budget Analysis	61
Full Assembly Testing	63
Challenges Faced	66
Future Work	69
Conclusion	69
References	70
Appendix A.	71
A1. House of Quality (HOQ)	71
A2. Quality Function Deployment (QFD)	71
Appendix B.	72
B1. SEMTE Business Office Receipt for Team 10	72
B2. Gantt Chart	72
Appendix C. Preliminary Parts and Engineering Drawings	73
Full Assembly Exploded	74
Magnetic End Effector (1)	75
Wrist Turntable (2)	76
Forearm (3)	77
Elbow Turntable (4)	78
Upper Arm (5)	79
Upper Arm Turntable (6)	80
Shoulder Pin (7)	80
Shoulder Hinge (8)	81
Shoulder Turntable (9)	82
Sample Module Kinematic Coupler (10)	83
Module Holder Tray (11)	84

Introduction

Remotely-controlled robots have been used to defuse or dispose of bombs for nearly fifty years (Lisle, 2020, p.1). While modern robots have gotten better and better at this, there are notable shortcomings for all of the commercially-available designs — namely cost and a lack of versatility. From initial research, objectives and goals for a new and improved, innovative arm were determined. Foremost among these considerations were enhanced controllability, reduced weight, and modular attachments that can quickly be swapped with minimal input from the operator. After these priorities were set straight, the project design was chosen and engineering analysis performed, both by hand and using Ansys. This allowed important design aspects such as motor specifications and construction material to be budgeted (originally totaling \$530) and ordered with confidence, knowing the minimum safety factor was 4.82.

Assembly began as material shipments arrived, starting with the test stand of the shoulder before moving through the shoulder and down towards the end effector. The design for each of these joints had to be iterated to include small details along the way, and the incoming parts had to be compared to their online drawings. Medium density fibreboard (MDF) was used for the stand, aluminum box channel was used for the upper and forearm, and the joints were all 3d printed using PLA that would then fit tightly around the box channel to connect the whole arm together. The electronics were mounted directly to the outside of the test stand so they would not be in the arm's path, and the wiring ran down the outside of the arm. In the end, all of these materials for assembly came successfully under budget.

After assembling the arm, controlling it quickly became the next priority. This was done using a Unity game engine, along with ROS (Robot Operating System), ROS#, and MoveIt, all paired with an Oculus Quest 1 controller and headset. Getting all of the software to appropriately communicate with each other proved to be a challenge. In summary, the process begins with the Oculus headset and the VR Unity application where the controller pose is obtained. The pose information is then sent through a Photon web server to the Unity desktop application where it is published directly to a ROS topic. MoveIt subscribes to this topic, performs inverse kinematics, and then publishes the joint angles to a separate ROS topic. Finally, this topic is subscribed to by the Arduino, which then sends the individual joint signals to the servos, moving the robot into position. After the controls were finished, prototype testing and demonstrations could begin.

Several tests were performed to verify the robotic arm's capabilities. The modular attachment swapping capability was tested by simply verifying the arm was able to successfully perform the sequence: detaching the current attachment in its holster and withdrawing the alternative attachment from next to it. The arm's consistency and repeatability was verified by pre-programming a path between two points and then measuring the horizontal positions. The arm was also tested at different speeds to determine which was most suitable for the necessary applications. Finally, the ability of the arm to track controller input was tested by connecting the headset and controller and feeding the arm inputs. Overall, the design successfully completed each test that was thrown its way, despite any obstacles that appeared. In terms of budget, the final tally revealed \$36.51 in excess funds, and although there is room for improvement, the project can be considered an all-around success. The rest of the report will now cover these topics in much further detail, starting at the very beginning with the problem formulation.

Problem Formulation

The use of robots to defuse bombs is a favorable method to reduce the risk of endangering personnel. Though this technology has been around for a few decades, these robots are still evolving today with new features. This project was intended to improve the design of these robots. The improvements would include, but not be limited to, more intuitive controls and smoother arm mechanics.

Market Example

The following example is from the robotics company RE². Their bomb defusal robot (Figure 1) has four degrees of freedom in each arm and a large control station for the operator. With few degrees of freedom, it limits the reachable workspace for the robot's arms. In addition, during an interview between TechCrunch and the robot's operator, the operator mentioned that it takes a few hours of practice to understand the robot's controls. When the interviewer attempted to use the controls, they noted that it was confusing to learn (Heater, 2017). This suggests that the remote controls are not intuitive. With this information, it was noted that an improved arm design would have more than four degrees of freedom, optimizing the arm's motion by increasing its reachable workspace. It is also important to design a controller that will be easy to learn and operate.



Figure 1. RE² robot shown with its operator. (Source: TechCrunch)

Project Needs

Given the research into various bomb defusal robots, there is a lack of modularity and dexterity in existing designs. The current solutions are almost prohibitively expensive, and they are specialized for specific situations such that the scope of tasks they can complete is relatively narrow. They are also often very difficult to control, requiring several hours of training to complete basic operations.

Project Goals

To address these problems and contribute to the development of bomb defusal technology, this new robotic system should be modular, flexible, and adaptable like a human arm. It should be easy to control, even for beginners, and it should be capable of completing tasks from multiple categories, such as grasping and manipulating objects and cutting wires.

Objectives

Several important objectives were identified (Table 1). The first objective is to make sure the arm has high fidelity to the controller position. This will make the controls easy for the operator and ensure the arm can reach any position within its range of motion. Second, it is important that recalibration is required as infrequently as possible to help with accuracy in the arm's motion. It is also desirable to have a quick settling time so the arm will quickly respond to a position command. Additionally, the desire to have an intuitive design means that a new user should be able to quickly learn the robot's remote controls and complete a given task. The arm should be as lightweight as possible to reduce stress on any equipment or robotic base which is conveying it. This will help achieve the control goals and minimize the mass of the arm. Finally, it is desired that the arm is compact. For this reason, the longest dimension of the arm while in storage should

be minimized, presumably by making the arm more foldable.

Table 1: Project Objectives

Objective	Measurement Basis	Units
High fidelity to controller position	Steady state error of end effector position	cm
Infrequent recalibration required	Position drift after 1 minute of use	cm
The arm should have quick response to motion	Time to reach position after VR controller settles	s
The arm should be easy to control for new users	Time for a new user to complete a given task	s
The arm should be lightweight	Total mass from shoulder to wrist	kg
The arm should be compact	Longest dimension when in storage	m

Constraints

One of the areas recognized for improvement in robotic arm technology was the ability to rapidly switch manipulators. To make this an asset, this should be done within 8 seconds. It is also desired that the arm shall be able to reach within tight spaces. Therefore, the diameter of the arm at every point shall be no more than 12 cm. Additionally, the arm must be capable of lifting a reasonably sized mass. This will bring flexibility in what size end effectors can be used. For this reason, the arm is specified to be able to lift 0.7 kg, at least. To give an intuitive and human-like work area, there needs to be a minimum arm length. This value was chosen to be 0.7 m, which resembles that of a normal human. Furthermore, the arm should have a range of motion that is intuitive and resembles a human-like motion. To achieve this, the shoulder needs to have a 170degree conical range of motion and 6 degrees of freedom in the arm from shoulder to wrist.

The full bulleted list of constraints is as follows:

- The arm shall change manipulator type (with no user input beyond a simple command) and restore the user-controlled position within 8 seconds.
- The arm shall be no wider than 12 cm in diameter (fits within a 12 cm cylinder when

straight).

- The arm shall be able to lift a 0.7 kg end effector.
- The arm shall be at least 0.7 m long from shoulder to wrist.
- The arm shall have a 170 degree conical range of motion on the shoulder.
- The arm shall have 6 degrees of freedom.

Lastly, during the problem formulation stage of this project, a House of Quality (HOQ) chart and Quality Function Deployment (QFD) chart (Appendix. A) were developed. The HOQ is used to compare engineering requirements of the design that are of interest. These requirements are compared by judging whether or not they have a positive or negative relationship to each other. In the QFD, the engineering requirements stated previously are compared to customer requirements. In the chart, the engineering requirements “control system response time” and “weight” satisfy the most customer requirements. The control system response time will ensure that the design is accurate, responsive, and easy to use. In addition, the engineering requirement “weight” will ensure the design is lightweight, inexpensive, will help with multi tool features, and be a compact design. These engineering requirements are given target values, shown at the bottom, that will further influence the final design. Lastly, market competitors are listed on the right side of the QFD. This area shows what customer requirements each competitor’s designs meet. Based on this section, it was found that a few of the competitors did not have a design that was inexpensive, had multi tool features, was compact, or easy to use. With this in mind, each group member generated their own concept design and presented it to the group to be judged and rated.

Design Prototype Concepts

Andrea Rio

The first concept to be presented is a simple arm design with a focus on the end effector connection. When looking at the design (Figure 2), there were some advantages and disadvantages that were noticed. The first advantage was the simple design because it can be fit to meet the dimension constraints. The second advantage is the large range the arm segments can rotate. However, these rotations are limited. When looking at the base joint, there are 2 degrees of freedom (DOF) and the elbow joint has 1 DOF. The constraints laid out for this problem state there must be 6 DOF, but this design only has 5. While researching ways to run electrical power

to the modular attachment, pogo pins were viewed as a potential solution. When looking at the end effector design (Figure 3), there were concerns that the design would not allow for a strong engagement between the end effector and the modular attachment. The third issue found was the thickness of the arm segments at the joints. Due to how thin they were designed, they may fail or cause damage to the arm. The last disadvantage found was the method designed to connect the end effector with the modular attachment. The design intended for the T-shaped rod to insert into the modular attachment, turn 90 degrees, and then sit locked in place. However, the design never specified what mechanisms would lock it in place. This resulted in concerns that the modular attachment would fall off when in operation. Though this design was simple, it displayed many shortcomings.

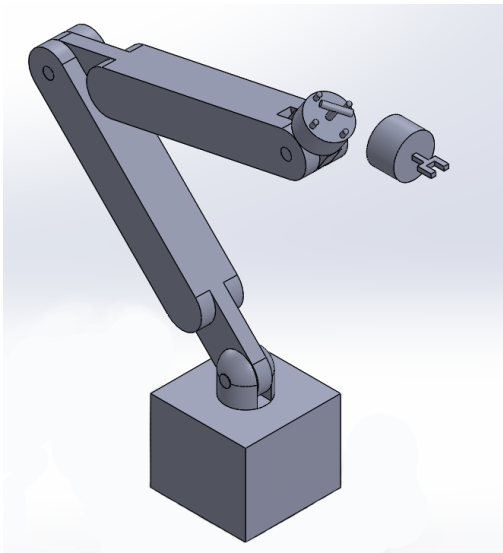


Figure 2: Isometric view of robot arm design

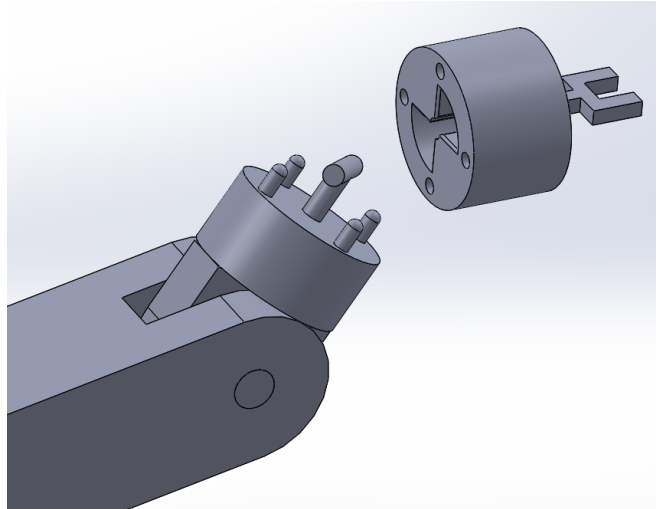


Figure 3: Close up of end effector connecting to modular attachment

Efrain Valero-Villavicencio

This design is simple and common among robotic arms. It can be found below in Figure 4. With this design, more data can be found through journals or online to help improve the project. Since it is a common design, there are many premade attachments readily available which could save some time and money.

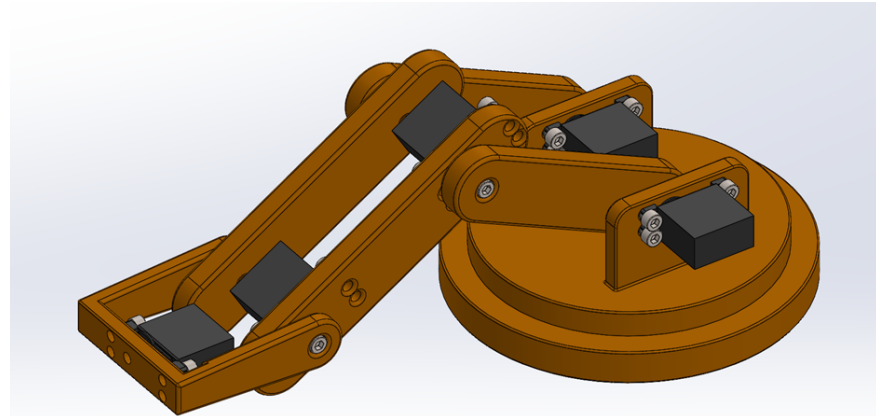


Figure 4: Simple Crane Concept design

This design also comes with a few drawbacks. This design lacks the degrees of freedom in most of the joints which means it would not be very compatible with our idea to closely mimic a human arm. The attachment point is not very well suited to allow for swappable attachments which is a main objective for the project. Another con is that due to the big base and the spacing between the members it would probably not satisfy some of the size constraints. The next con in this design is that the motor that rotates the base is mounted underneath and that could potentially conflict with mounting options to mimic a human arm. This design would need a lot of changes to work with our project idea.

For the second design found in Figure 5, there are a few pros. The first pro in this design is that it has two degrees of freedom at every joint which satisfies the project goal of six. This allows the arm to be able to mimic the movement of a human arm well. Another advantage is that due to the offset members, it would allow the robotic arm to fold to a compact size suited for storage. Next, the joints allow for the scaling of motors to increase the arm's capabilities.

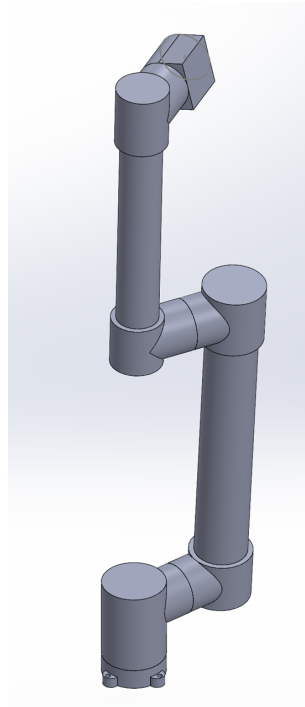


Figure 5: Tube arm with offset members

This design has a couple of cons. First, the attachment point is not ideal and might conflict with some of the constraints and/or objectives. Secondly, the way the base motor is attached to the bottom member may not be the best way to model a human arm depending on how it is mounted. This design would need a few tweaks to work very well with our idea, mainly at the attachment point and the base.

Cariappa Devaya

This design has several advantages. This robotic arm is primarily made up of 7 components and the assembly is shown below with all of the components labeled. The arm has 6 degrees of freedom and each component has a considerable amount of range of angular motion, ranging from 170 degrees to 320 degrees. The range of motion for each component and the axes about which they rotate, relative to the given coordinate system, is labeled as well. This gives the arm greater flexibility and maneuverability, thus allowing it to reach any position within its wide range of motion.

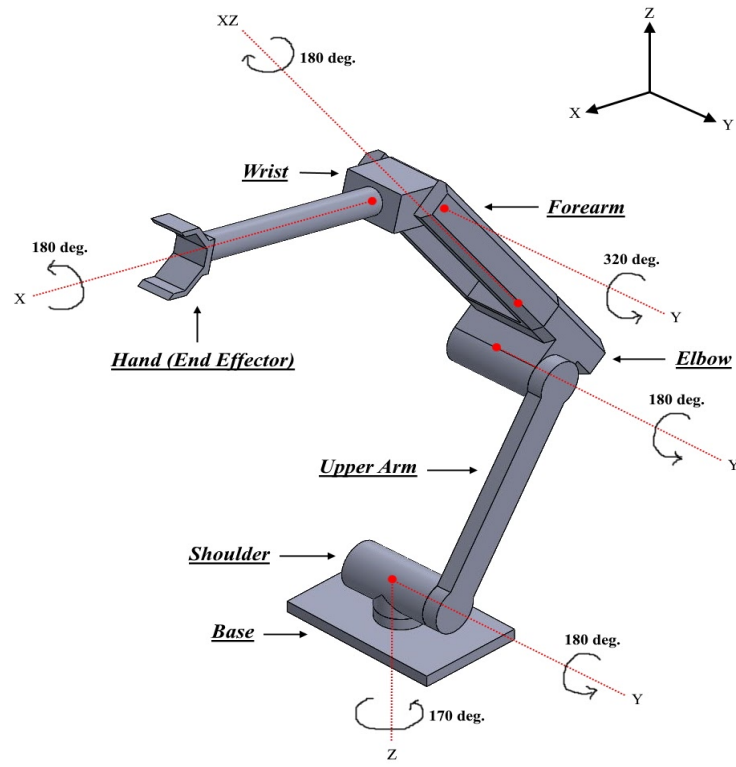


Figure 6: Concept of assembly in SOLIDWORKS

The arm is designed such that it meets the given dimension constraints to ensure ease of storage. It was decided that the diameter of the arm at every point shall be no more than 12 cm and the arm shall be at least 0.7 m long from shoulder to wrist. As seen in the picture, the arm becomes very compact when folded, therefore the storage space is minimized, allowing it to fit within a 12 cm. cylinder when straight and upright. Also each component is designed such that there is adequate space to fit sensors, motors and wires using hollow sections within each component.

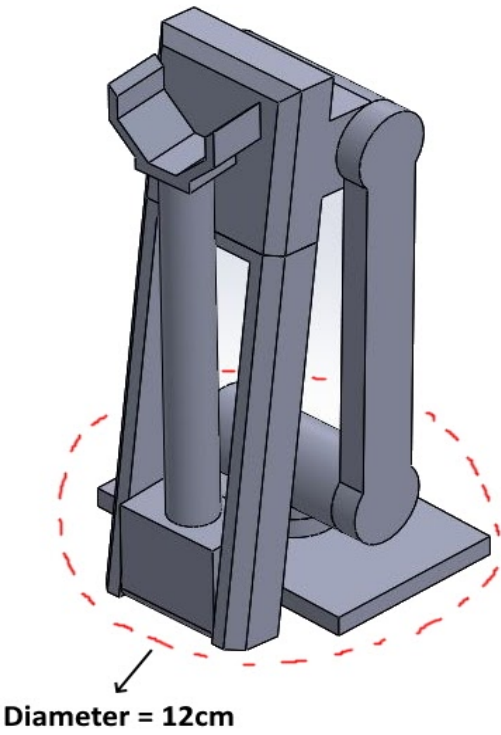


Figure 7: Arm in its folded position

There are, however, some downsides to this design. There is no degree of freedom near the end effector and this is a disadvantage when working in a very tight space where only the rotation and turning of the end effector is required. This could also make the process of attachment and detachment of different end effectors difficult and more complicated. Another disadvantage exists with the thickness of the upper arm. Because the upper arm is relatively thin compared to the other components, it could become more prone to buckling when dealing with compressive loads. The upper arm is also slightly offset from the center, therefore it has to deal with tensile loads and bending moments as well. As a result, failure or fracture could occur along the cross section where the arm is most thin. The upper arm can be approximated as a cantilever beam.

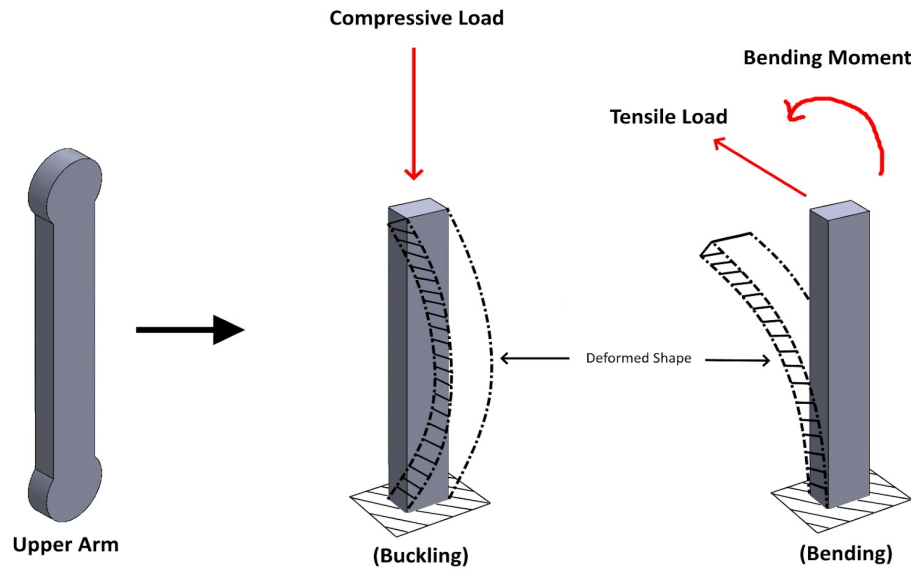


Figure 8 : Two possible modes of failure for the upper arm

Benjamin Miller

Below, in Figure 9, is an isometric view of another robotic arm concept. In this case, the arm is mounted in a position similar to that of a human arm, elevated off the floor. The arm is mounted to a wooden base for demonstration and testing purposes. A simple gripper is shown as the attachment, though the system is modular and more trays could be added in a matrix below the shoulder with the arm programmed to swap attachments on command.

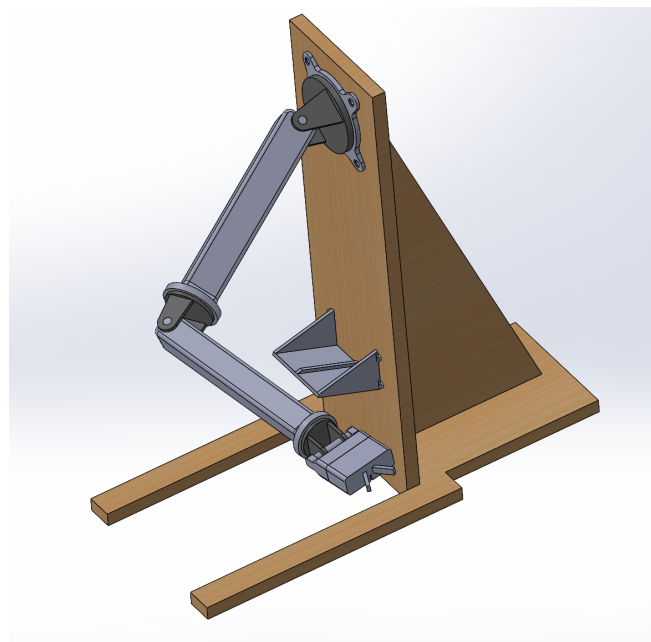


Figure 9: Isometric arm view

Below, in Figure 10, is an image showing the pins which attached the module along with the backside of the module. The pins and holes for this module attachment are rounded to give a mechanical means of assisting in alignment.

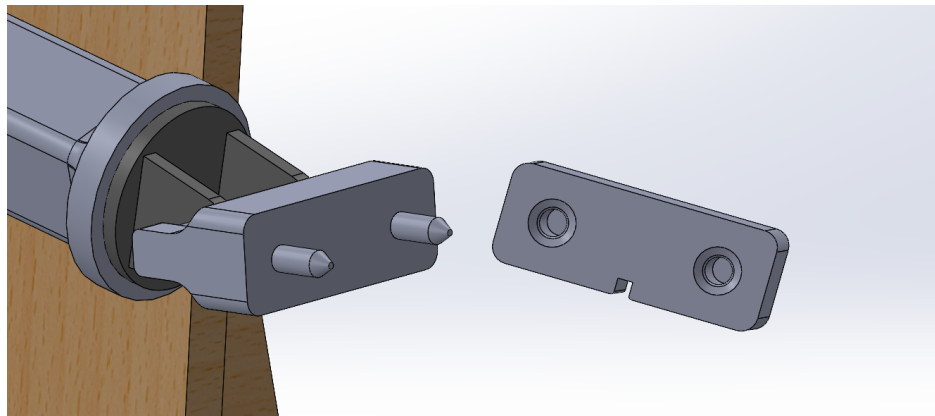


Figure 10: Close-up view of module connection interface

This design has many benefits. First, the shoulder is mounted in a human-like position and the joints are similarly-positioned to that of a human arm as a six degree of freedom arm can be. Additionally, the attachment of a large variety of modules to this arm should be quite easy. Moreover, the design for each compound joint is the same, just to different dimensions. Therefore, the analysis and design is simplified greatly as much can be reused. Finally, if copper alignment pins were used, the same part could carry electrical current for powering the attachment while simultaneously ensuring alignment.

This design does, of course, have some downsides. One downside is that both motors on the shoulder would have to be strong enough to hold the arm's full weight, given the orientation of the mounting point. This is because there exist arm orientations in which either motor would be taking the entire weight of the arm. Moreover, if a mechanical latch was used for the module attachment, some slop could exist in this when the attachment joint is under tension. Any amount of play would reduce the precision of the end effector. Finally, it is physically possible for a module to be mounted upside down depending on the arm's orientation compared to where the program thinks it is mounted. This could be counteracted through code, but it is an engineering best practice to reduce the possible errors that could occur at a later time through negligence.

Mason Keck

The next arm being presented was designed with simplicity in mind. When given the choice between simple and satisfactory or overly complex and perfect, it chooses the former.

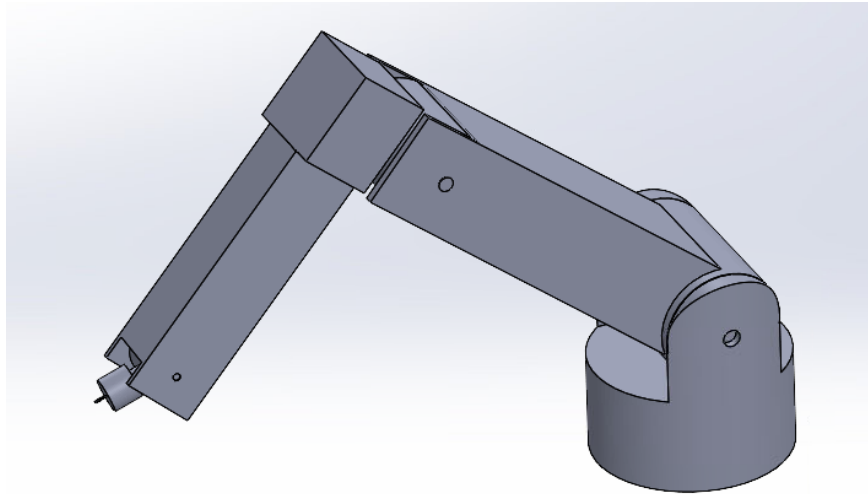


Figure 11: Isometric View of Design

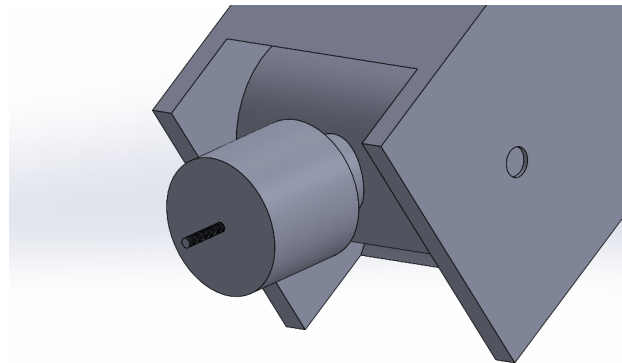


Figure 12: Close Up View of End Effector

This design has a total of six degrees of freedom — two at each joint. This gives the arm fair mobility in most circumstances, especially when considering the end effector. It was designed to be able to make small movements in cases where fine manipulation is needed. Also, this end effector is one of the most simple designs, making for relatively straightforward and inexpensive manufacturing. Next, the large connections at each joint grants large storage spaces for internal workings such as motors, sensors, and other electronics. This may allow the robot to have more powerful motors, and therefore provide better fidelity when commanding the arm.

There are, however, disadvantages to this design. Because of the focus on simplicity, the design ended up being generally large and clunky. This means the arm may be difficult to manufacture to the project's size constraints. Also, the attachments for the end effector would have to be relatively complex, while simultaneously being limited in scope and weak. This is because the end effector does not provide any power to attachments, and instead would rely on mechanical advantages to cut or clamp. In some cases, the weight of the object itself could be what clamps the attachment, creating possible issues if the object is too small or light. Finally, this arm may not closely emulate human arms. This could create conflicts with the project's objectives, as it aims to have intuitive controls that can be learned quickly and with relatively little training.

Matthew Nolan

The sixth robotic arm concept was developed with a focus on robust end effector coupling, a large work area, and neatly packaged electronics. The arm, shown below in Figure 13, has six degrees of freedom, meaning that it is fully actuated to achieve nearly any 3D position and angle of its end effector. The arm consists of two joints at the base, two at the elbow, and two at the wrist, with each pairing containing one axial joint and one hinged joint.

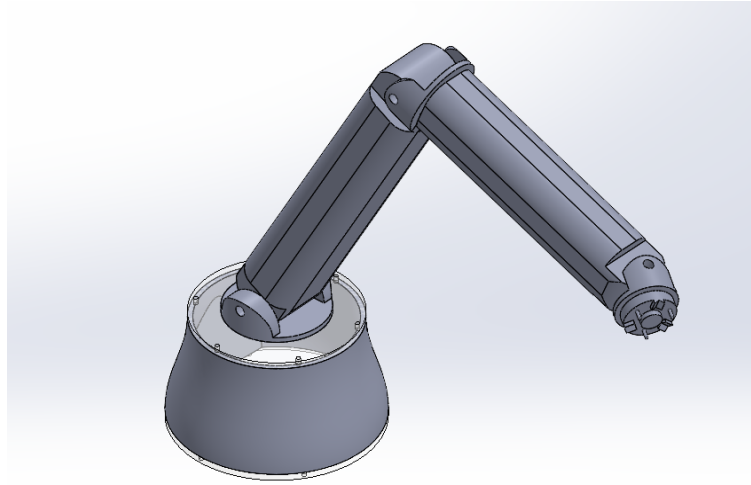


Figure 13: Basic concept model of the robotic arm. The motors are placed in-line with each limb. As seen above, this design mounts onto a simple pedestal, which contains all of the arm's electronics and serves as a simple mount for the first axial joint (the "shoulder rotate" joint). The orientation of the arm, as determined by the pedestal, allows for the robot to reach behind itself as much as the base motor permits, increasing the work area if the operator were to turn in place. Because the center of mass of the arm does not necessarily sit above the pedestal throughout the

arm's entire range of motion, there is a cutout in the back of the base that allows the project to easily be clamped to a table for testing purposes. This is shown more clearly in Figure 14.

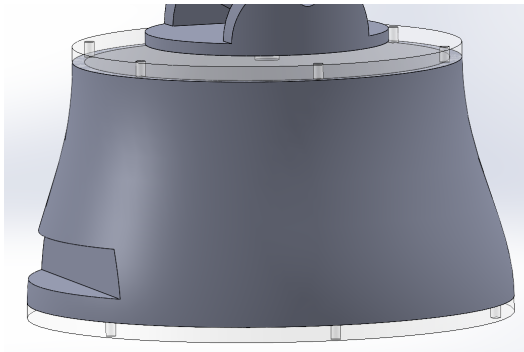


Figure 14: The base of the robot arm has a simple cutout to allow for it to be clamped to the surface of a table.

A variety of modular end effectors can be attached to the arm through the use of a kinematic coupling. This ball-and-divot structure ensures precise and consistent alignment of the tool even if the motion to pick up said tool is not perfect. The tool will be held in place axially with an electromagnet, which may serve as its own end effector in order to manipulate ferromagnetic objects. The normal force from the electromagnet combined with the ball-and-divot structure prevents the tool from rotating in its mount. Three spring-loaded pogo pins will facilitate the use of active tools such as grabbers and wire cutters, passing power through the wrist and into the end effector. This system is shown in greater detail in Figure 15 below.

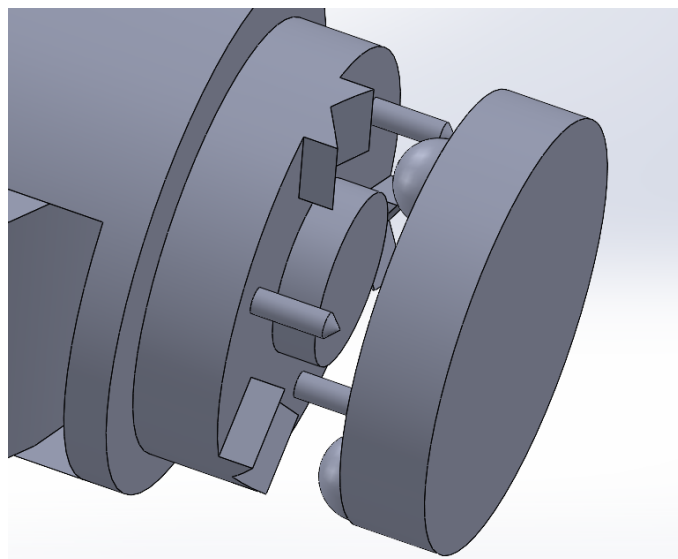


Figure 15: Close-up view of the kinematic coupling with electromagnet and pogo pins. The wrist side (left) has divots that couple to balls on the tool side (right).

The primary benefit of this design is the robust, precise, and highly repeatable method of attaching both active and passive end effectors. Accurately locating the arm's tool ensures that it can repeatedly swap between several tools without risking a misalignment that might result in an unstable connection or compromise the ease of control. Additionally, the six degrees of freedom combined with the mounting configuration means that the arm has a large usable work area and can reach behind itself. All of the electronics and motors are enclosed, resulting in a tidy and well-integrated design. Finally, the concept's structural components would be relatively easy and cheap to manufacture purely with additive manufacturing and laser cutting.

This concept has some drawbacks in areas that other designs perform well. Notably, the orientation of the arm and distribution of joints between the limbs is dissimilar from a human arm, which is elevated relative to the work area, oriented horizontally, and has one joint at the elbow rather than two. This has the potential to undermine the intended intuition behind the arm's control. It would also likely mean that the device does not end up mimicking the arm shape of the human operator, simply copying the hand's position and orientation. Additionally, the somewhat bulky nature of the limbs means that the design can not fold up as much as other concepts presented here, giving it a relatively large storage footprint.

Connor Nail

The concept seen in the figures below is for a robotic arm that consists of six joints and attached to an upright tower. Starting at the top, the first two joints in the arm include an axial revolute joint and a hinged revolute joint. These two joints model the shoulder motion of a human arm. This is followed by another axial joint to represent the upper arm rotation of a human. Next, there is another hinge joint and axial joint representing the elbow and forearm rotation respectively. There is then a final hinged joint to represent a portion of a human's wrist movement. The connection between the end effectors and the arm is an electromagnetic coupling system that allows the arm to switch between different types of end effectors.

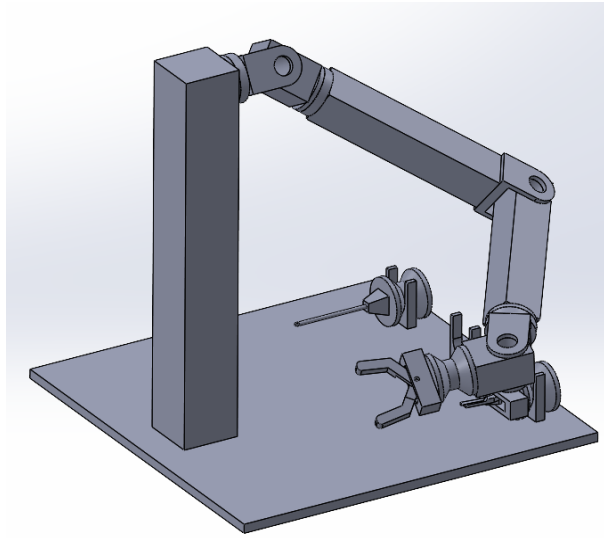


Figure 16: Isometric View of Arm

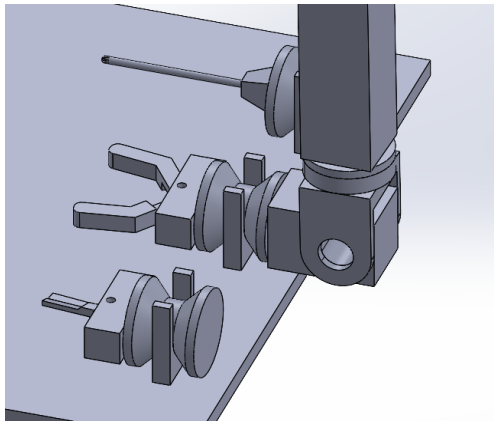


Figure 17: Enlarged View of End Effector Connection

The main benefits of this design come from its similarities to a human arm both in terms of location of joints and length of limbs. This is critical due to the emphasis our requirements place on the ease of use of the system. Having this type of geometry will allow for the system to more easily mimic the positioning of a human's arm while holding a VR controller.

This concept also provides a very modular system for the end effectors. Each end effector has a modular base meaning that nearly any type of end effector could be modified to interface with this system. The number of end effectors that could be made selectable by the system is also scalable with the amount of space on the base being the only limiting factor.

There are also a few downsides to this concept. The electromagnetic end effector connection system would require activation. This increases the complexity required to change end effectors and could possibly be improved by integrating a passive mechanical connection system. In addition to this, the magnetic connection may not be strong enough under loads in specific directions making the use of certain end effectors impossible. The final disadvantage to this design is the requirement that the motors be mounted externally. This may or may not be an issue depending on the degree to which the motors limit the rotation of each joint.

There were many similarities between all of the concepts that were generated. However, there were also a few key differences that needed to be considered as the team moved toward a final design. First, the shoulder mounting orientation had to be determined; both horizontal and vertical mounting configurations were observed in the concepts. The joint positioning was also strongly considered as it affects the workspace that the end effector can reach, as well as the orientations it can achieve inside that workspace. Next, the joint and linkage geometry was evaluated. There were many different configurations proposed between the concepts that will need to be considered. Finally, the way in which the arm interfaces with the end effectors had to be determined. With these points under consideration, the team believed that it would be best to combine favorable aspects of many of these concepts into one robotic arm system that meets our goals. In order to do this, characteristics of the arm had to be prioritized based on the project's goals and objectives.

Decision Making

Design Criteria

To determine the design criteria, the team looked to the objectives and constraints to help brainstorm. A few different criteria were considered, but most were either similar or were difficult to give a measurement to which led to the following criteria:

1. Longest dimension while in storage, which will be measured in inches.
2. Mass, which will be measured in pounds.
3. Dexterous work area which will be measured in cubic feet.
4. Similarity to a human arm.
5. Cost in USD (\$).
6. Quality of module swapping.

The first one came from the previously-defined objective that "the arm should be compact in

storage.” The purpose is to ensure the designs can fold up in a compact manner, which is useful for getting through confined areas and for storage. The second relates to the objective that “the arm should be lightweight.” This helps with other objectives and constraints by allowing it to have less mass to move thus making it quicker and/or reducing torque requirements of the motors. The third criterion relates to two constraints: “the arm shall have a 170-degree conical range of motion on the shoulder” and “the arm shall have six degrees of freedom” which just refers to having good reach and motion. The fourth criterion is very important because it relates to the constraint that “the arm shall have six degrees of freedom” as well as the objective that “the arm should be easy to control for new users”. This is achieved by allowing the movements to be intuitive. The cost criterion is just to stay within budget and within a reasonable cost. The last criterion is a big part of the project and relates to the constraint “the arm shall change manipulator type (with no user input beyond a simple command) and restore user-controlled position within 8 seconds.” This was used to determine which connection type was best and to ensure it will be able to perform the tasks required without failing.

After selecting the criteria, an Analytical Hierarchy Process was used to compare the six criteria and weigh them by order of importance. This process can be seen in Table 2 below.

Table 2: Analytical Hierarchy Table

	Longest Dimension While in Storage	Mass	Dexterous Work Area	Similarity to Human Arm	Cost	Quality of Module Swapping	Rating	Normalized Rating
Longest Dimension While in Storage	1	8	4	3	7	5	2.05	0.03
Mass	1/8	1	1/4	1/2	1	1/3	19.00	0.28
Dexterous Work Area	1/4	4	1	5	3	2	6.28	0.09
Similarity to Human Arm	1/3	2	1/5	1	3	4	10.08	0.15
Cost	1/7	1	1/3	1/3	1	1/3	18.00	0.26
Quality of Module Swapping	1/5	3	1/2	1/4	3	1	12.67	0.19

Once completed, the two most important criteria were established to be “Mass” closely followed by “Cost”. These two criteria were the most important since they both strongly affect the quality of the robotic arm relative to the market, as well as its ability to function. Additionally, they are the most measurable. The next most important criteria were “Quality of Module Swapping” and “Similarity to Human Arm” which were both given a similar weighting. While less important than “Mass” and “Cost”, these two criteria still received relatively high weightings due to their close relation to the project objectives. These criteria directly relate to the arm’s ability to quickly and autonomously swap modules and maintain a simplistic and effective user control system. Lastly, “Dexterous Work Area” and then “Longest Dimension While in Storage” were weighted

as least important to criteria decision making. “Dexterous Work Area” received a higher rating than “Longest Dimension While in Storage” since it relates to the usability of the robotic arm. The “Longest Dimension While in Storage” criteria was seen as more of a welcome feature and not something that would hugely affect the functioning of the arm itself.

Numerical Scales

The following numerical scale was developed to numerically evaluate the qualitative performance level of each design for each criterion:

Table 3: Qualitative Evaluation Scale

Performance Level	Value
Perfect	10
Excellent	9
Very good	8
Good	7
Satisfactory	6
Adequate	5
Tolerable	4
Poor	3
Very poor	2
Inadequate	1
Useless	0

After developing this table, the top and bottom thresholds were identified for each criterion. Five inches was considered to be the perfect size for the longest dimension in storage, while 36 inches was determined to be too long. For mass, one pound was found to be ideal, while ten pounds was labeled as useless. Dexterous work area is a criterion that must be weighted qualitatively in lieu of complex modeling which can be performed at a later stage for the chosen design. Although some robotic arms may be able to reach unique directions, a human will be controlling the robot with arm movements. This means the arm could never be commanded in that direction. Therefore the perfect arm will be able to reach all end-effector orientations and positions possible by a human arm. An arm that could not move at all would be unusable in the target applications. The similarity to a human arm was rated similarly, with equal proportions to a human arm being perfect, and being dissimilar or unrecognizable would be rated as useless. Simply enough for cost, \$100 was considered to be ideal and anything over \$1000 was decided

to be too expensive. Finally the quality of module swapping was again scaled qualitatively. If the end effector is attached relatively quickly and robustly, it is considered perfect. If the end effector is unusable or falls off, it is considered useless. These scales are shown in the table below and later used to score each criterion.

Table 4: Numerical Scales

Longest Dimension While in Storage		Mass		Dexterous Work Area		Similarity to Human Arm			Cost		Quality of Module Swapping		
	[in]		[lb]										
Perfect	5	Perfect	1	Reach all end effector orientations and positions possible by a human arm.	10	Same motion at human arm joints. Same dimensions as human arm.	10	Perfect	100	Fast and robust.	10		
	8		2		9		9		200		9		
	12		3		8		8		300		8		
	15		4		7		7		400		7		
	19		5		6		6		500		6		
	22		6		5		5		600		5		
	26		7		4		4		700		4		
	29		8		3		3		800		3		
Useless	33		9		2		2		900		2		
	36	Useless	10	No movement	1	No similarities to a human arm.	1	Useless	1000	Cannot swap modules and/or avoid detaching unexpectedly	1		

Decision Matrix

A decision matrix was generated from the numerical scales and relative weights in order to quantitatively assess the value of each design concept by assigning all of the designs a raw score for each criterion. This matrix is shown below in Table 5.

Table 5: Decision Matrix

Design Options															
Criteria		Units		Normalized Weights			3M			EV			MK		
Criteria	Units	Normalized Weights	Raw Score	Value on Std. Scale	Relation Value	Raw Score	Value on Std. Scale	Relation Value	Raw Score	Value on Std. Scale	Relation Value	Raw Score	Value on Std. Scale	Relation Value	
Longest Dimension While in Storage	in	0.03	19	6	0.1807627074	12	8	0.2410169432	15	7	0.2108898253				
Mass	lb	0.28	5	6	1.674389327	3	8	2.232519103	6	5	1.395324439				
Dexterous Work Area	m^3	0.09	9	9	0.8305852319	8	8	0.7382979839	9	9	0.8305852319				
Similarity to Human Arm	rating	0.15	10	10	1.481002256	7	7	1.036701579	8	8	1.184801804				
Cost	USD (\$)	0.26	800	3	0.7931317865	700	4	1.057509049	600	5	1.321886311				
Quality of Module Swapping	rating	0.19	8	8	1.488346068	1	1	0.1860432586	7	7	1.30230281				
			Total:	6.448217377		Total:	5.492087916		Total:	6.245790422					
Design Options															
Criteria		Units		Normalized Weights			AR			CD			MN		
Criteria	Units	Normalized Weights	Raw Score	Value on Std. Scale	Relation Value	Raw Score	Value on Std. Scale	Relation Value	Raw Score	Value on Std. Scale	Relation Value	Raw Score	Value on Std. Scale	Relation Value	
Longest Dimension While in Storage	in	0.03	17	6	0.1807627074	5	10	0.301271179	16	6	0.1807627074				
Mass	lb	0.28	4	7	1.953454215	2.5	8.5	2.372051547	5	6	1.674389327				
Dexterous Work Area	m^3	0.09	6	6	0.553723488	9	9	0.8305852319	9	9	0.8305852319				
Similarity to Human Arm	rating	0.15	5	5	0.7405011278	8	8	1.184801804	6	6	0.8886013534				
Cost	USD (\$)	0.26	500	6	1.586263573	500	6	1.586263573	650	4.5	1.18969768				
Quality of Module Swapping	rating	0.19	8	8	1.488346068	1	1	0.1860432586	10	10	1.860432586				
			Total:	6.503051179		Total:	6.461016594		Total:	6.624468885					
Design Options															
Criteria		Units		Normalized Weights			CN			Alternative					
Criteria	Units	Normalized Weights	Raw Score	Value on Std. Scale	Relation Value	Raw Score	Value on Std. Scale	Relation Value	Raw Score	Value on Std. Scale	Relation Value	Raw Score	Value on Std. Scale	Relation Value	
Longest Dimension While in Storage	in	0.03	19	6	0.1807627074	16	6	0.1807627074							
Mass	lb	0.28	5	6	1.674389327	4.5	6.5	1.813921771							
Dexterous Work Area	m^3	0.09	9	9	0.8305852319	9	9	0.8305852319							
Similarity to Human Arm	rating	0.15	10	10	1.481002256	10	10	1.481002256							
Cost	USD (\$)	0.26	900	2	0.5287545243	800	3	0.7931317865							
Quality of Module Swapping	rating	0.19	6	6	1.116259551	10	10	1.860432586							
			Total:	5.811753598		Total:	6.959836338								

The scores are standardized using the numerical scales discussed previously, and then a final score is calculated using the normalized weights for each criterion. These relation values are

added to get a final score for each design. From the matrix, it is demonstrated that the new alternative design option, highlighted in green above, scores the highest at 6.96 points, indicating that it is the best option overall. While relatively costly, it demonstrates excellent work area, similarity to the human arm, and module swapping quality. Matthew's design came second at 6.62, followed by Andrea's at 6.50 and Benjamin's at 6.45. Because this alternative option clearly scores higher than all of the other designs, and because it combines the most promising aspects from each of the other concepts, the team will be exclusively focusing on this option moving forward.

Top Design

The top design selected by the team was an alternative concept that combines the favorable aspects of multiple designs. It inherits the upright mounting position from some of the previous designs which make the arm closer to a human form, leading to more intuitive human control and allowing the arm to replicate the human arm's range of motion. Here, it is shown with a wooden testing stand for prototyping purposes, though of course in real use it could be mounted on anything.

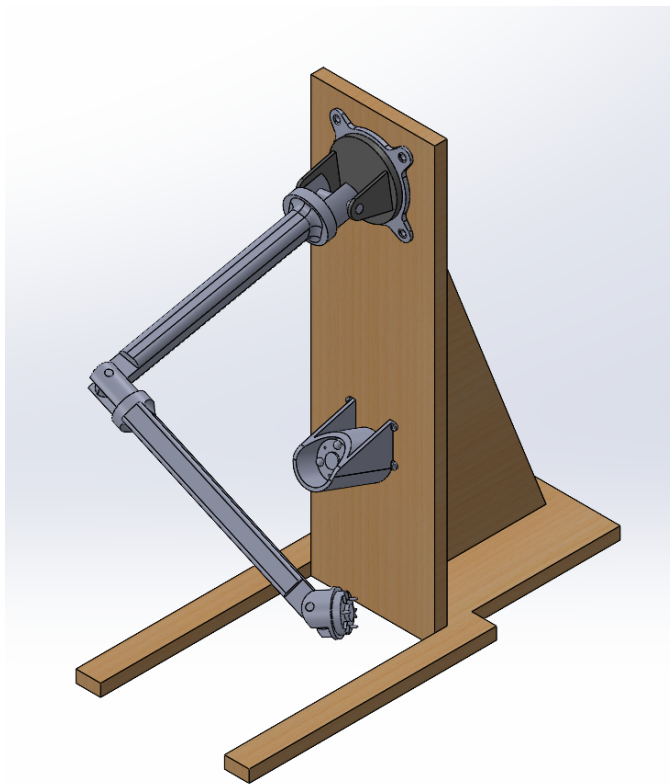


Figure 18: Full view

The positions of the joints were chosen very deliberately. The arm needs to have six degrees of freedom (DOF); this is accomplished by placing three DOF at the shoulder, two DOF at the elbow, and one DOF at the wrist. This allows the mass of the motors and their respective gearboxes to be placed as close to the shoulder as possible, reducing the torque requirements of the motors by reducing the moment of inertia about each joint as much as possible while still attaining the range of motion expected of a six DOF arm. This design is also able to curl enough to have a largest dimension in storage of 16 inches, though this could be improved with further design optimization. This folded configuration is seen in Figure 19 below.

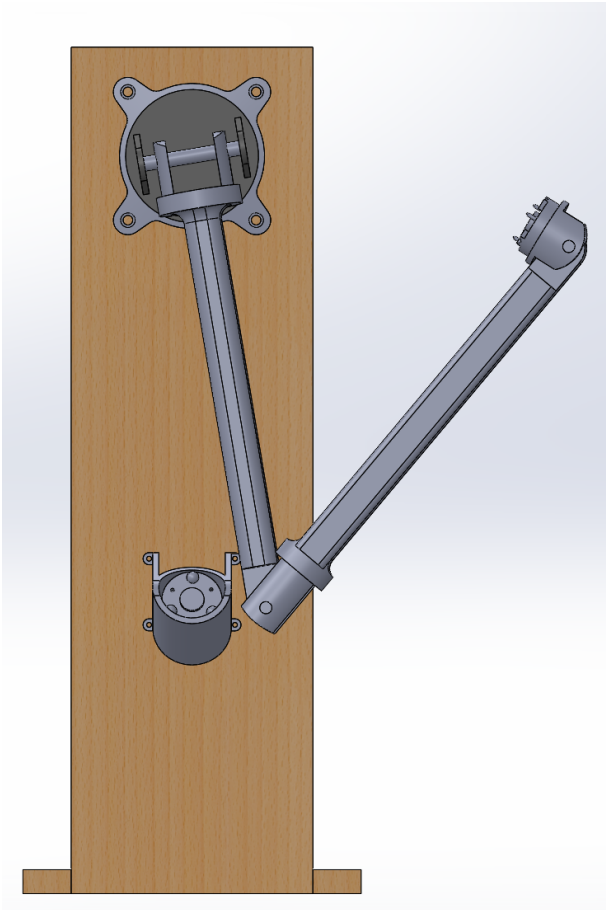


Figure 19: Robotic arm folded

This design has circular module trays, which can be arranged in a matrix at the base of the testing stand, that help to guide the arm in to pick up or release a modular attachment. This is seen in Figure 20 below. The kinematic coupling is inherited from one of the previous designs, and it helps to align the module with the arm with an electromagnet to robustly hold the tool. This electromagnet can itself act as a useful tool.

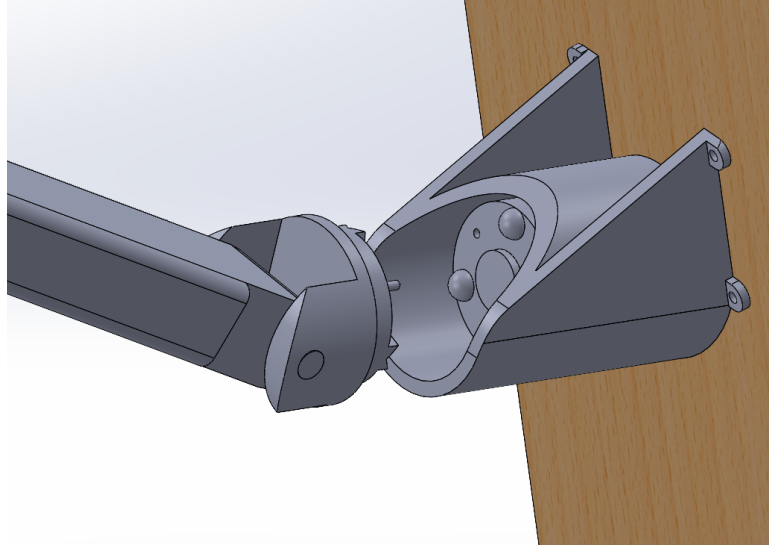


Figure 20: New tray design and kinematic coupler

Engineering Analysis

The purpose of the Intuitive Human-Controlled Robotic Arm is to create a robust, accurate, and intuitive robotic arm which can be remotely operated. The mechanical design of this arm is essential to accomplishing this goal, as software and controls can only optimize the operation of the motors; however, each arm segment needs sufficient torque in the motors to support and move the mass of the arm. Moreover, the arm must not deflect significantly so that accurate control can be guaranteed, and critical points of the arm cannot be allowed to yield under the expected stresses.

The options have been narrowed down to a singular design which incorporates the best parts of each generated design. It is desired to analyze the torque required for motors at each joint along with the stresses which will be developed in worst-case scenarios. To accomplish this, analysis of the whole arm in ANSYS with bonded conditions between joints has been completed, along with more detailed calculations for individual parts given the expected mass and centers of mass and ANSYS simulations for parts of interest.

Overall, a minimum structural safety factor of 4.82 was found with the original geometry (if aluminum alloys are used) and the motor torque requirements are not excessive. The sections are organized as follows (labelled in the figure below):

- Section 1: Wrist
- Section 2: Lower Arm
- Section 3: Upper Arm
- Section 4: Shoulder Joint

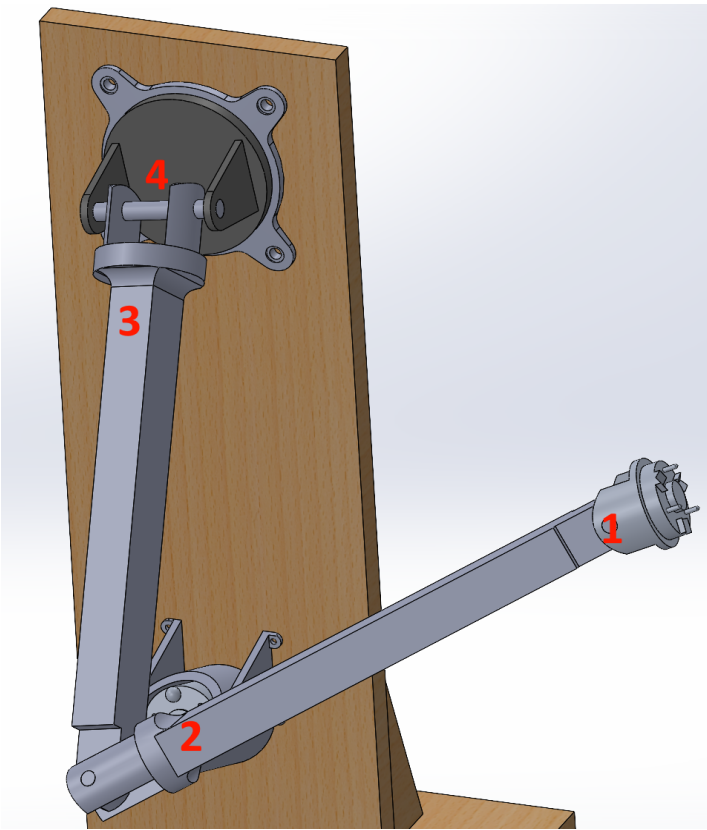


Figure 21: Labelled arm sections

Whole Arm

ANSYS analysis was completed of the whole arm with a bonded condition at each joint and a 0.7 kg aluminum block as a stand-in for the end effector. The entire arm was modeled as an aluminum alloy. Besides just looking at the maximum stress anywhere on the arm, certain key positions were noted on the surface of joint pins. As seen in the table below, the deformation and stresses developed in the shoulder pin do not appear to increase as element size decreases, so this analysis is valid.

Table 6: Maximum stresses with various element sizes in a geometric series

Element Size (mm)	Von Mises Stress Total, MPa	Von Mises Stress (Shoulder pin, MPa)	Von Mises Stress (Elbow, MPa)	Von Mises Stress (Wrist pin, MPa)	Deformation (mm)
20	56.86	56.86	5.04	3.20	2.61
10	46.70	46.70	6.75	4.25	2.71
5	49.48	40.25	8.91	9.65	1.91
2.5	45.57	45.57	12.70	2.43	2.57

The maximum deformation across simulations was about 2.7 mm, which is relatively insignificant. So, it is not anticipated that the deformation of the arm sections will be a major cause of steady-state error.

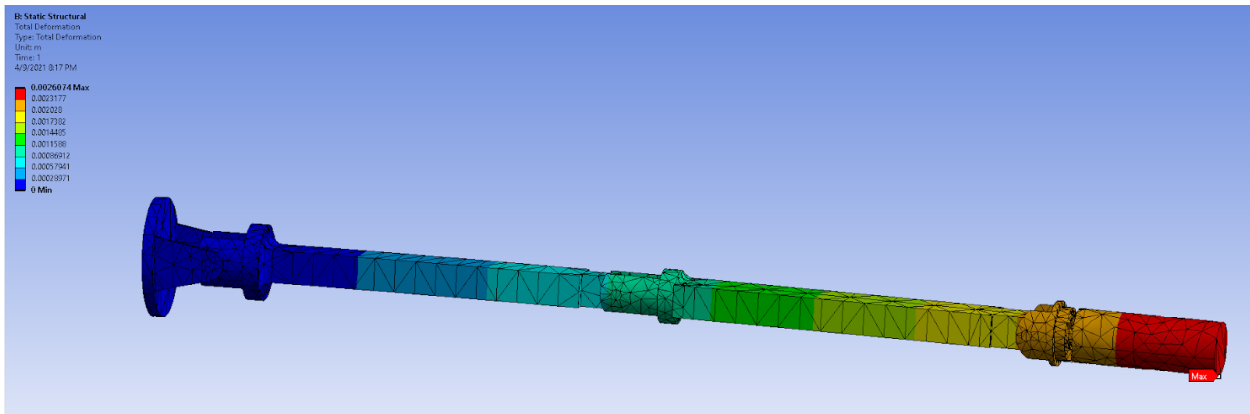


Figure 22: Maximum deformation (20 mm mesh)

The maximum von Mises equivalent stress developed across simulations was about 57 MPa (shown below), whereas the yield strength of a 6061 aluminum alloy is 275 MPa (Campbell, p. 494). This results in a safety factor of 4.82 if such an alloy is used, which is very good.

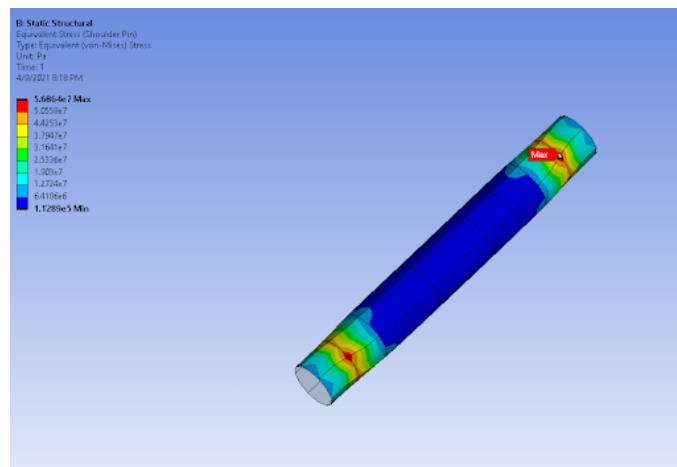


Figure 23: Point of maximum stress, shoulder pin (20 mm mesh)

Wrist (Section 1)

The robot's wrist consists of an axle powered by a servo motor which connects to a mount for an end effector, which can be up to 0.7 kg. The equation for the stress expected in the wrist axle (and therefore the minimum yield strength) is demonstrated in the figure below, and is made up of shear components.

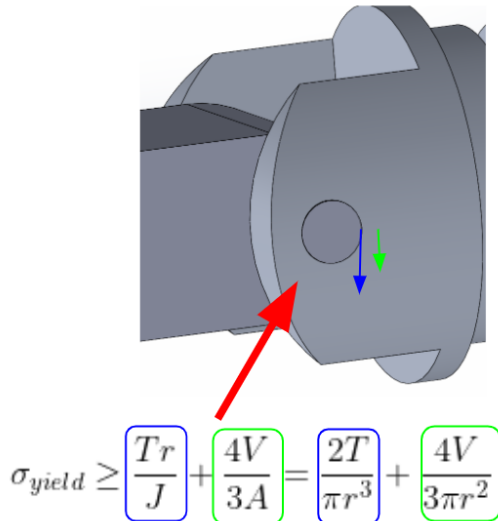


Figure 24: Relevant stress equations and labelled stresses

In the table below, the input specifications are given. This includes the mass of the end effector, and that center of mass's distance from the wrist. A stall torque multiplier of 1.5 is used to calculate the torque required for the motor not just to hold up the end effector but to accelerate it in a direction opposed by gravity. A safety factor of 2 was also multiplied by this to output the minimum value of yield strength required by the axle material and the minimum rated stall torque required by the motor. The outputs (motor and shaft requirements) are also shown in another table below.

Table 7: Wrist Specifications

Wrist Inputs						
Mass: 0.7 kg	Center of mass distance from wrist: 0.05 m	Factor of safety: 2	Stall torque multiplier: 1.5	Gear reduction: 1	Shaft radius 5 mm	

A value of the stall torque was also given in kg*cm, since this is commonly used for motor stall torque specifications.

Table 8: Wrist motor and shaft requirements

Wrist Outputs		
Motor stall torque req.	Yield strength req'd:	
1.03005 N*m	5.479157198	MPa
10.50 kg*cm		

Based on these specifications, there are numerous low cost and low weight motor options available for the wrist. Additionally, with the currently-planned shaft radius, any standard aluminum alloy will have more than enough yield strength even with a generous safety factor. In order to better understand the behavior of the wrist member under load, two loading conditions were considered in ANSYS. The first simulation observed the wrist and end effector together in a vertical orientation, with the end effector pointing downward. For this case, the deformation in the wrist shaft was not considered, and the wrist shaft holes were assumed to be fixed. A downward force was applied to the end effector to more accurately depict its maximum allowable weight (the length of the stand-in end effector was chosen based on how far the expected center of mass of the real end effector is from the wrist axis of rotation, and as such weighs slightly less than the maximum weight of the real end effector, so extra force was applied to compensate). An upward force of 37 N (a fairly standard value found in small electromagnets on the market) was also applied to the end effector to simulate an electromagnet pulling on it. A test moment of 1 N*m was also applied to the cylindrical face of the end effector in order to observe the effects of torsional stress on the kinematic coupling. The total deformation and equivalent stress for these simulations are shown below in Figures 25 and 26 respectively.

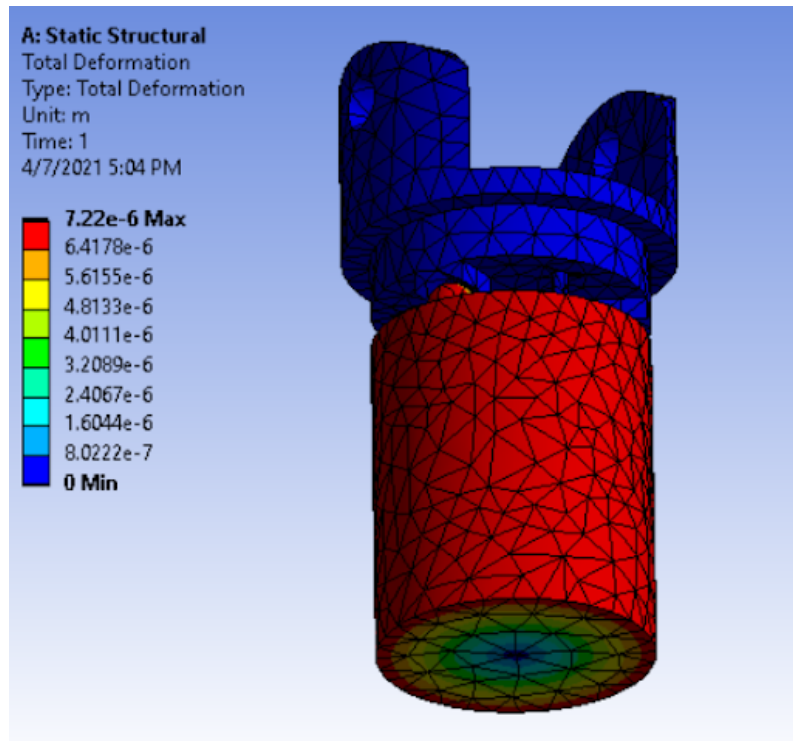


Figure 25: Total deformation for the vertical orientation of the wrist

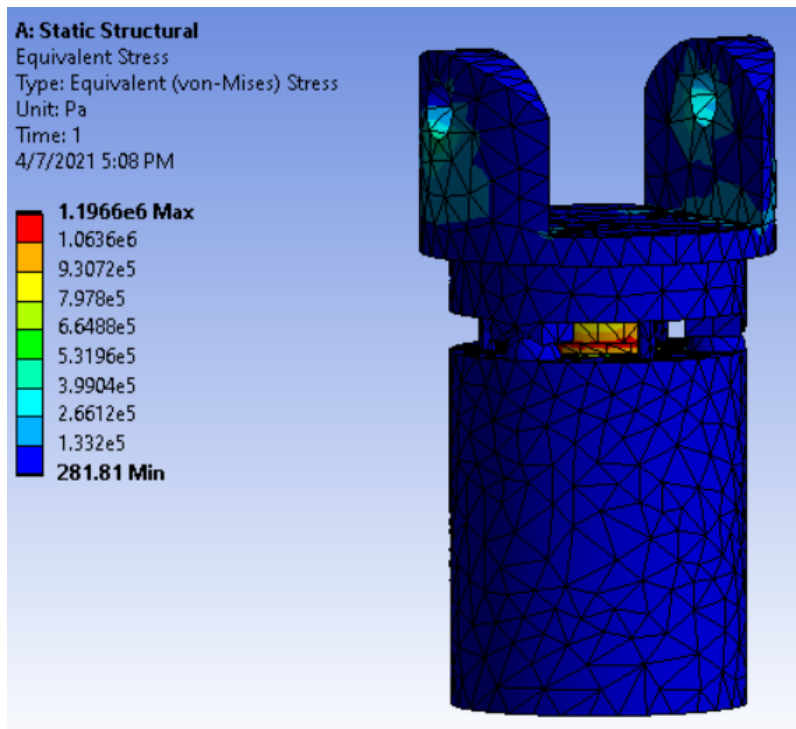


Figure 26: Equivalent (von Mises) stress for the vertical orientation

As expected, the deformation is maximum along the circumference of the end effector and zero at the cylinder's center. The small deformation around the circumference is about 7.22 microns and can be considered negligible. The maximum equivalent stress is about 1.6 MPa, which is considerably lower than the yield strength of aluminum. This maximum stress appears to occur at the circumference of the magnetic interface of the kinematic coupling between the wrist and the end effector, which is largely due to the bonded condition between the parts in ANSYS and the stress singularity that would seem to arise from this junction. Notably, the stress in the wrist is higher around the shaft holes and at the sharp interior corners of the wrist flanges, which is consistent with the theoretical implication of such geometric stress risers.

The second simulation placed the wrist and end effector in the horizontal orientation such that gravity acts downward, inducing a bending moment in the wrist. As in the previous case, an additional downward force was applied to the edge of the end effector (again, at the presumed center of mass of the real manipulator) to compensate for the effects of using a lighter stand-in for now. Like before, the shaft holes were considered to be fixed, a 37 N force was applied to the end effector acting toward the left (to simulate the electromagnet pulling it toward the wrist), and a moment of 1 N*m was applied about the circumference of the end effector. The total deformation and equivalent stress for these simulations are shown below in Figures 27 and 28 respectively.

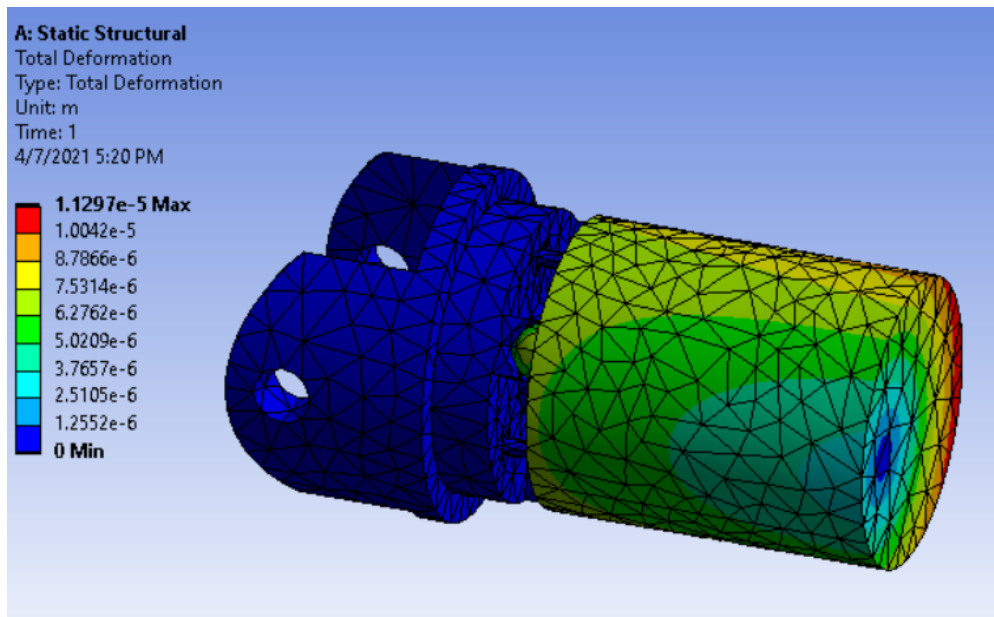


Figure 27: Total deformation for the horizontal orientation of the wrist

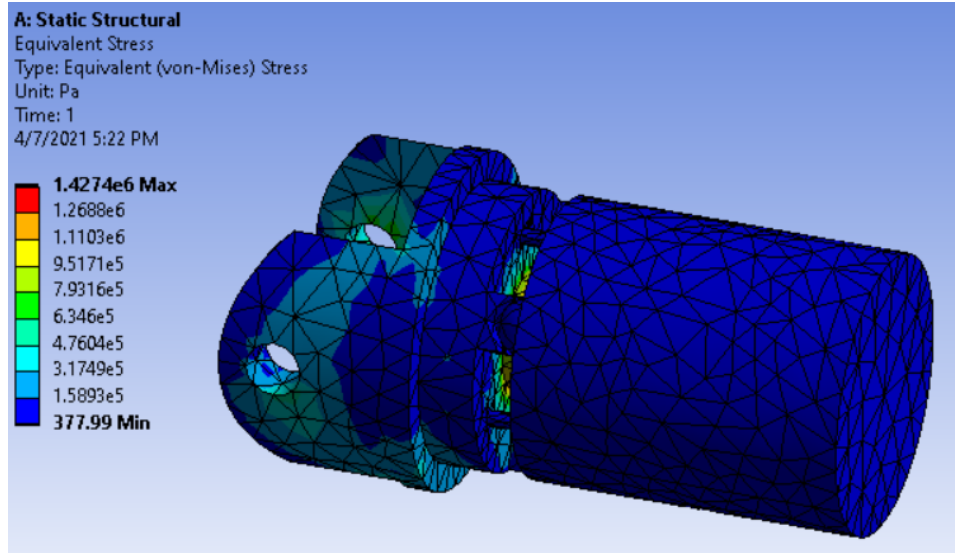


Figure 28: Equivalent (von Mises) stress for the horizontal orientation

Like before, the maximum deformation is observed near the circumference of the end effector. However, this deformation is not uniform about the circumference. Furthermore, the zero-deformation-axis through the end effector is no longer in the center of the cylinder. This is because of the downward bias of gravity, which combines with the moment about the end effector to effectively offset the deformation. Gravity applies a negative (downward) deformation throughout the model, while the moment applies a positive deformation on one side of the cylinder and a negative deformation on the other side. This has the effect of shifting the zero deformation axis to the left, as elements that would deform negatively due to gravity then have a positive deformation due to the torsion, resulting in a net zero change.

The maximum equivalent stress appears to be about 1.4 MPa, which is again substantially lower than aluminum's yield strength. Once again, this maximum stress appears to occur at the magnetic interface between the components and is due to the bonded condition and subsequent stress singularity at that edge. Similar to the previous case, the equivalent stress is higher near the shaft holes and the sharp corners of the flanges, which remains consistent with theory.

Lower Arm (Section 2)

The lower arm is part number 2. This arm was modeled as a simple cantilever system with the end effector acting on the free end. This part was given a hollowed squared cross section that has a thickness of 0.0015 m, a width and height of 0.04 m. The arm's length was set to be 0.4 m and the end effector had a weight of 0.7 kg. The figure below shows the model with dimensions.

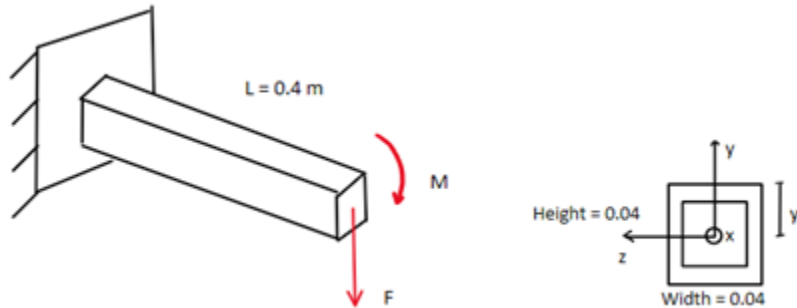


Figure 29: Illustration of cantilever model and cross section

To continue with the mathematical model the free body diagram, FBD, is needed and is shown below. From the FBD the reaction forces can be found by assuming the arm is in static equilibrium.

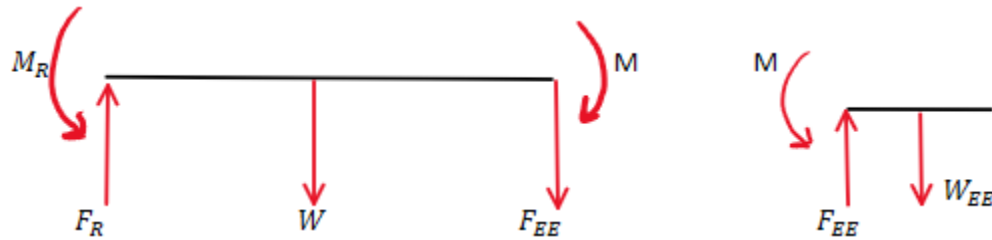


Figure 30: Free Body Diagram of Lower Arm (Left) and End Effector (Right)

From the reaction forces the maximum stress, torque for the hinge at the elbow, and the torque for axial rotation at the elbow can be found and are shown below in Table xx.

$$\sigma = \frac{My}{I}$$

Table 9: Lower Arm Calculation Results

Lower Arm Outputs	
Maximum Stress	3.08 MPa
Torque for Hinge at Elbow	4.66 N*m
Torque for Axial Rotation at Elbow	0.343N*m
Maximum Deflection	0.0712 mm

The maximum deflection is also included in the table above and is shown in the equation below. However, to be able to calculate the maximum deflection some material properties are needed. This section is assumed to be made of aluminum which has a modulus of elasticity, E, of 68 GPa. Using this equation, the maximum deflection can be found.

$$\delta_{max} = \frac{FL^3}{3EI}$$

The yield strength of aluminum is about 275 MPa (Campell, p. 494) which can be compared to the maximum stress and determine that the safety factor for this part is nearly 100. The maximum deflection can be seen to be extremely small. Due to the material and design choices the stress and deflection should not be an issue for the lower arm.

To continue the analysis of the lower arm a static structural simulation was run in ANSYS. The model that was used comes from the initial concept and was modified to more closely represent the final arm link. This model was fixed at the elbow joint, and a force and moment were applied to the wrist joint. This force and moment were calculated from the weight that is expected to be applied by the wrist and end effector.

Due to the singularity at the fixed support, the maximum stress in the link could not be determined from this simulation. It was, however, possible to collect information on the stress distribution throughout the link in areas farther from the singularity and found it to be far less than the yield strength of aluminum as seen in the figure below.

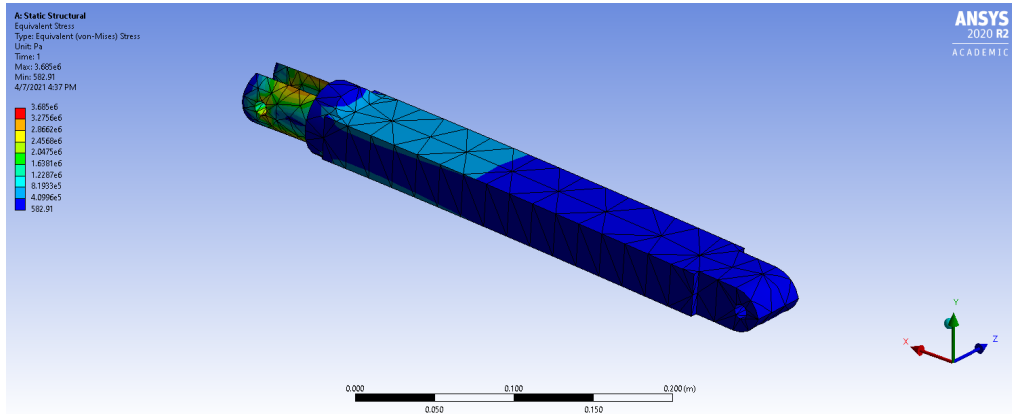


Figure 31: Stress Distribution in Lower Arm

The maximum deformation of the arm was found to be 0.08 mm as seen in Figure 32. This deflection is very small and shows that the deflection in the arm is negligible.

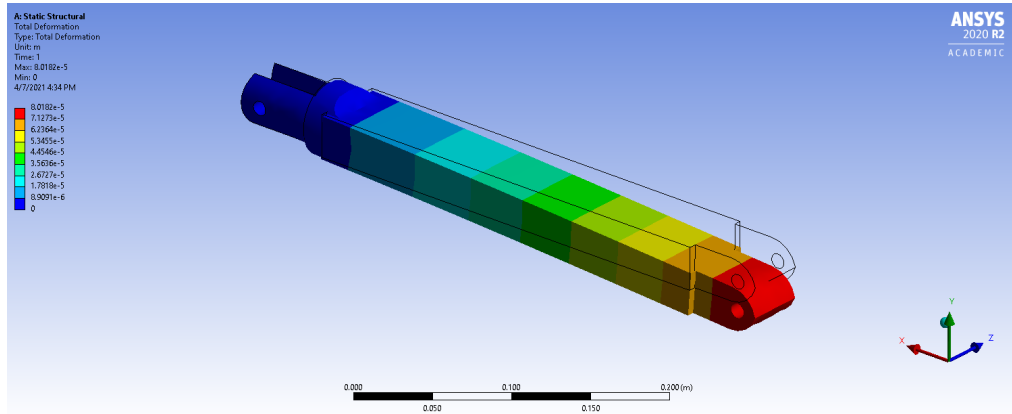


Figure 32: Deformation of Lower Arm

In addition, it was possible to find the reaction force and moment that will be acted upon the joint to be 22 N and 6.4 Nm respectively. These values closely match the values found during our previous analysis with the differences most likely being due to the difference in geometry and thus mass.

Upper Arm (Section 3)

The third component of this design is the upper arm. This arm segment is located nearest to the shoulder base. When conducting the engineering analysis for this part, it was important to find the sources of large torsional and bending stresses in the upper arm. These stresses were analyzed with static analysis and then further looked at using ANSYS.

When conducting the analysis for the upper arm, the torque reactions, torsional shear stress, and bending stress were of most interest. These stresses in the upper arm were found for two conditions of the arm's orientation. Condition 1, Figure 33, models the arm as static, fully extended, and parallel to the ground. Condition 2, Figure 34, models the arm with the elbow bent at 90 degrees and the entire arm parallel to the ground. The static analysis for condition 1 found the reaction torque near the shoulder and the bending stress in the upper arm. The bending stress was found due to the weight of the lower arm and wrist when the material was assumed to be aluminum. For condition 2, the torque reaction near the elbow and the torsional shear stress were able to be approximated.

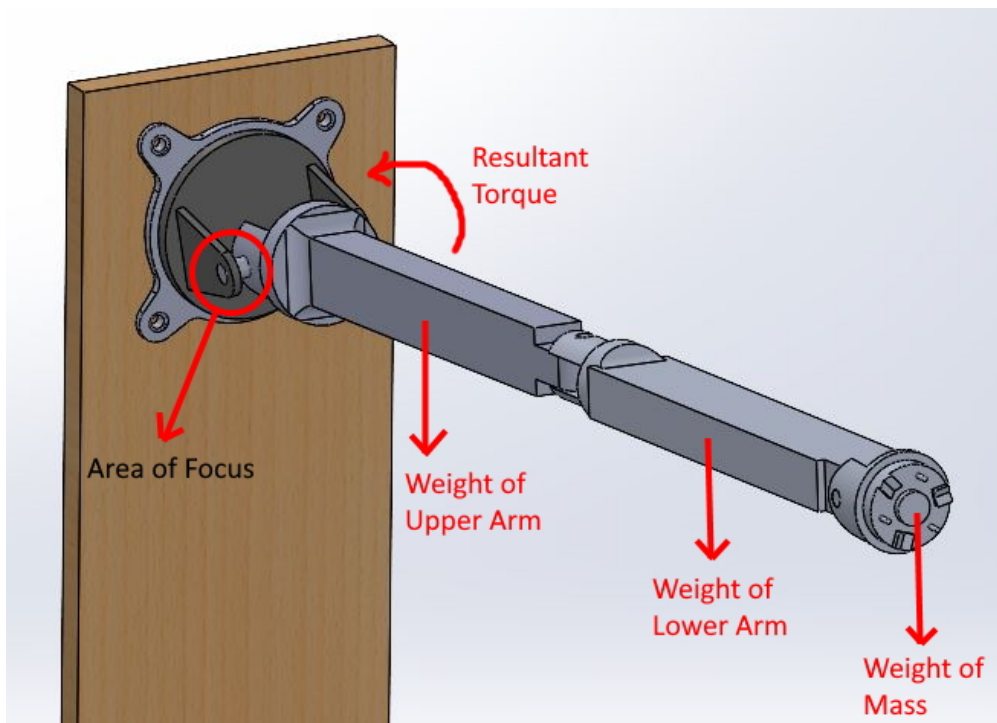


Figure 33: Condition 1 - Robotic arm is fully extended in a static position

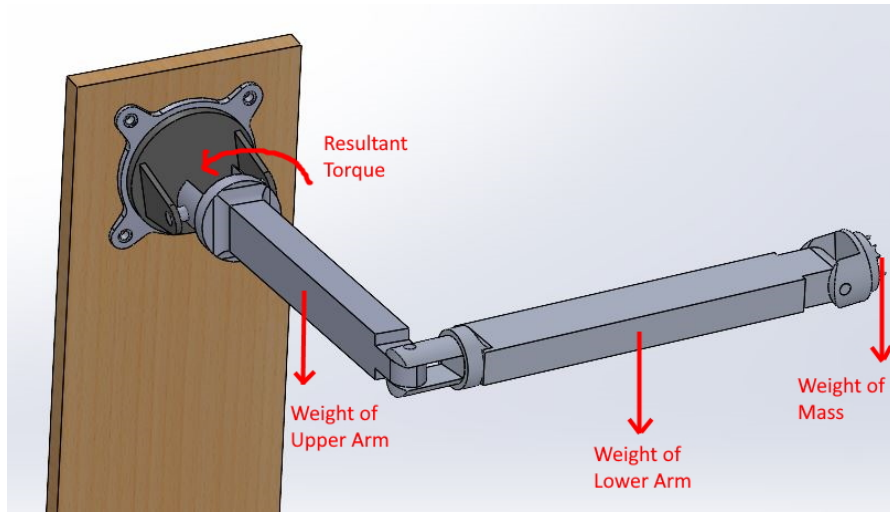


Figure 34: Condition 2 - Robotic arm is bent at a right angle and held static in position

Below, the results of the static analysis are shown in Tables 10 and 11.

Table 10: Static analysis of the upper arm under condition 1

Torque Reaction near the shoulder [Nm]	10.92
Bending Stress [MPa]	1.9
von-Mises Stress [MPa]	1.9
Factor of Safety	126.38

Table 11: Static analysis of the upper arm under condition 2

Torque Reaction near elbow [Nm]	4.36
Bending Stress [MPa]	1.14
Torsional Shear Stress [MPa]	0.53
von-Mises Stress [MPa]	1.46
Factor of Safety	164.16

These values were calculated by approximating the geometry as a simple hollow shaft with a rectangular cross section. This means that the weight and geometry of any joints or pins in the design were not accounted for when calculating the reaction torques and stresses. To obtain a better analysis of the part, ANSYS was used to simulate any torques or weight forces experienced by the upper arm. Below are the ANSYS simulations conducted to observe the stresses in the upper arm.

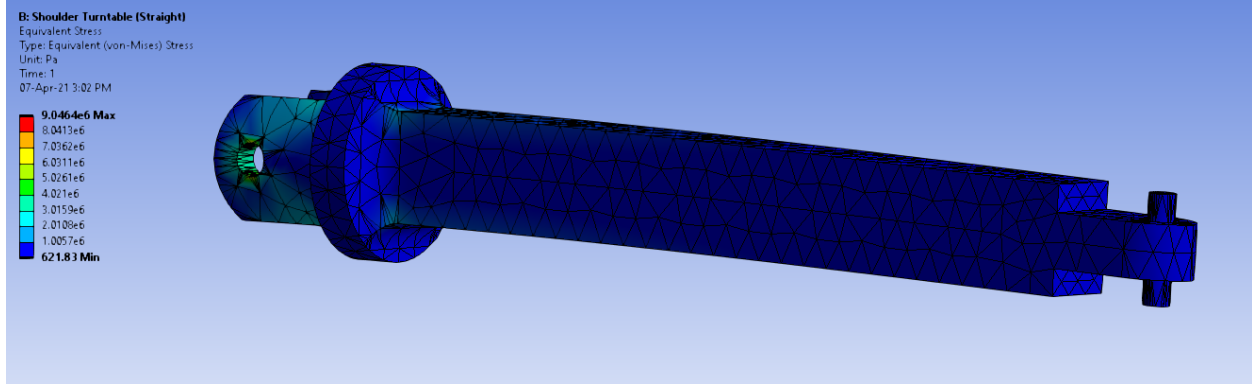


Figure 35: Stress Distribution for shoulder turntable, condition 1

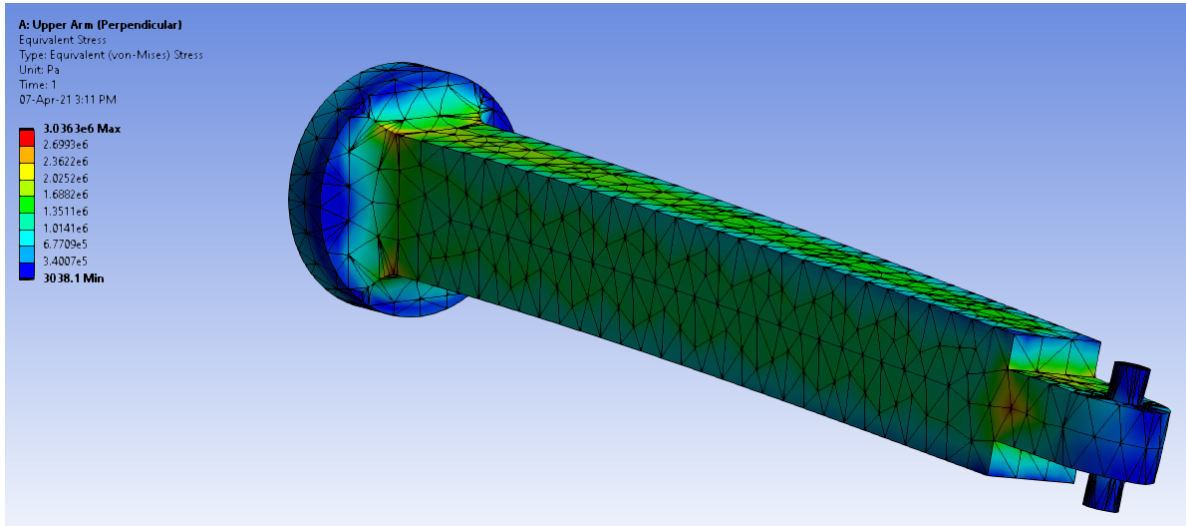


Figure 36: Stress Distribution for upper arm, condition 2

It can be seen that the maximum von-Mises stresses are higher than the calculated stresses, however this may be due to stress concentrations present in the fillets at the base and the pin holes, resulting in stress singularities. Despite this phenomenon, the maximum von-Mises stresses are still considerably lower than the yield strength of aluminum and large safety factors are obtained.

Shoulder Joint (Section 4)

To start analyzing the shoulder joint, hand calculations were performed in order to determine the stall torque that would be required in order to operate the two degrees of freedom that the shoulder has. Since the robot can be both fully extended out in front, and fully extended out to the side, the stall torque needed by the motors can be considered to be equivalent. The figure below shows the spreadsheet and free body diagram used for calculations.

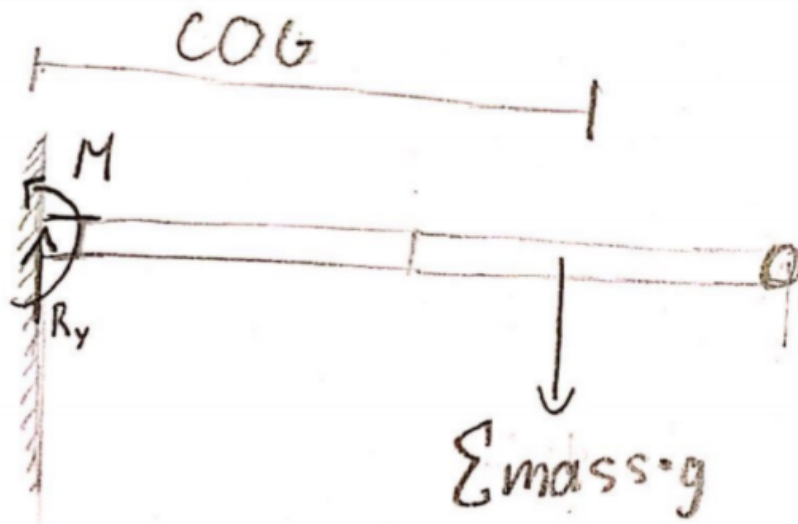


Figure 37: Free body diagram of whole arm

The calculations assume the following:

1. The length of each arm is a maximum of .4 meters and weigh a maximum of .6 kg each.
2. The elbow and wrist motors weigh 0.1 kg and 0.06 kg, respectively.
3. The end effector weighs .7 kg and has a center of gravity .05 meters past the wrist joint.
4. A factor of safety of 1.5 so that the arm can move with great fidelity.

The above assumptions were then used to calculate the center of gravity and weight of the arm. The minimum stall torque required was then found by multiplying the weight by the center of gravity. This answer was then multiplied by the factor of safety and the fidelity multiplier to find that both motors need to have approximately 13 Newton meters of torque to satisfy the project needs.

The next factor that is of key significance is the strength of the material and the stress it will be under. Since the shoulder has the force of the entire system acting on it, the ANSYS analysis for the shoulder is covered under the “Whole Arm” section of this report. It was found when the arm is fully outstretched in front of the base, a position shown previously in Figure 24. The maximum stress in the shoulder was found to be approximately 30 MPa in the pin. This is supported by the same equation below used for the wrist pin (combined shear stress due to twist and shear force).

$$\sigma_{yield} \geq \frac{Tr}{J} + \frac{4V}{3A} = \frac{2T}{\pi r^3} + \frac{4V}{3\pi r^2}$$

Using the above equation with a torque of approximately 13 N*m (solved above), and a 12 mm diameter solid shaft, the theoretical stress is approximately 38 MPa. When considering a generic yield strength value for aluminum of approximately 240 MPa, that gives a factor of safety of approximately 6.3 for the shoulder. This is a sufficient factor of safety for this component, therefore, the design of the shoulder can be considered satisfactory.

Design Progression

After selecting an alternate concept design and determining the required specifications, parts were selected. With the parts selected the concept design could be changed to accommodate them. The updated designs were broken up into multiple stages. Stage one included the base, shoulder and upper arm. Stage two included the elbow joint. The third and final design stage included the wrist and end effectors. Figure 38 contains the CAD design for the base, shoulder, and upper arm segment.

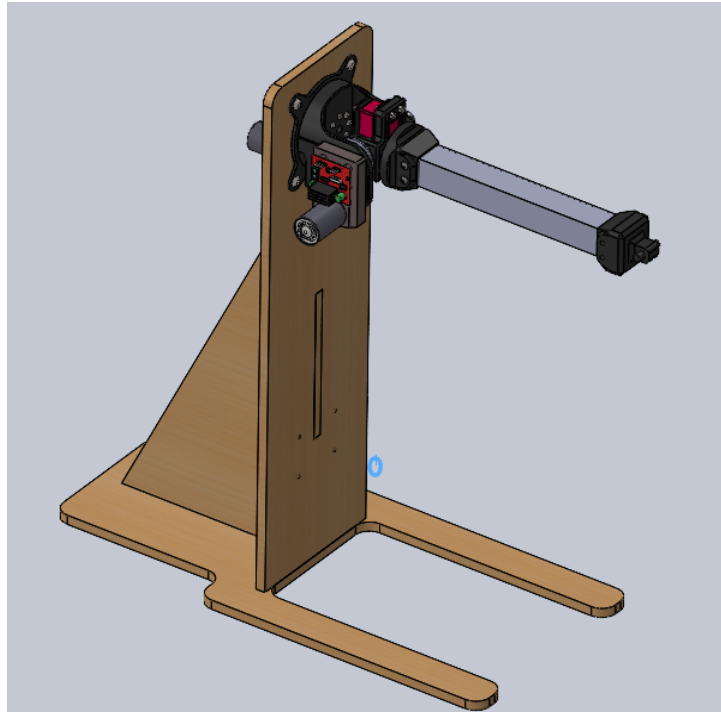


Figure 38: Isometric view of base, shoulder and upper arm.

Figure 39 shows an exploded view of the shoulder assembly. The MDF stand is shown with a wood grain texture, and the four 3D printed components are shown in dark gray. All of the necessary hardware, such as bearings, shafts, shaft collars, bolts, and nuts are included as well.

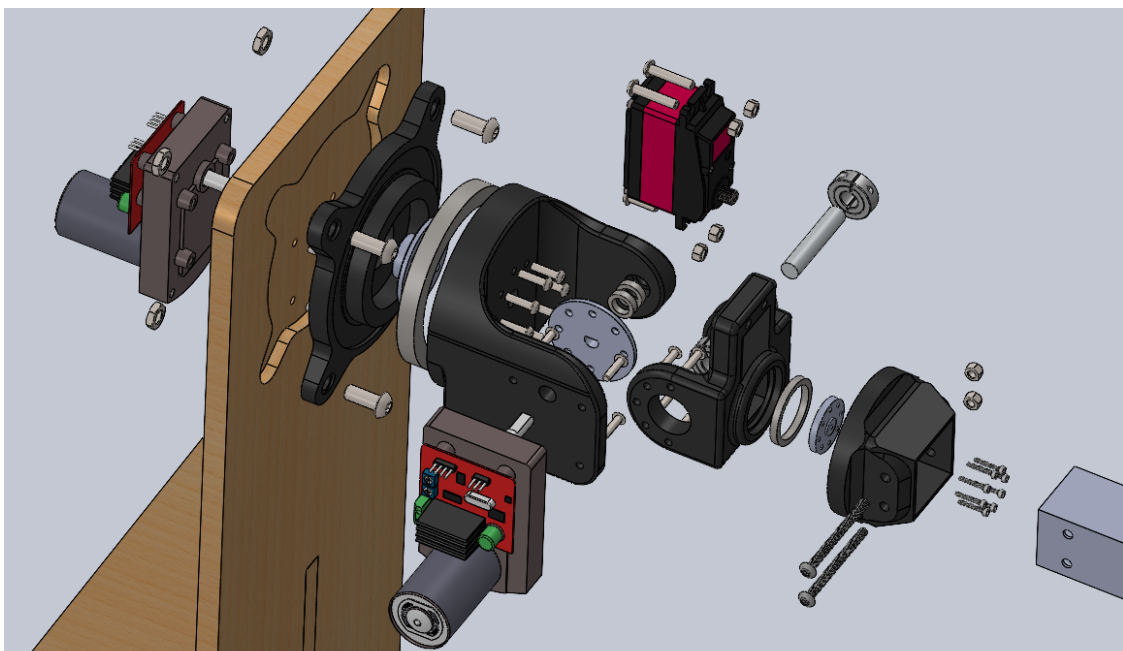


Figure 39: Exploded view of the robotic arm's three shoulder joints

All three axes are supported with bearings to minimize stresses on the motor shafts. The servo horns are made of aluminum and feature threaded circular hole patterns, which enable simple and compact attachments between motor shafts and their respective joints.

The next design stage was the elbow joint. Shown below in Figure 40 and Figure 41 are an isometric view and a top view of the elbow joint section. The leftmost motor enables motion about the x-axis and the inner motor enables motion about the z-axis.

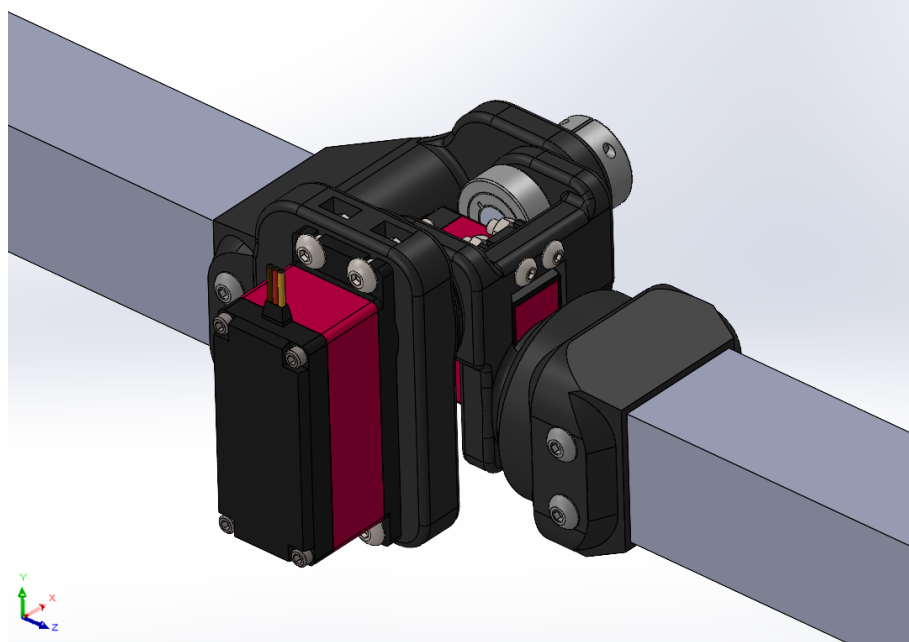


Figure 40: Isometric View of Elbow Joint

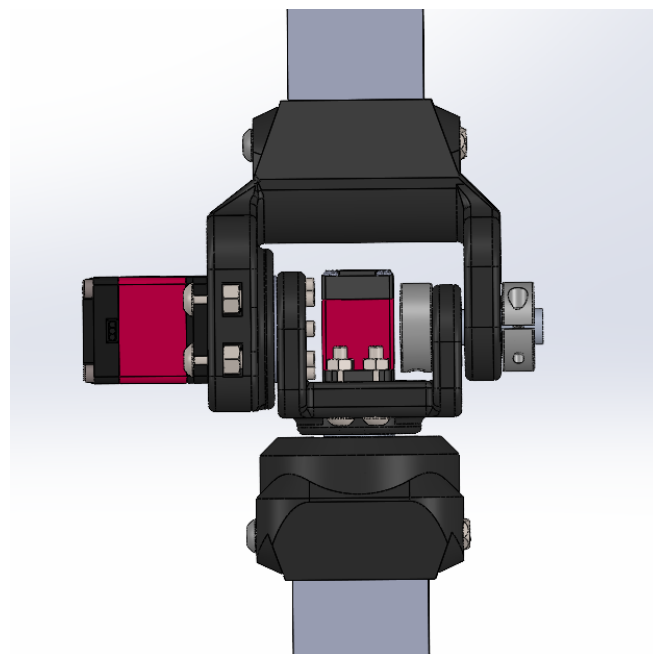


Figure 41: Top View of Elbow Joint

Note that the rotational axis of the left motor is placed higher than the box channel as seen in the isometric view. This allows the arm to reach around back toward the test stand like a human arm is able to do. In Figure 42 below, is the exploded view of the elbow joint assembly with all the parts labelled in Table 12.

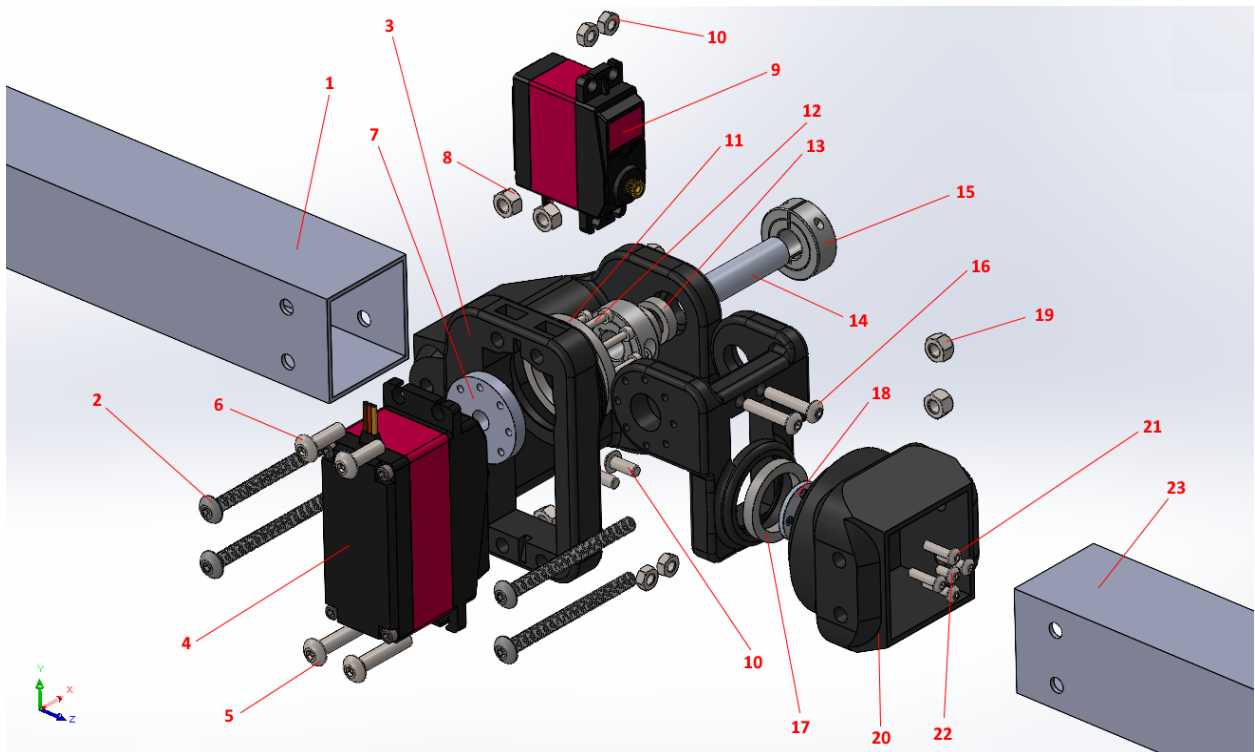


Figure 42: Exploded View of Elbow Joint

Table 12: Elbow Joint Parts

Part #	Part Name	Quantity
1	Upper Arm Box Channel	1
2	Button Head Hex Drive Screw	4
3	Upper Arm Bottom End-Cap	1
4	Servo 60 kg-cm	1
5	Socket Button Head Cap Screw (5 x 0.8 x 25 SBHCS)	2
6	Socket Button Head Cap Screw (5 x 0.8 x 16 SBHCS)	2
7	60kg Servo Horn	1
8	Hex Nut (M5 x 0.8)	4
9	Servo 20 kg-cm	1
10	Hex Nut (M4 x 0.7)	4
11	Joint 3 Bearing	1
12	Socket Head Cap Screw (2.5 x 0.45 x 12 Hex SHCS)	8
13	10x15x4mm Bearing	2
14	Joint 5 Shaft	1
15	Clamping Shaft Collar	2
16	Socket Button Head Cap Screw (4 x 0.7 x 20 SBHCS)	2
17	Joint 5 Bearing	1
18	Small Servo Horn	1
19	Torque Hex Nut (AM-M5-N)	4
20	Lower Arm Top End-Cap	1
21	Socket Button Head Cap Screw (3 x 0.5 x 12 SBHCS)	4
22	Socket Button Head Cap Screw (3 x 0.5 x 6 SBHCS)	1
23	Lower Arm Box Channel	1

The next and final design stage was the wrist and end effectors. Shown below in Figure 43, Figure 44, and Figure 45 are an isometric view, a side view of the wrist and an isometric view of the cutter end effector. The leftmost motor enables rotation of the wrist about the y-axis and the other motor allows the gripper to open and close in order to grasp and manipulate objects.

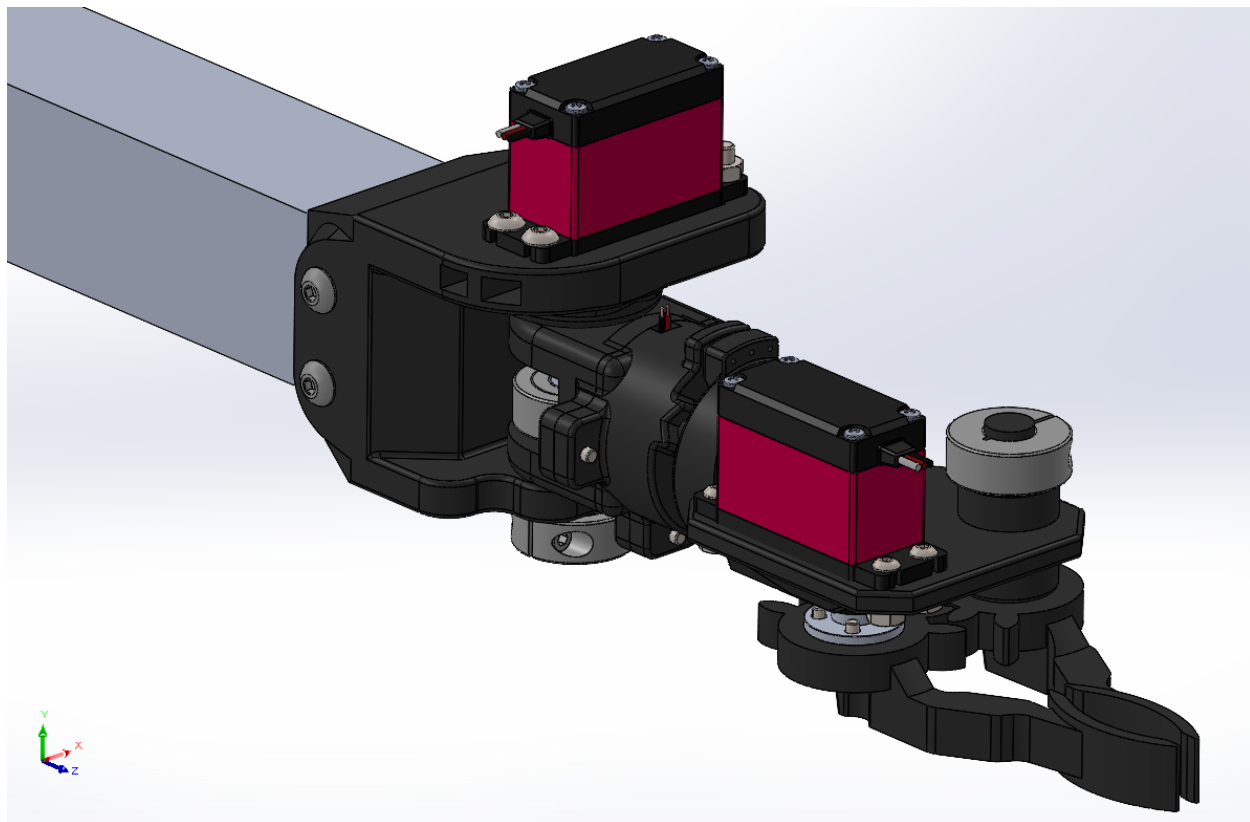


Figure 43: Isometric View of Wrist Joint with Gripper End Effector

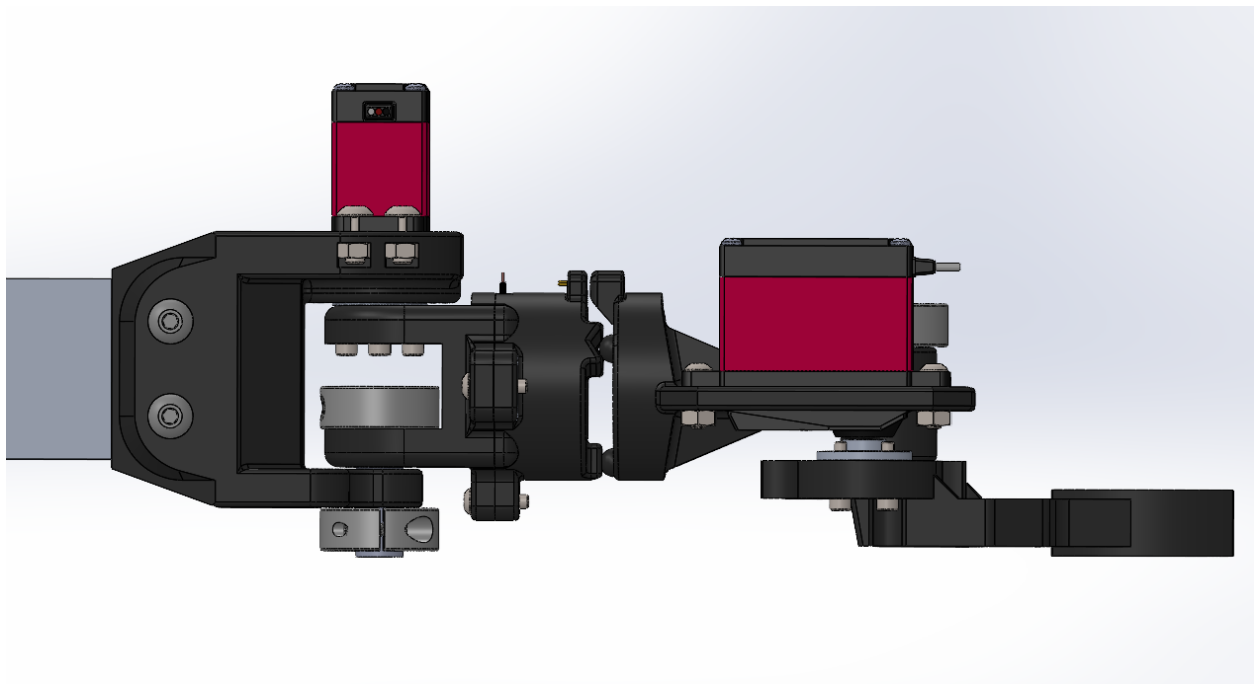


Figure 44: Side View of Wrist Joint with Gripper End Effector

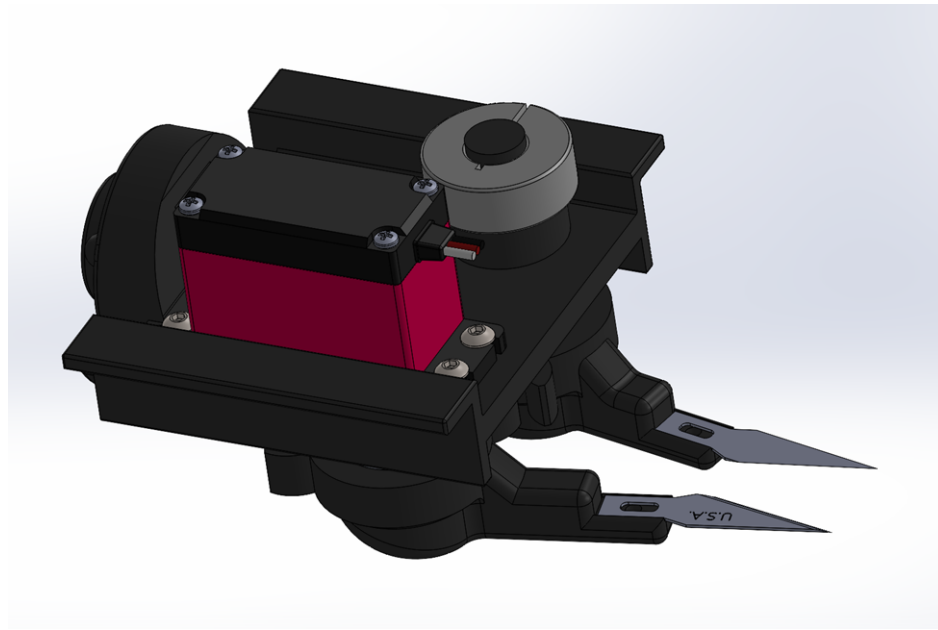


Figure 45: Isometric View of Cutter End Effector

Figure 46 shows an exploded view of the wrist followed by Table 13 containing all of the parts labelled with their respective part numbers, part names and quantities. A total of 49 parts are required for the assembly. In the exploded view, the electromagnet can be seen in the middle, and was not previously visible in the isometric and side views. The electromagnet is crucial in

enabling the swapping of end attachments as in when needed, while also still providing enough strength to hold the end attachments in place when in use.

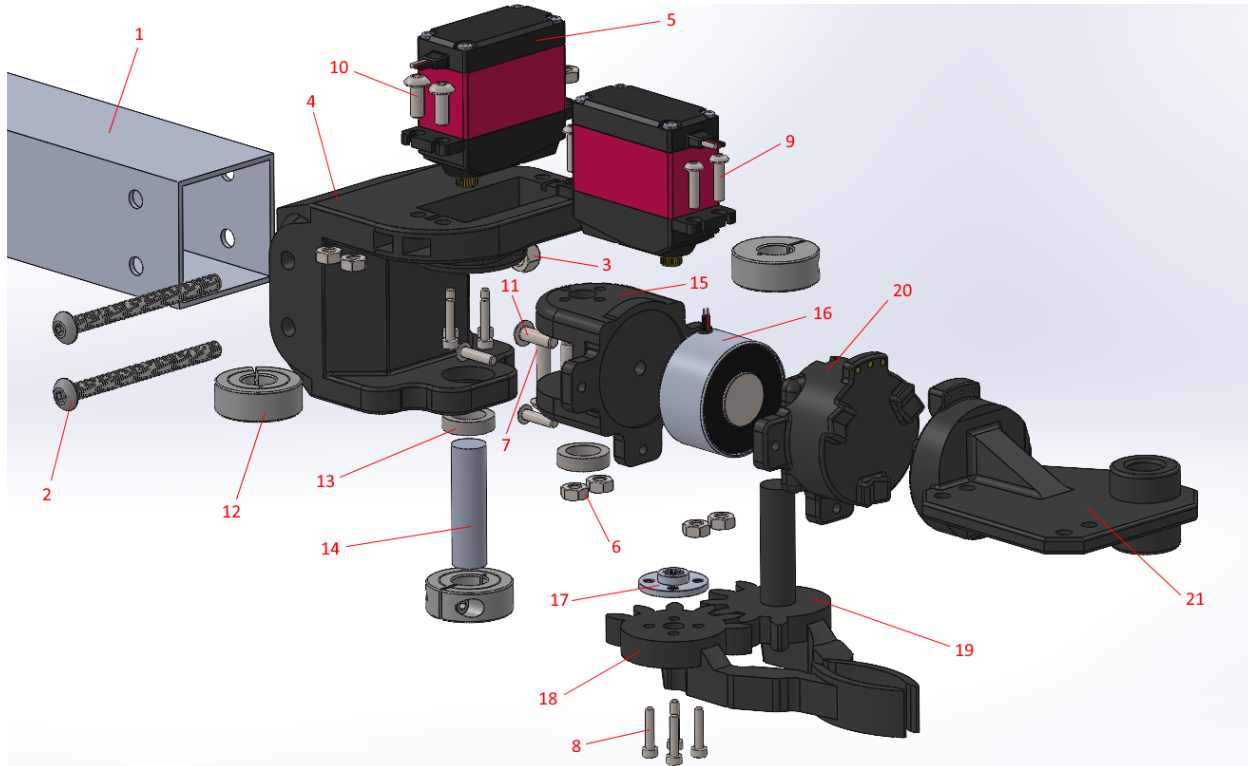


Figure 46: Exploded View of Wrist With Parts Labeled

Table 13: Wrist Joint Parts

Part #	Part Name	Quantity
1	Lower Arm Box Channel	1
2	Button Head Hex Drive Screw	2
3	Prevailing Torque Hex Nut	2
4	Lower Arm Bottom End Cap	1
5	Servo 20 kgcm	2
6	Hex Nut (M4 x 0.7)	8
7	Socket Button Head Cap Screw (4 x 0.7 x 20 SBHCS)	2
8	Socket Head Cap Screw (2.5 x 4.5 x 12 Hex SHCS)	8
9	Socket Button Head Cap Screw (3 x 0.5 x 12 SBHCS)	7

10	Socket Button Head Cap Screw (4 x 0.7 x 10 SBHCS)	2
11	Socket Button Head Cap Screw (4 x 0.7 x 12 SBHCS)	1
12	Clamping Shaft Collar	3
13	10x15x4mm Bearing	2
14	Joint 6 Shaft	1
15	Wrist	1
16	Electromagnet	1
17	Small Servo Horn	1
18	Gripper (Powered Half)	1
19	Gripper (Unpowered Half)	1
20	Wrist Cap	1
21	Gripper Casing	1

With all of the robotic arm design stages complete, a few minor changes were made to the stand to allow its full range of motion while still accommodating the end effectors. The final CAD design is shown below in Figure 47.

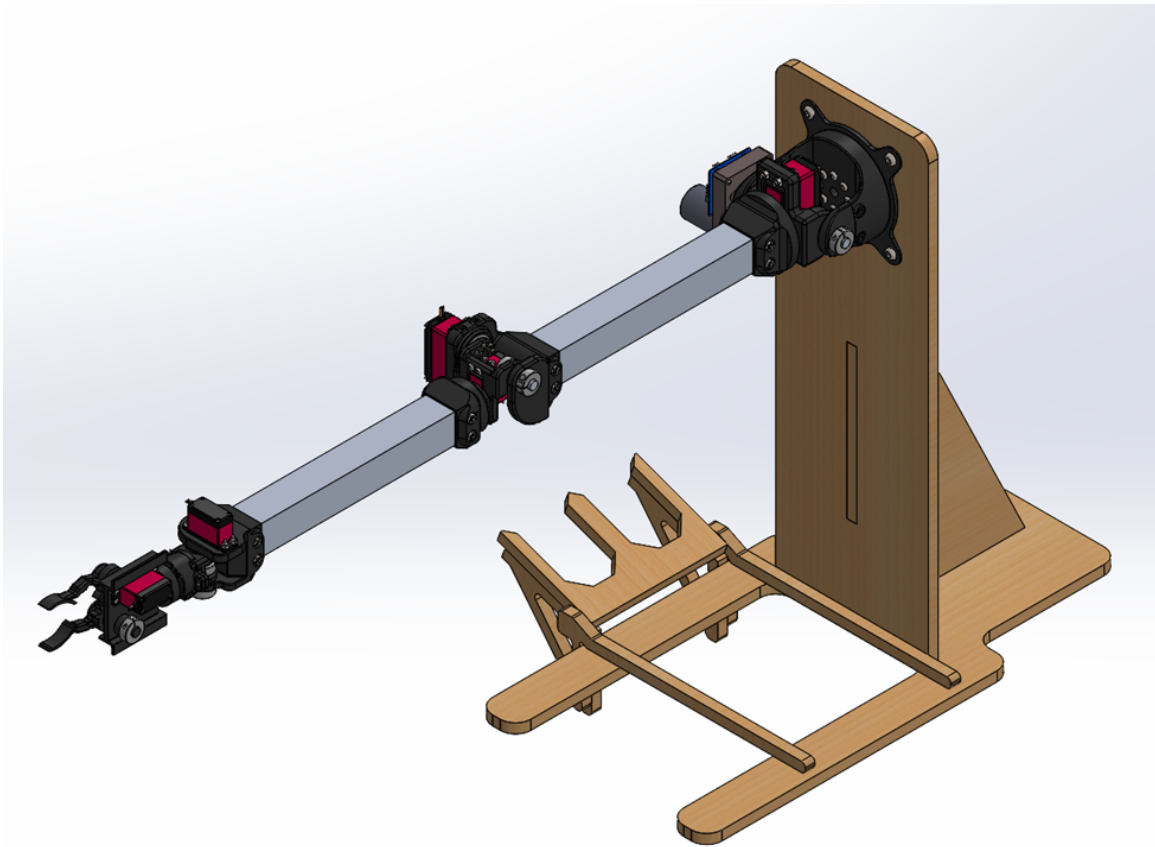


Figure 47: Final CAD Design of Robotic Arm

Parts Receiving

The robotic arm prototype required several commercial off-the-shelf (COTS) components such as motors, bearings, shafts, and aluminum stock. In order to streamline the purchasing process and ensure that purchased components arrived in a timely manner, the team made a point to source most of the COTS parts from Amazon. All of the electronics, motors, and bearings were purchased from Amazon, and McMaster-Carr was used to source some of the more specialized hardware components such as aluminum box channel and shaft collars. Most of the COTS components were partied out at the end of the Spring 2021 semester, and only minor edits were made to the Bill of Materials as the low-level design progressed. As such, almost all of the components were ordered within the first eight weeks of the Fall semester. This allowed the prototype construction to proceed unhindered. Figure 48 shows the first round of COTS parts that were purchased for this project.

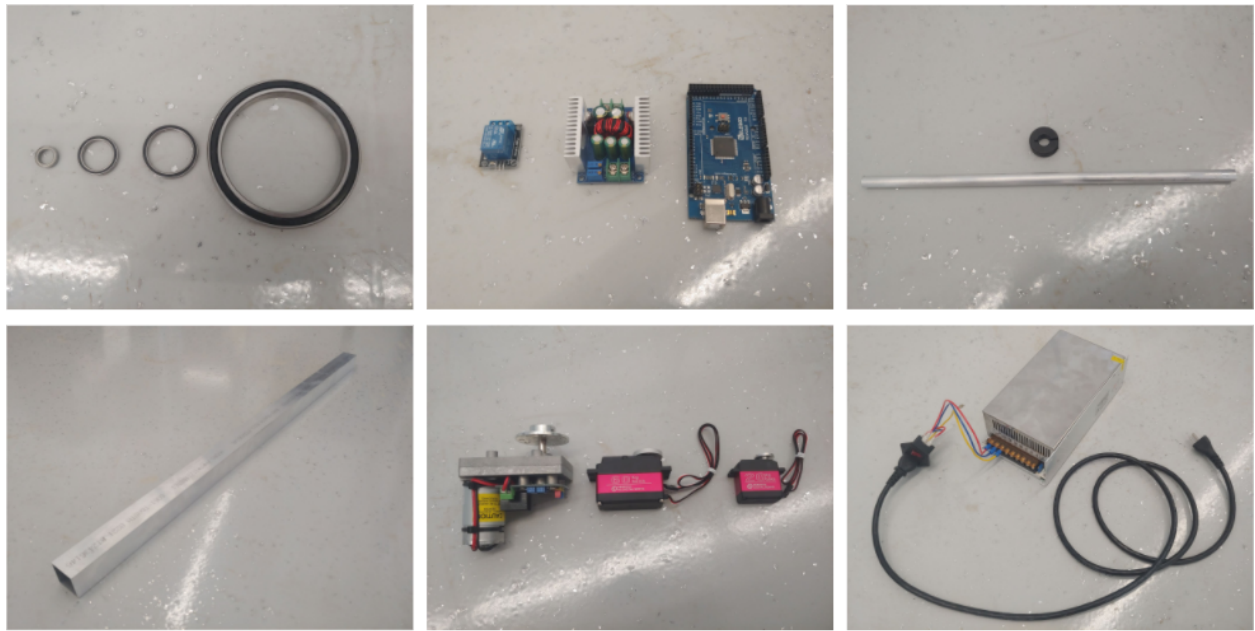


Figure 48: Initial round of purchase orders for off-the-shelf components (duplicates omitted)

The top left image in Figure 48 depicts the various sizes of bearings that support each joint and take some of the radial load off of the motor horns. The top middle image shows the three main electronics modules: the Arduino Mega (right) communicates with the joint group controller on the laptop and sends motor control signals, the buck converters (middle) regulates the 24V power supply down to voltages that are usable by the medium and small motors, and the relay module (left) allows the Arduino to switch the 24V power going to the electromagnet. The Arduino Mega was chosen over other Arduino variants because most other controllers do not have enough PWM pins to support 7 servo motors simultaneously. The top right image shows a shaft collar and an aluminum shaft, which are used to further support the joints. The bottom left image depicts the aluminum box channel, which makes up the upper and lower arm segments of the robot. The bottom middle image shows the three different types of motors and their associated servo horns. The large motors (left) are used for joints 1 and 2, the medium motors (middle) are used for joints 3 and 4, and the small motors (right) are used for joints 5 and 6, as well as for the end effectors. The bottom right image shows the AC-DC converter that accepts 120 V_{AC} wall power and converts it to 24V_{DC} to feed into the rest of the system.

A few weeks after all of the above items were received, a final purchase order was made for the components shown below in Figure 49. These items include the electromagnet and supplies for wiring and wire management.



Figure 49: The final major components of the prototype that were purchased

Assembly Overview

The robotic arm was assembled from the base to the wrist in a mostly linear fashion. The tight component placement required a very specific order of assembly at each of the joints, but there were no major hurdles to the assembly process when this order was followed. The assembly took place over the course of several weeks in the ECG eSpaces during their daily open project hours. All of the test stand components were machined out of MDF using a CNC router, and all of the custom joint components were 3D printed out of ABS on a Stratasys Mojo desktop 3D printer at the FSE 3D Print and Laser Cutter lab. The team had initially intended to use nylon as the primary material for the printed components, but ABS was ultimately chosen because the nylon parts kept warping during the printing process. While not as tough as nylon, ABS is stiffer and more temperature stable, so the group decided it would be a usable substitute.

In general, the assembly process took place in stages. The required parts for each stage were manufactured a few days before each assembly meeting so that components could be test-fit. Some of the 3D printed parts underwent a few design revisions to ensure that they bolted to the motors snugly because of this testing. As seen in Figure 50 below, the first stage of the assembly process revolved around the test stand for the arm.

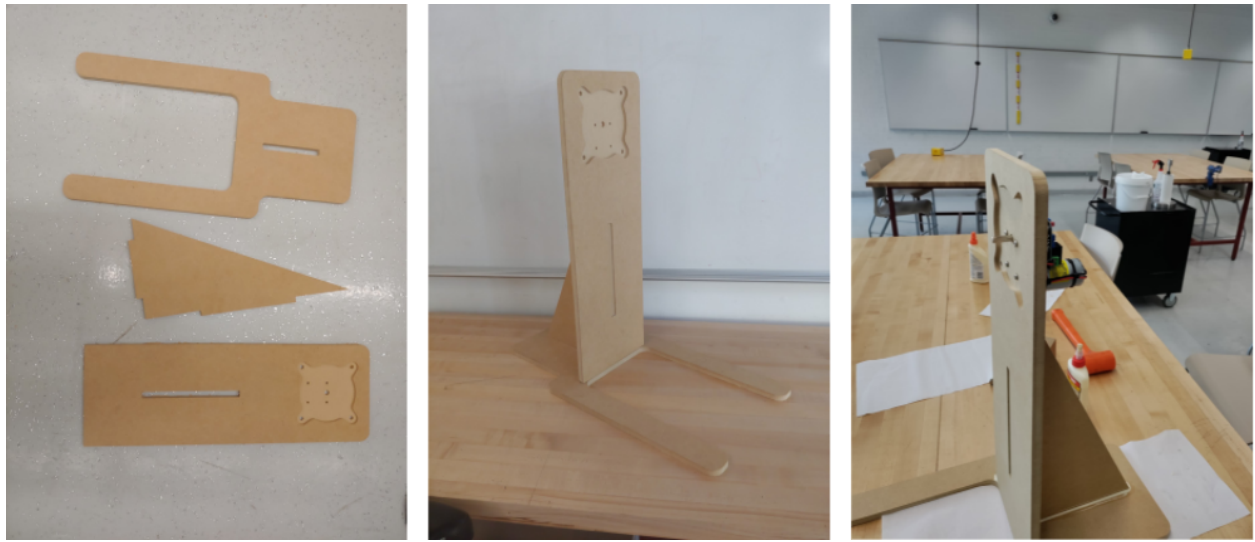


Figure 50: Assembly process for test stand

The test stand is composed of three main MDF components (seen on the left in the above image) that were cut out on a CNC router. These pieces simply slot together, and their connections were made permanent by using wood glue and clamps. This resulted in the assembly seen in the center of Figure 50. On the right, the joint 1 motor has been attached to the stand to prepare for mounting the shoulder assembly.

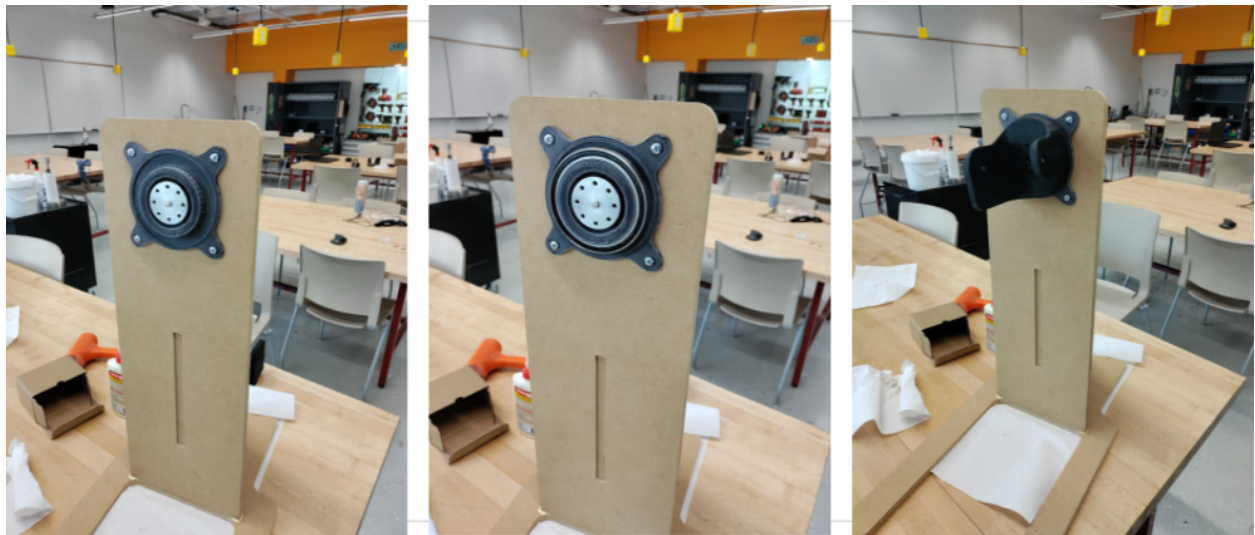


Figure 51: Attaching the base pivot mount and the turntable

Figure 51 shows the first steps of the shoulder assembly process. As seen in the left image, the base pivot mount was bolted into the routed pocket on the test stand, and the joint 1 servo horn was attached. The center image shows the large turntable bearing press-fit onto the pivot mount,

and the right image shows the turntable pressed onto this bearing and bolted to the joint 1 servo horn. This assembly supports the weight of the rest of the robot arm.

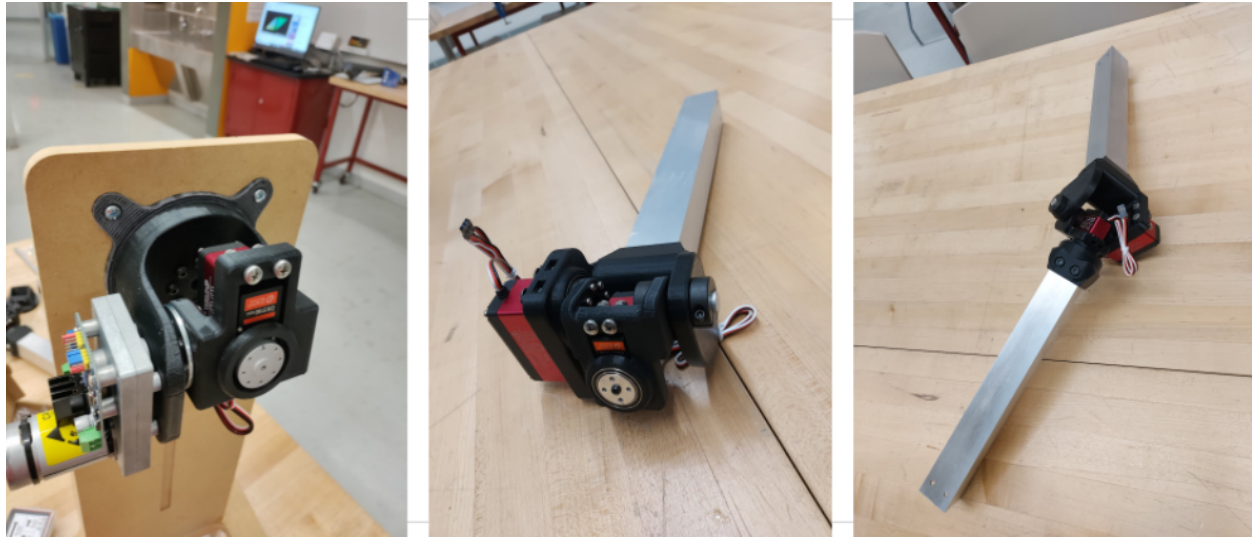


Figure 52: Finishing the shoulder and elbow assemblies

The left image in Figure 52 depicts the final steps of constructing the shoulder assembly. The large joint 2 motor was mounted to the side of the turntable, followed by the joint 3 bracket and its associated medium servo motor, horn, and bearing. The rest of the arm assembly attaches to the light gray joint 3 servo horn seen in the center of the left image. This concluded the 3-DOF shoulder assembly.

The elbow joints and their respective aluminum box channel segments were assembled apart from the rest of the robot. The center image of Figure 52 shows the 2 joints that make up the elbow, with a medium motor for joint 4 and a small motor for joint 5. This assembly is bolted to the upper arm segment, and in the right image it is bolted to the lower arm segment as well, forming a separate 2-DOF subassembly that can then be mounted to the rest of the robot.

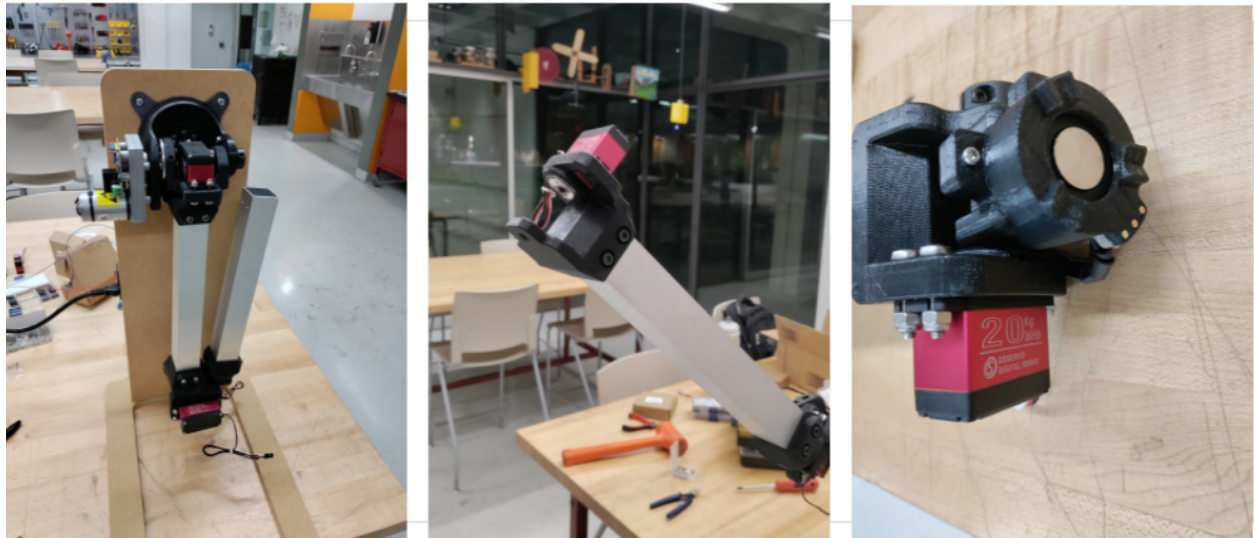


Figure 53: Mounting the elbow assembly and constructing the wrist

The left image in Figure 53 shows the previously assembled elbow joints and their associated box channel segments mounted to the shoulder assembly. This grouping makes up 5 of the 6 degrees of freedom on the robot (excluding the grippers). The wrist joint was then attached to the end of the upper arm segment with a small servo motor, as seen in the center image above. The right image shows the electromagnet and brass-colored pogo pin contacts assembled into the final permanent link of the manipulator. The electromagnet cap also contains the divot-side kinematic coupling geometry that allows the end effectors to index to the wrist consistently during a tool change. This marks the mechanical completion of the main structure of the robot arm.

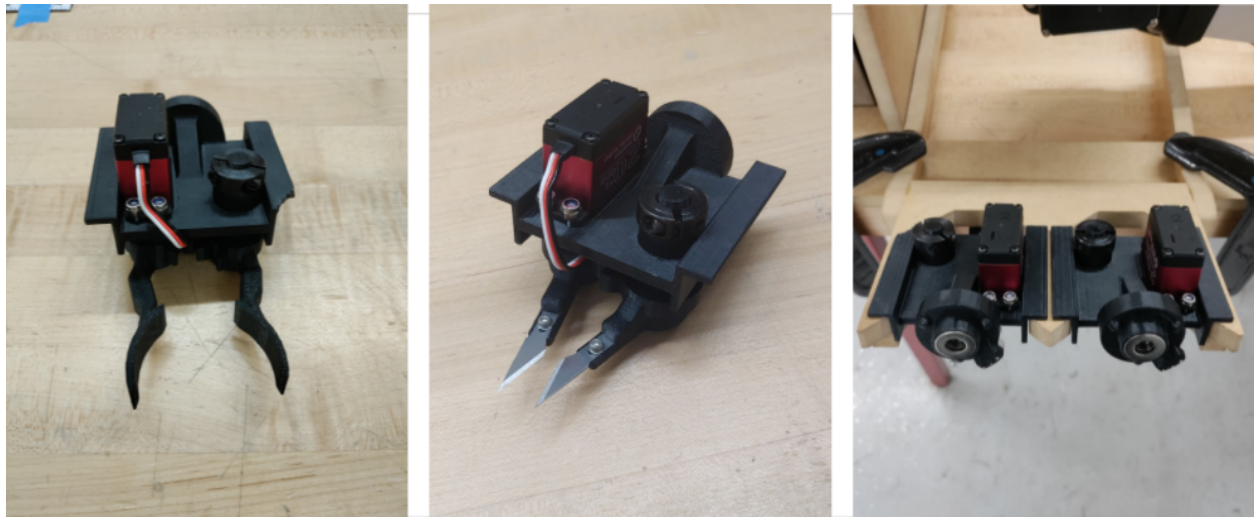


Figure 54: Assembling the 2 swappable end effectors and the tool holder

The left image in Figure 54 shows the grabber end effector, while the center image shows the cutter end effector. The two assemblies use an identical body structure. A small servo motor powers one of the moving arms, and the other arm is passively constrained to rotate equally in the opposite direction through a set of spur gear teeth modeled into the arms themselves. The moving arms are very similar as well except for at the extremities; the gripper version has a contoured grabbing surface while the cutting version allows an Xacto blade to be mounted. The right image of Figure 54 shows both of the grippers placed into the tool rack. From this perspective, the permanent ring magnets, brass pogo pins, and ball-side kinematic coupling geometry are visible. The tool rack is made of MDF and its components were routed on the CNC router and wood glued together. It is simply clamped to the arm's stand using table clamps. After the mechanical assembly of the robotic arm was finished, the team moved on to the electrical wiring. Figure 55 below shows the final state of the wiring at the rear and front of the robot arm.

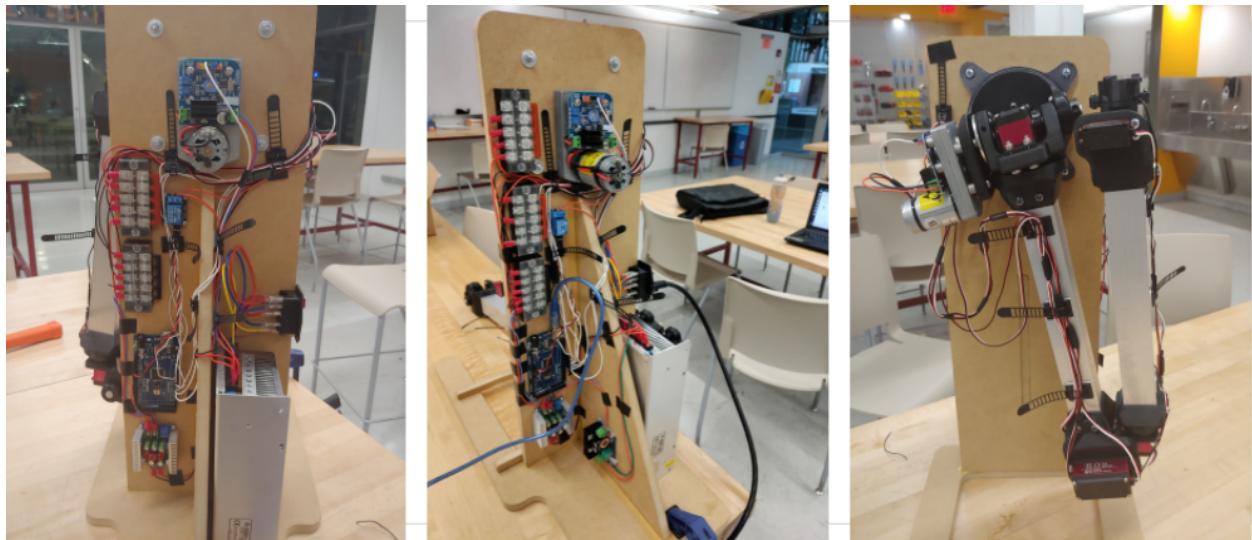


Figure 55: Completed electrical wiring for the robotic arm

The left and center images in the above figure show two different perspectives of the rear of the test stand after the wiring was completed. Although a production machine would certainly take care to cover up as much of the exposed wiring as possible, both for safety and aesthetic reasons, the team did not consider this to be a worthwhile endeavor for a prototype because the focus was on the mechanical design and the controls. As such, the wiring is exposed, although all live points of contact are either insulated or covered in protective housings, meaning that there is very little risk of accidentally damaging the system.

All of the medium and small motor wiring connects to the motors via servo connectors, and it connects to the regulated positive and negative bus bars via ring terminals. The large motor wiring connects to the attached control boards with screw terminals, and it connects directly to the output of the 24V power supply. The motor control wires connect to the Arduino Mega with Dupont connectors. The wiring is secured to the frame using a combination of electrical tape and wire straps.

The right image in Figure 58 shows the front of the robotic arm system, with the arm folded up in a storage position. The wiring can be seen running down the lengths of the upper and lower arm segments and is attached with wire straps. This wiring is given a loop of slack at the elbow and shoulder joints in order to allow those joints to move freely without pinching or breaking the wiring. These wiring loops are wrapped in a protective plastic spiral wrap (not shown in the figure above but visible later in Figure 61).

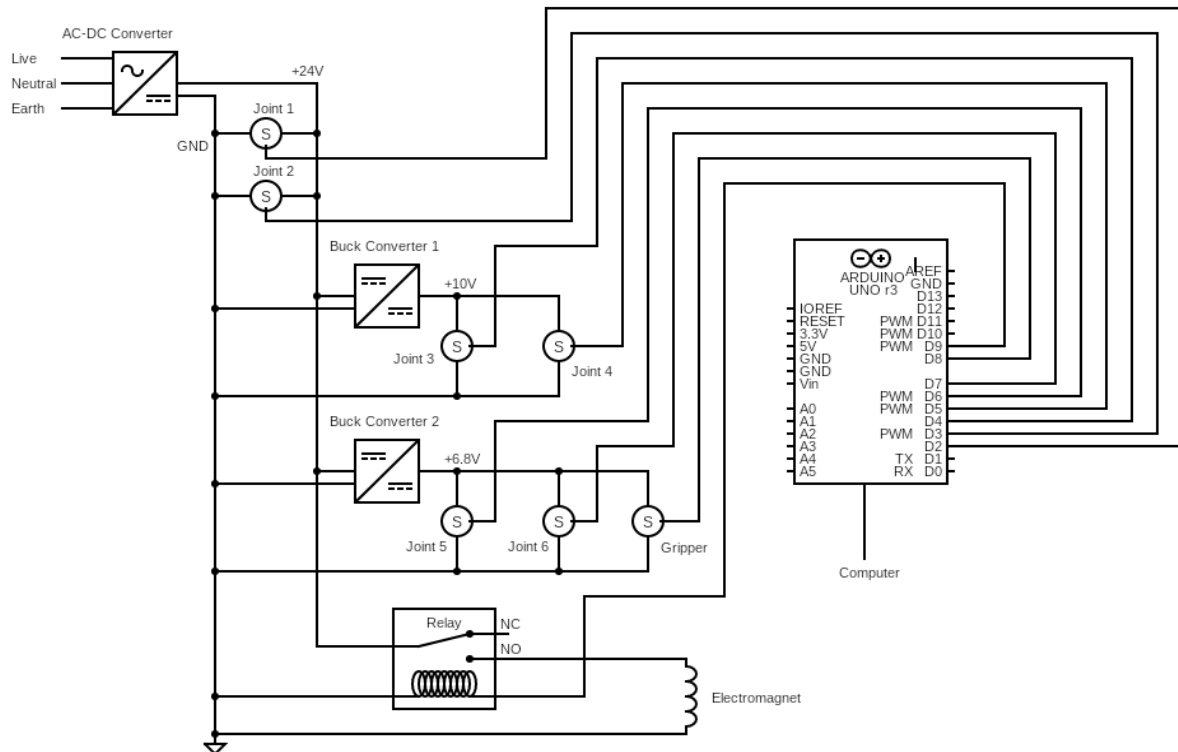


Figure 56: Electrical diagram

The full electrical diagram for the robotic arm system is shown above in Figure 56. Power enters the system from the wall outlet at $120V_{AC}$. The AC-DC converter reduces and rectifies this voltage to $24V_{DC}$. This voltage is fed directly into the large motors powering joints 1 and 2. It also connects to the relay, which acts like a switch that the Arduino can use to energize the

electromagnet to 24V at will. The 24V is also fed into two DC-DC buck converters. One of these converters regulates the voltage down to 10V and powers the medium servos of joints 3 and 4. The other converter regulates down to 6.8V and powers the small servos of joint 5, joint6, and the end effector. Two buck converters are desirable because the medium servos are able to tolerate a higher voltage than the small servos, and the design requires that the medium motors operate near the maximum power they are able to. Each of these servo motors has a control wire that is routed to a PWM pin on the Arduino Mega (note that the electrical diagram depicts an Arduino Uno in order to conserve space). The Arduino then connects to the common ground of the entire circuit so that its command signals will not float, it connects to a computer to receive joint control messages from the control system.

Control System Update

Overview

To control the robot the system in Figure 57 was designed. In this system all inputs are received from the user through a Unity program running on the Oculus VR headset. These inputs are then sent by the VR program to a Unity desktop application. The data is sent through a Photon server. Using this kind of server allows for the user to be connected to the system from anywhere in the world as long as they maintain an internet connection. Once received the desktop application performs operations on the data, packages it, and then sends it to the ROS server. To accomplish this a Unity library called ROS# is used to package the data and a RosBridge web server connection is used to send the data to ROS. Once in ROS, a custom listener script time stamps the data to align the machine clocks. This data is then published to a topic where it is ready to be used by the controller. The controller that is used for the real time inverse kinematics is a combination of MoveIt, Gazebo, and a ROS library called Real Time Servoing. This process outputs joint angles to a topic which is then subscribed to by the Arduino on the robot. The Arduino receives this data through a serial connection with the computer and publishes the joint angles to each corresponding servo.

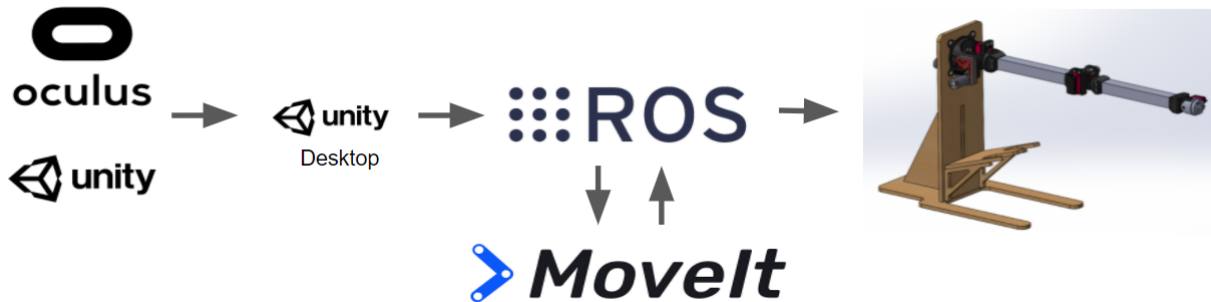


Figure 57: Control System Outline

Oculus Headset

The Unity application on the Oculus headset was designed to receive four different user inputs. The main input from the user was the active tracking of all six degrees of freedom of the VR controller. The hand trigger on the controller acted as a clutch by only allowing for pose data to be relayed to ROS when the trigger was held down. This allowed the user to control when they wanted the software to track their hand movement. Next the main controller trigger acted as a toggle for the end effector activation. When the trigger was pressed the end effector would be commanded to activate and upon releasing the trigger the end effector would be commanded to deactivate. Finally, the A button acted as a toggle for the equipped end effector module. By pressing this button control of the robot was lost and the robot would instead enter a preplanned set of motions to swap the attached end effector module. No operations were performed on these user inputs while the data remained on the Oculus headset. Instead all of the data was sent through a Photon server to the Unity desktop application.

Desktop Application

Once the data was received from the Photon server, many different operations were performed. First, in order for ROS to receive the position data it needed to be sent as a TwistStamped message. This type of message is a collection of three linear velocities, three angular velocities, and a header which includes information on the data ordering.

To find the linear velocities the position information was numerically integrated. The rotational velocities were more complicated since Unity saves all rotational information in terms of quaternions. When these quaternions are converted to euler angles some velocity information for certain axes is lost. To overcome this, the quaternion from the pose data was used to calculate a difference quaternion. From this an axis-angle representation of the quaternion could be found

and broken down into its components. These difference angles were then divided by the time difference between frames to find the angular velocities. This process ensured that all rotations were taken with reference to the world frame as desired and not the local frame.

Additionally, this program was responsible for handling the clutch logic for the hand trigger data passed from the VR headset. If the trigger was held down, the TwistStamped message was sent to ROS; if not, the data was withheld. This program also packaged the trigger and A button toggle data and passed this to the unityButtonChatter ROS topic. All of the data packaging was set up using the ROS# Unity library and sent to ROS using a RosBridge server.

ROS

Once the TwistStamped message was sent to ROS, a custom listener script made slight adjustments to the message. For the data to be used in real time the message needed to be time stamped. Since the ROS server runs on a virtual machine and the Unity application runs on the desktop itself there are discrepancies in the time stamp. This script compensated for this by restamping the data with the virtual machine time. The script then republished the message to the input topic for the control loop.

Real Time Servoing

To accomplish real time inverse kinematics, a ROS library called Real Time Servoing was implemented alongside MoveIt and Gazebo. To set up this system the program would first be launched using a joint trajectory controller. This was used to plan and execute the simulated robot arm to the correct starting configuration as seen in Figure 58. The controller was then switched to a joint group position controller. This controller read from the input topic where the TwistStamped data was published by the listener script and performed inverse kinematics. This resulted in each joint angle being outputted to an output topic by the controller and the resulting simulation can be seen in the simulation tracking video seen in references.

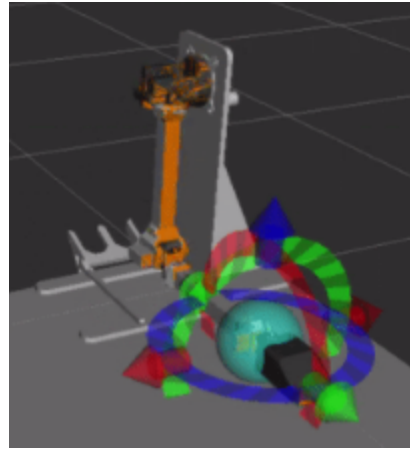


Figure 58: Rvis Robot Simulation

Arduino

The output topic, created by the controller, was subscribed to by the Arduino on the robot through a serial connection. The joint angles in this topic were then taken and assigned to their corresponding servos as the topic was updated. The arduino also subscribed to the unityButtonChatter topic that Unity originally published the button information to. The Arduino handled the logic for both activating the module swapping and the end effector. The preplaned paths for module swapping were manually programed into the Arduino script using preset joint angles and timers. When the signal was sent that the A button on the controller was pressed the path routine would run. Ultimately once completed the arm returned to it's starting position with the new end effector module.

Budget Analysis

The team has successfully built a robotic arm within the \$700 budget provided at the start of this project. Much of the money was dedicated towards the electronics of the robotic arm and any servo motors and accessories needed. In Table 2 it shows the parts that have been purchased, or yet to be purchased. This table shows estimated values of our total project costs, along with an estimated leftover budget. This table does not account for tax or any shipping and handling costs from any purchases made.

Table 2: Updated Bill of Materials

Item	Link	Unit Cost	Quantity	Subtotal	Notes	Ordered?	Total:	\$650.18	Remaining:	\$49.82
High Torque Robot Servo	https://www.amegastore.com	\$67.99	2	\$135.98	170 kg*cm @ 24V, for joints 1+2	<input checked="" type="checkbox"/>				
60kg Servo	https://www.amegastore.com	\$36.98	2	\$73.96	65 kg*cm @ 7.4V, for joints 3+4	<input checked="" type="checkbox"/>				
20kg Servo	https://www.amegastore.com	\$28.99	2	\$57.98	21.5 kg*cm @ 6.8V, 2-pack, for joints 5+6 and 2 end effectors	<input checked="" type="checkbox"/>				
20kg Servo Horns	https://www.amegastore.com	\$11.99	1	\$11.99	25T, 10-pack	<input checked="" type="checkbox"/>				
60kg Servo Horn	https://usa.banggood.com	\$6.99	2	\$13.98	18T, 1 each	<input checked="" type="checkbox"/>				
Aluminum Rod	https://www.mcr.com	\$2.64	1	\$2.64	10mm x 1 ft, for joint shafts	<input checked="" type="checkbox"/>				
Bearings	https://www.amegastore.com	\$7.99	1	\$7.99	10 x 15 x 4mm, for joints 2,4	<input checked="" type="checkbox"/>				
Bearing	https://www.amegastore.com	\$15.39	1	\$15.39	80 x 100 x 10mm, for turntable	<input checked="" type="checkbox"/>				
Bearing	https://www.amegastore.com	\$9.99	1	\$9.99	30 x 37 x 4mm, for joints 3,4	<input checked="" type="checkbox"/>				
Bearing	https://www.amegastore.com	\$9.79	1	\$9.79	20 x 27 x 4mm, for joint 5	<input checked="" type="checkbox"/>				
Shaft Collar	https://www.mcr.com	\$7.58	6	\$45.48	10mm bore, for joint 2	<input checked="" type="checkbox"/>				
Power Supply	https://www.amegastore.com	\$45.99	1	\$45.99	24V 25A	<input checked="" type="checkbox"/>				
Buck Converter	https://www.amegastore.com	\$14.79	1	\$14.79	300W, 20A output	<input checked="" type="checkbox"/>				
Power Socket w/ Switch	https://www.amegastore.com	\$8.99	1	\$8.99	10A @ 120VAC	<input checked="" type="checkbox"/>				
IEC Power Cord	https://www.amegastore.com	\$6.79	1	\$6.79		<input checked="" type="checkbox"/>				
Arduino Mega	https://www.amegastore.com	\$15.99	1	\$15.99		<input checked="" type="checkbox"/>				
5V Relay Module	https://www.amegastore.com	\$5.50	1	\$5.50	for controlling the electromagnet	<input checked="" type="checkbox"/>				
Aluminum Square Tubing	https://www.mcr.com	\$14.36	1	\$14.36	1-1/2" x 3ft	<input checked="" type="checkbox"/>				
Alloy 910 Filament	https://www.makergear.com	\$80.00	0	\$0.00	Nylon, 1 kg, 2.85mm, for motor / shaft mounts, free to us through FSE 3D Print Lab	<input checked="" type="checkbox"/>				
Magnetic Connector	https://www.amegastore.com	\$14.50	2	\$29.00	For passing power to end effector servos	<input type="checkbox"/>				
Electromagnet	https://www.amegastore.com	\$10.99	1	\$10.99	180N @ 24V	<input checked="" type="checkbox"/>				
Servo Cables	https://www.amegastore.com	\$13.99	1	\$13.99	For wiring up the motors	<input checked="" type="checkbox"/>				
Copper Strips	https://www.amegastore.com	\$7.98	1	\$7.98		<input checked="" type="checkbox"/>				
Pogo Pins	https://www.amegastore.com	\$11.52	1	\$11.52		<input checked="" type="checkbox"/>				
Cable Straps	https://www.amegastore.com	\$10.98	1	\$10.98		<input checked="" type="checkbox"/>				
Metric Hardware Kit	https://www.amegastore.com	\$28.09	4	\$28.09		<input type="checkbox"/>				
MDF Wood Sheet	https://www.homecenter.com	\$39.45	1	\$39.45	1/2" x 48" x 96", for test stand / electronics panel	<input checked="" type="checkbox"/>				

A breakdown of the spent budget was created using an updated receipt chart from the SEMTE Business office. This receipt chart can be found in the Appendix section A1. This receipt accounts for any tax and/or shipping and handling from all purchases made. The breakdown of how the budget was spent is seen in Figure 59. The chart breaks down the budget based on the component category and any leftover funds out of the \$700. This chart shows that almost half of our budget has been dedicated to servo motors and accessories.

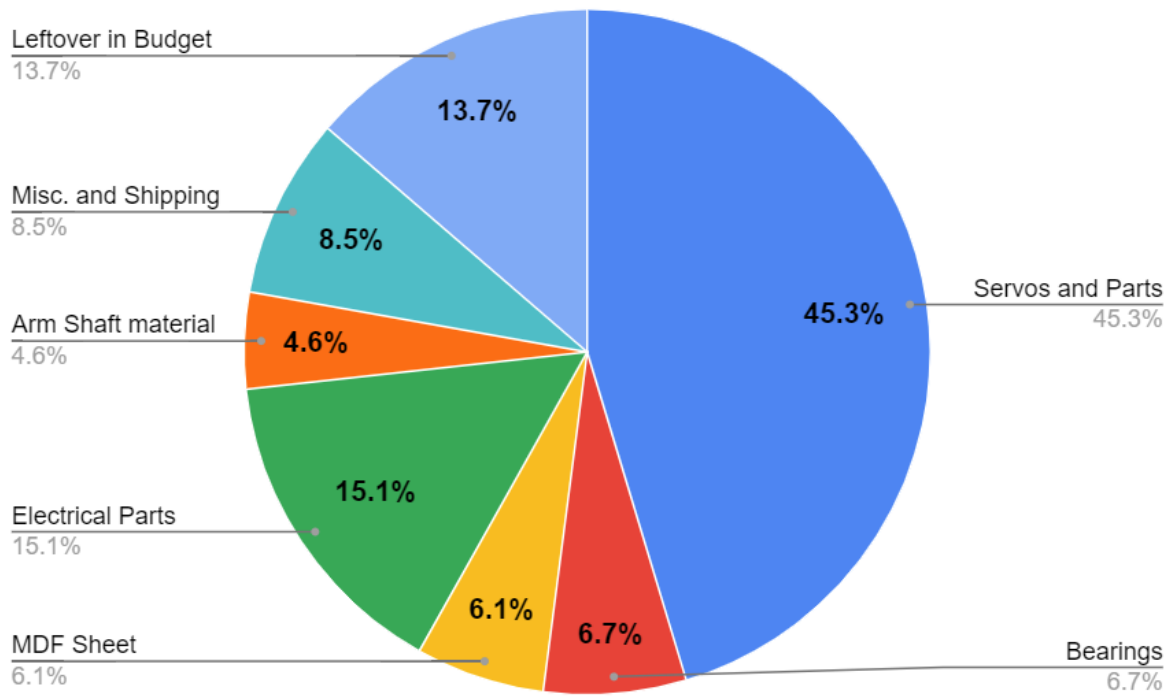


Figure 59: Budget breakdown for different component categories

Full Assembly Testing

A series of tests were performed. YouTube video links of each demonstration are available in the References section of the report. In the first test, commands were issued to the servo motors to demonstrate individual operability of the motors as well as sufficient strength to hold up and move the arm. An image from that demonstration is shown.

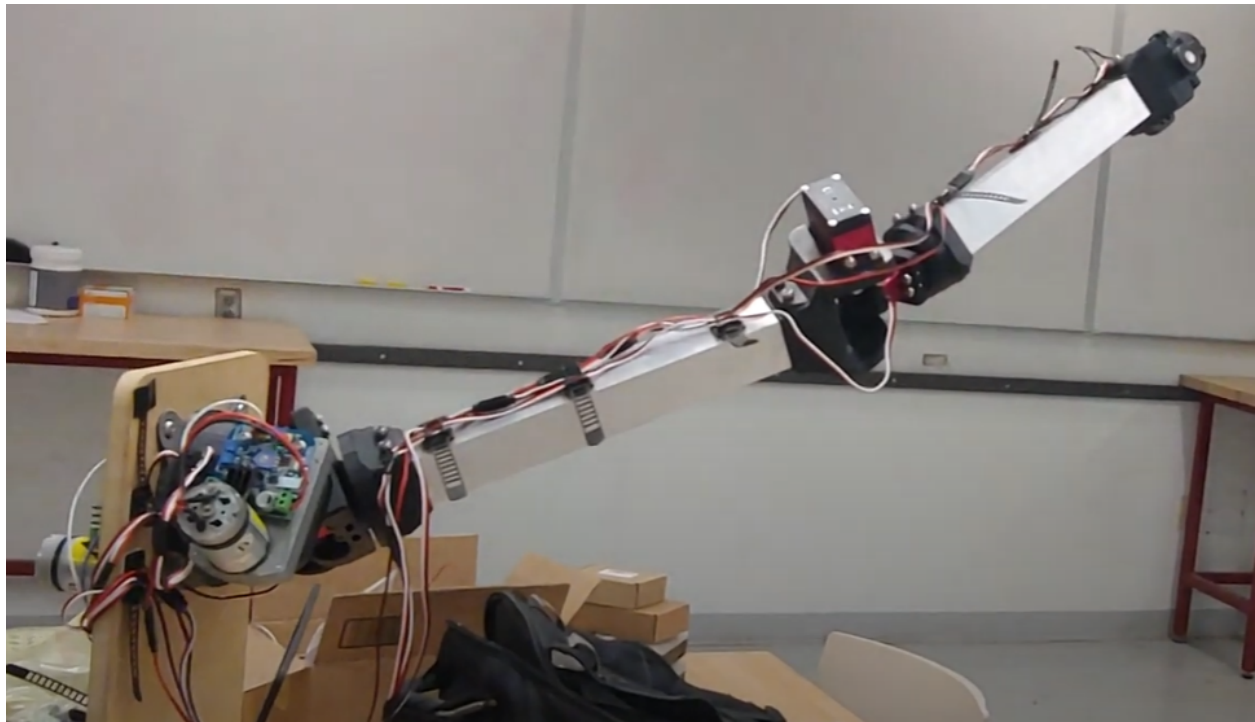


Figure 60: Still picture from joint-by-joint demonstration video

In the next test, control of the arm with a VR controller was demonstrated. The operator successfully picked up a cardboard box with the gripper attachment and dropped it in the hand of a group member.

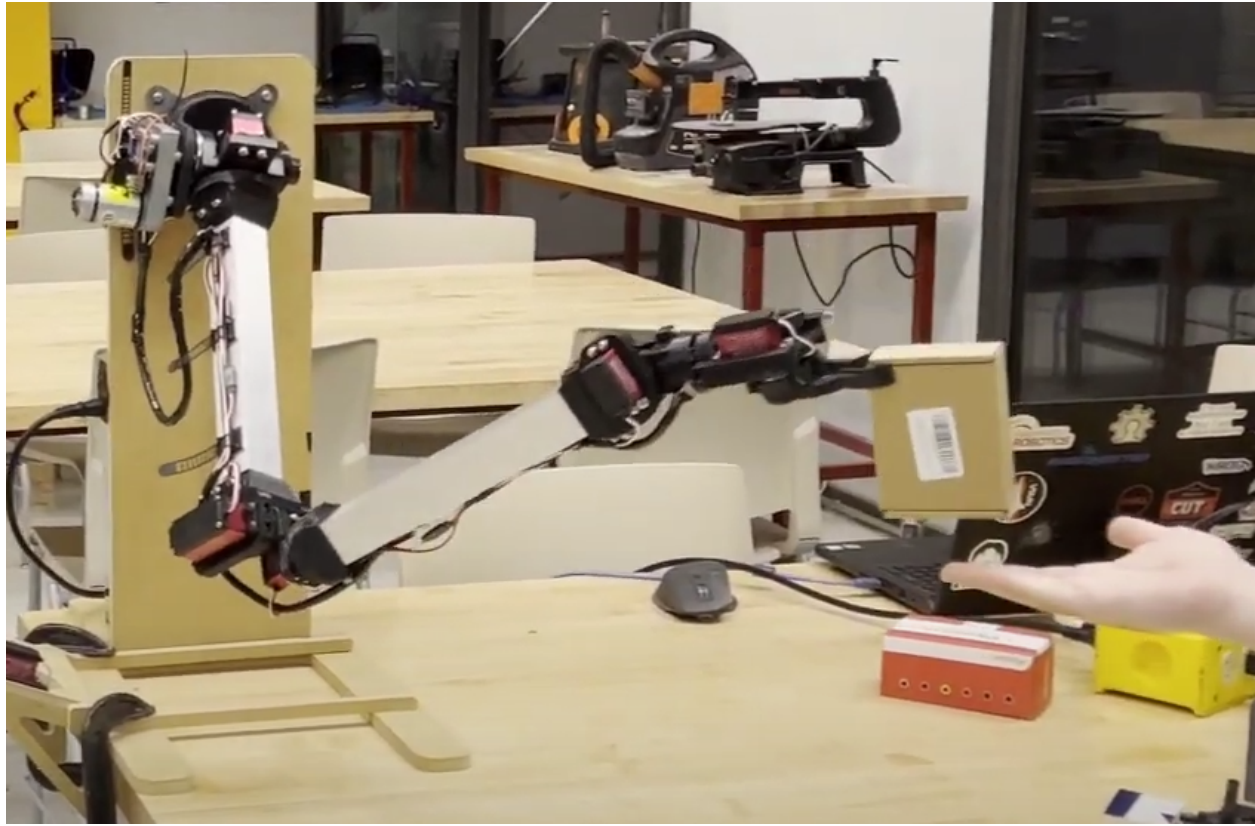


Figure 61: Still picture from VR control demonstration video

Lastly, a video was created of the arm's tool changing routine. The arm is programmed to enter the tool changing routine at the press of a button by the operator. This program keeps track of which attachment is currently on the arm. When commanded, the arm will place the current end effector in the tool rack and mate with the other end effector which is waiting for it in the other tool rack slot.

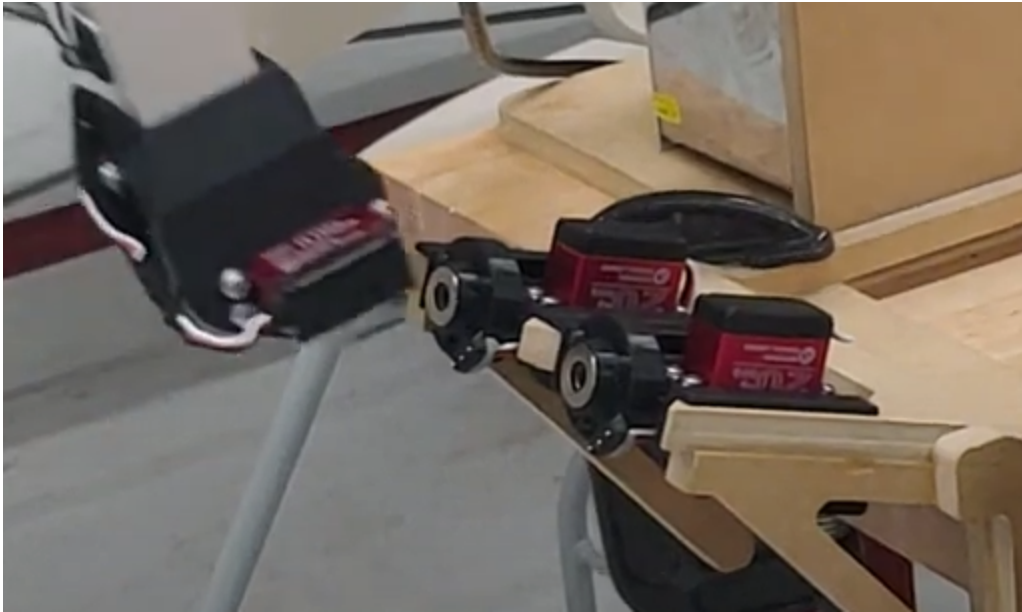


Figure 62: Still picture from tool change demonstration video

Further, the group performed a test of various arm movement speeds: the standard speed which has been used for all pre-programmed movements as well as a slower and faster speed. The faster speed qualitatively had more oscillations, but these seem to be due to backlash in the motors (the ability of the output axle to move without encountering resistance from the electromechanical system) as well as possibly a need to strengthen the materials of the arm's shoulder. This video, like all of the others, is available in the References section.

Finally, the group performed a movement repeatability test. There is no practical way to correspond a sense of absolute position in ROS to position in the real world. However, the human operator moves the VR controller while looking at the robotic arm as a feedback loop; so, this should not be an issue anyway. The group tested moving back and forth between two pre-programmed positions and measured the horizontal position to gauge repeatability. With measurement resolution of $\frac{1}{8}$ ", the two positions had a standard deviation of 0.133" and 0.044" in eight back-and-forth motions.

Challenges Faced

Moving on to some of the challenges that were faced, there were both structural issues with certain components, and issues with the controls of the arm. The shoulder joint had snapped due to the over tightening of screws, as seen in the picture below. The quality of the 3D print as well as the direction in which the fibers were printed, may have also had an effect on the shoulder

joints' resistance to transverse loads. To counter this issue, spare shoulder joints were 3D printed with different fiber orientations. Having spares meant that any faulty shoulder joints could be replaced quickly without causing further delays in testing.

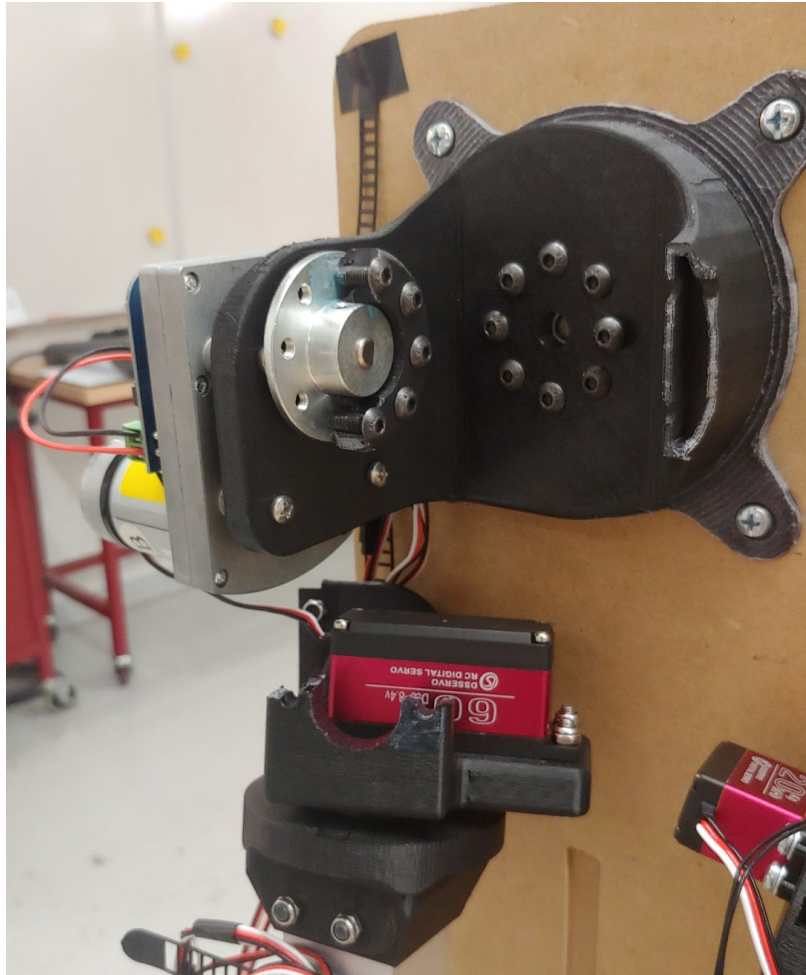


Figure 63: Shoulder joint failure along the 3D-printed layer lines

In the initial design stage, there wasn't much clarity about which specific motors would be used at each joint and what their dimensions would be. As the project progressed to the build stage where the design was updated, it became clear as to what motor requirements were. It is at this stage it became apparent that one of the initial design constraints (the arm not exceeding 12-cm in diameter) would have to be abandoned because of the size of the motors. This is illustrated in the picture below, where the red cylinder represents the area within which the entirety of the arm is supposed to fit.

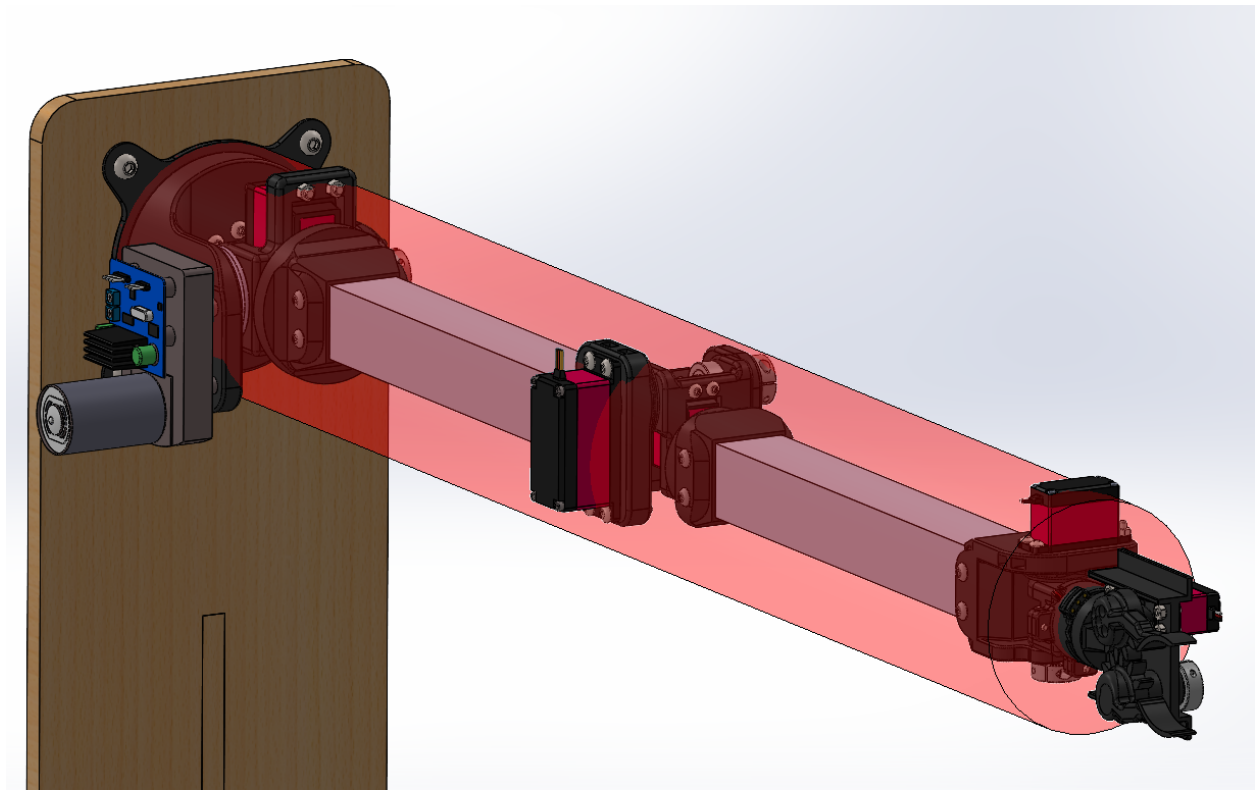


Figure 64: Diameter constraint of the arm

Moving on to issues with the controls, there were initially issues with smoothing the joint motions. The smoothing filter for the motor commands ended up adding delay and wobble because of conflict with smoothing that MoveIt was trying to do by default. The sensitivity of the large motors was also turned down via a potentiometer on the control board, thus reducing the oscillations in those joints. There were also problems with getting Unity to talk to MoveIt as the communications setup in ROS was more complicated than anticipated, and also the documentation was poor. Another challenge faced was that the buck converter was current limiting and as a result it was preventing the medium motors from drawing enough power. The medium motors appeared to not have enough torque. The solution to this problem was turning off the current limiting, thus allowing joints 3 and 4 to move properly. Lastly, during a software upload, Arduino unexpectedly sent abnormal motor values to the wrist motor, causing the wrist motor to break. The motor had to be taken off the cutting end effector and put on the wrist.

Future Work

To expand upon this project and further improve the performance of the arm, better controls could be developed with more advanced motors and sensors. The servo motors do not give feedback to the microcontroller but instead are their own closed loop system. They could be replaced with motors and sensors which give information to the microcontroller. Better quality motors would also have less backlash, which would result in the arm achieving greater precision. As far as the structural design is concerned, something that could be done without much of an increase in budget is increasing the strength, size and area of the joints at the shoulder. This marginally increases the moment of inertia of the arm or torque requirements. Furthermore, a stronger shoulder joint would result in less bending or sagging from the weight of the entire arm, thus reducing the risk of yielding or fracture.

Conclusion

Overall, despite minor setbacks with the failure of certain components and controls related issues, the team was able to keep to schedule throughout the build stage and have a working prototype ready. During the final prototype demonstration, the user, while using an Oculus VR headset and controller to move the arm, was able to demonstrate the arm successfully replicating the movement and motion of the user's hand with very minor delays. The robotic arm was also able to demonstrate successful completion of tasks such as picking up objects with the gripper and switching end effectors placed on a tool rack. Out of the 6 design constraints that were initially set, the prototype fully satisfies 5, with the abandoned constraint being the diameter requirement. However, it is important to note that the arm only fails the diameter requirement in a few places, particularly at the joints. This project was completed without exceeding the allocated budget as the final expenditure for the entire project stands at \$663.49, which is \$36.51 less than the allocated budget of \$700. Finally, With less limitations with the budget and additional investment, it was concluded that the performance of the arm could be further improved with the use of higher quality components such as more advanced motors and sensors. Minor design changes to make the shoulder joint stronger and bigger, and further testing would also yield improvements in performance.

References

Lisle, D. L. (2020). Making safe: The dirty history of a bomb disposal robot.
Security Dialogue, 1. <https://doi.org/10.1177/0967010619887849>

MoveIt Quickstart in RViz. MoveIt Quickstart in RViz - moveit_tutorials Noetic documentation. (n.d.). Retrieved December 1, 2021, from
https://ros-planning.github.io/moveit_tutorials/doc/quickstart_in_rviz/quickstart_in_rviz_tutorial.html

MoveIt Setup Assistant. MoveIt Setup Assistant - moveit_tutorials Noetic documentation. (n.d.). Retrieved December 1, 2021, from
https://ros-planning.github.io/moveit_tutorials/doc/setup_assistant/setup_assistant_tutorial.html

Realtime Arm Servoing. Realtime Arm Servoing - moveit_tutorials Noetic documentation. (n.d.). Retrieved December 1, 2021, from
https://ros-planning.github.io/moveit_tutorials/doc/realtime_servo/realtime_servo_tutorial.html

Simulating Robots with Ros and Unity. Unity Resources. (2021, August 9). Retrieved December 1, 2021, from
<https://resources.unity.com/unitenow/onlinesessions/simulating-robots-with-ros-and-unity>

Joint-wise control: <https://youtu.be/GrYs0maNXb0>

VR tracking: https://youtu.be/_19oKAfcOmY

Simulation tracking: <https://www.youtube.com/watch?v=JftjxaKjExk>

Tool Changing: https://www.youtube.com/watch?v=tp3Tb9I_O9M

Arm speed demonstration: https://www.youtube.com/watch?v=i1y_S35qO3g

Bill of Materials:

https://docs.google.com/spreadsheets/d/1d4_-5JI5_yLZmJNfimuZ_uEBtmQKV2tSQflwyJY8dAY/edit?usp=sharing

ROS workspace repository: <https://github.com/manff/capstone-robot-ros>

Desktop application: <https://github.com/manff/capstone-robot>

Appendix A.

A1. House of Quality (HOQ)

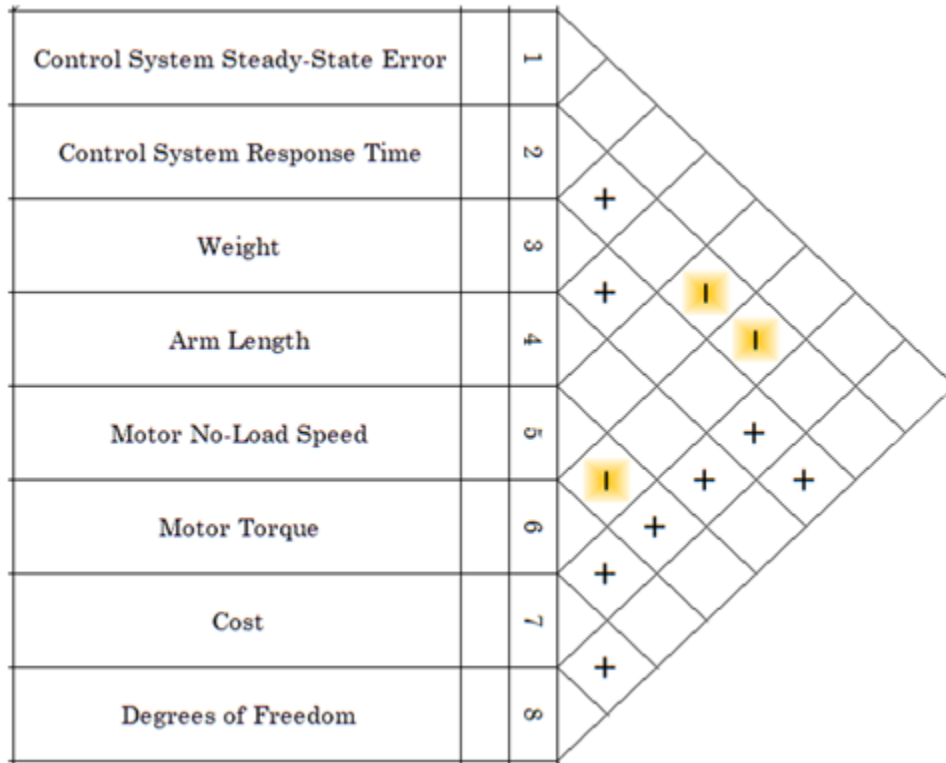


Figure 38: House of Quality

A2. Quality Function Deployment (QFD)

Table 12: Quality Function Deployment

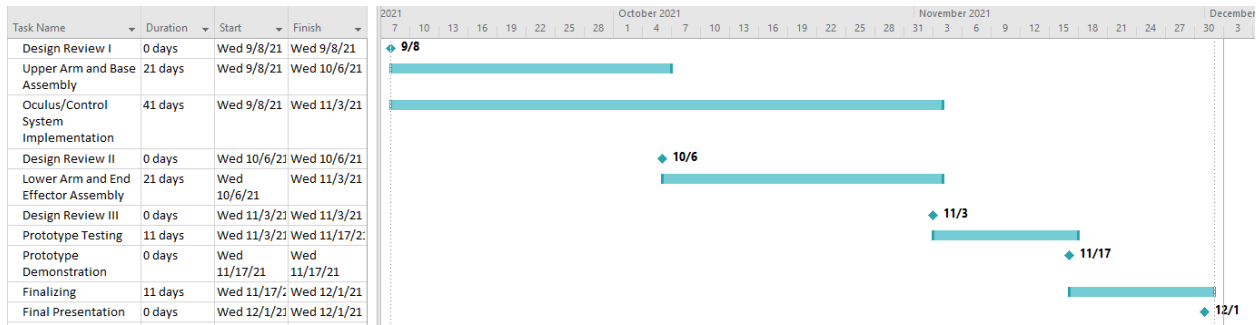
	Engineering Requirements								Benchmarks			
	Control System Steady-State Error	Control System Response Time	Weight	Arm Length	Motor Speed	Motor Torque	Cost	Dof	Ref2	Northrop Grumman	XTEK	Pollen Robotics
Customer Requirements												
Accurate	x	x			x	x			x	x	x	x
Lift Light Objects			x		x				x	x	x	x
Responsiveness		x		x					x	x	x	x
Easy to Use		x						x				x
Lightweight			x			x			x		x	x
Able to Reach in All Directions				x					x	x	x	x
Inexpensive			x				x					
Multitool			x									
Compact			x	x							x	x
Units	cm	sec	kg	m	RPM	N*m	\$	#				
	5	0.5	7	0.7	3000	7	700	6				
Engineering Targets												

Appendix B.

B1. SEMTE Business Office Receipt for Team 10

Team 10						
1. Benjamin Miller						
2. Matthew Nolan	REQ-22-00016178 - \$235.84	HomeDepot - \$42.72	Banggood \$14.26	REQ-22-00020330 \$92.17	REQ-22-00020348 \$31.17	
3. Connor Nail	REQ-22-00017472 \$129.50	McMaster \$27.53	Amazon-\$59.13			
4. Andrea Rio	REQ-22-00020348 \$31.17					
5. Cariappa Kalianda Devaya						
6. Efrain Valero-Villavicencio						
7. Mason Keck						

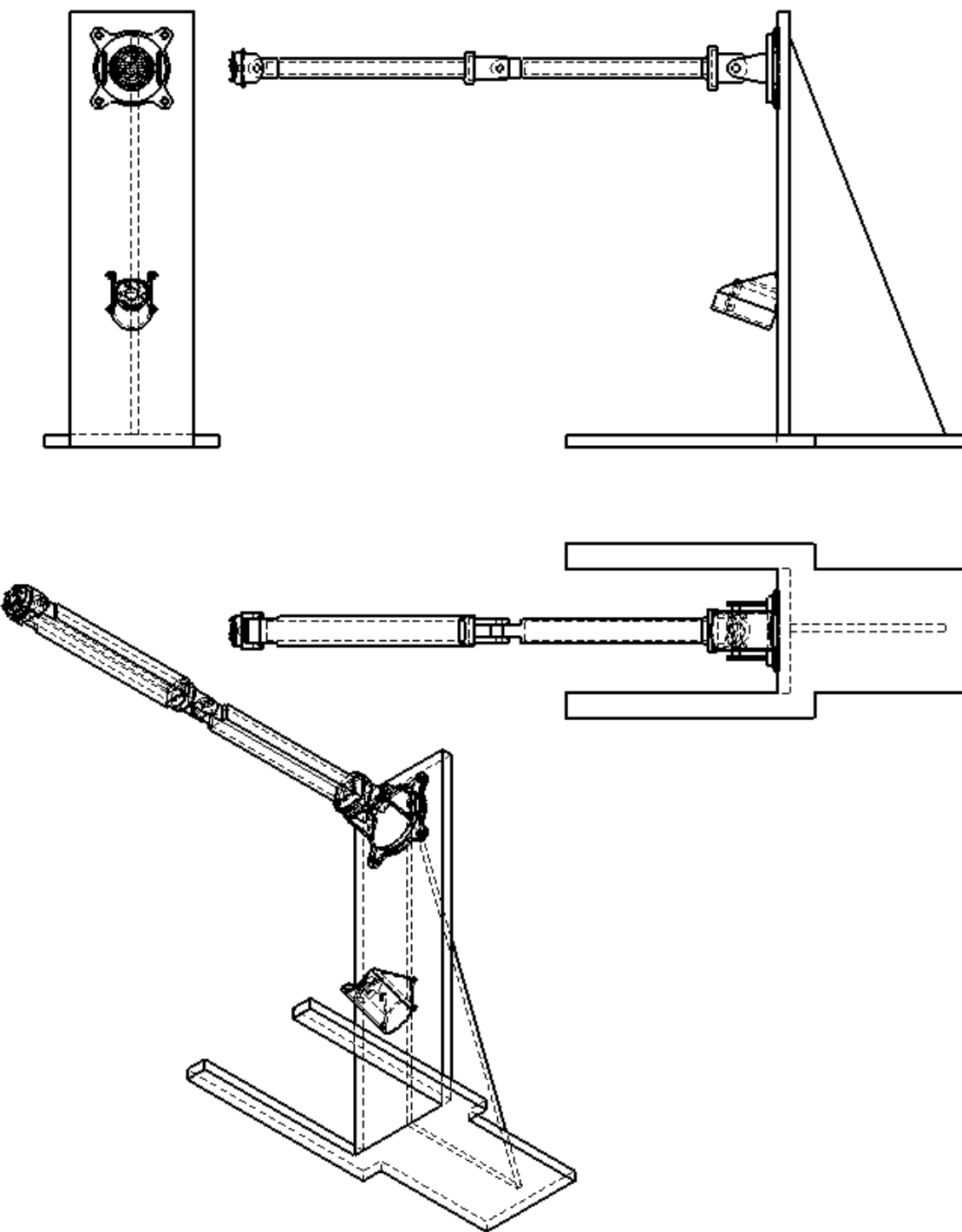
B2. Gantt Chart



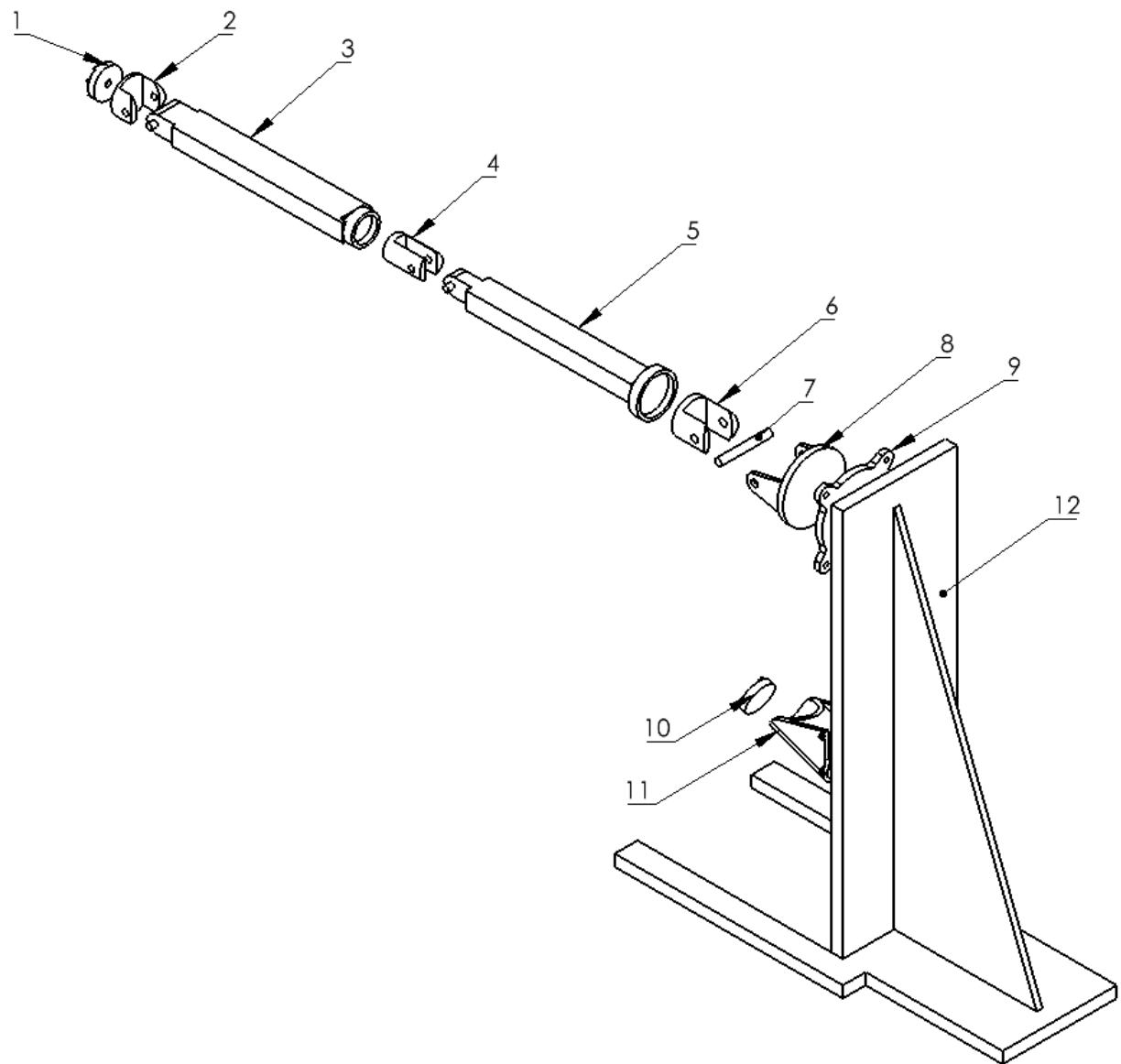
Appendix C. Preliminary Parts and Engineering Drawings

All dimensions in mm.

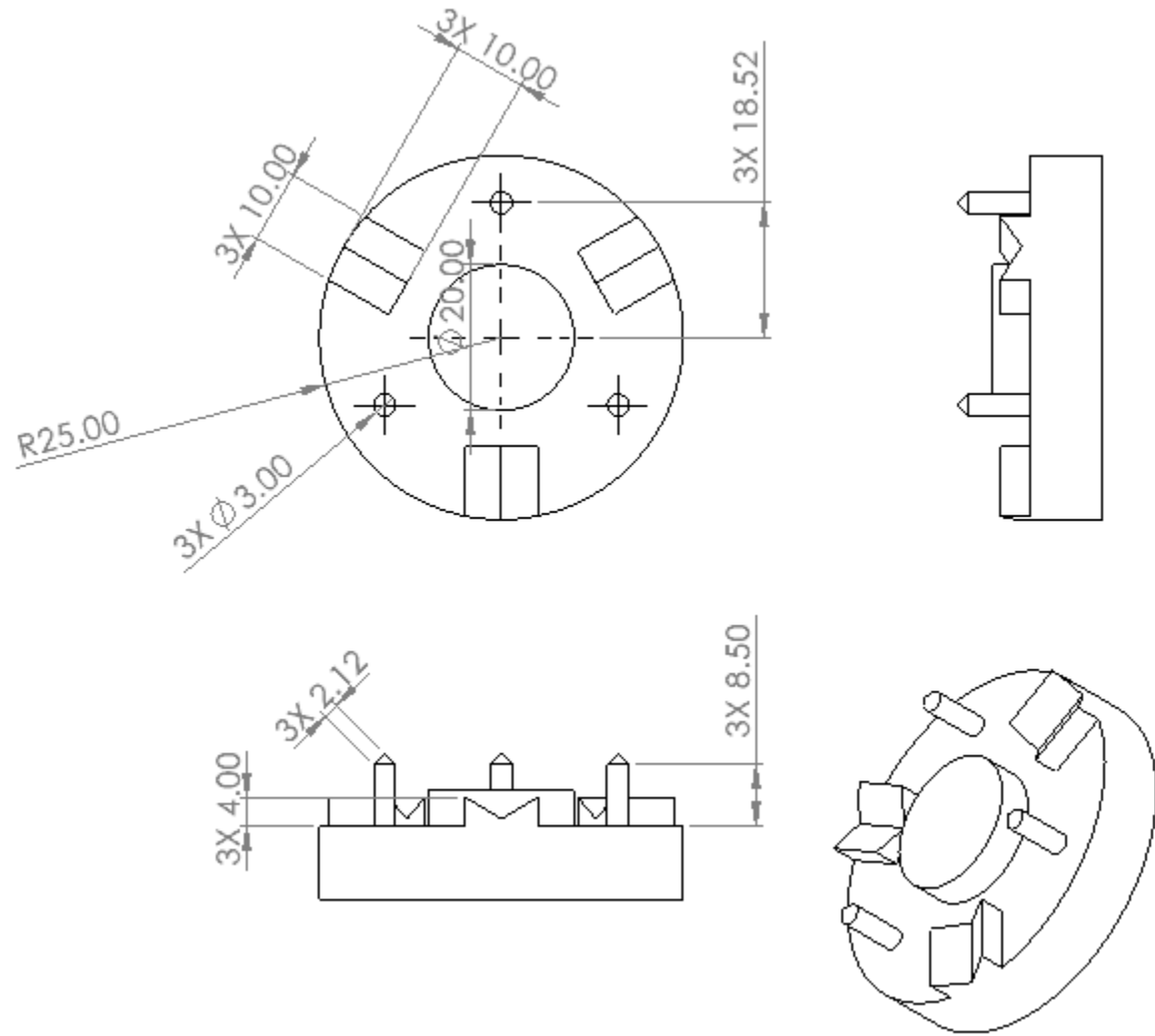
Full Assembly



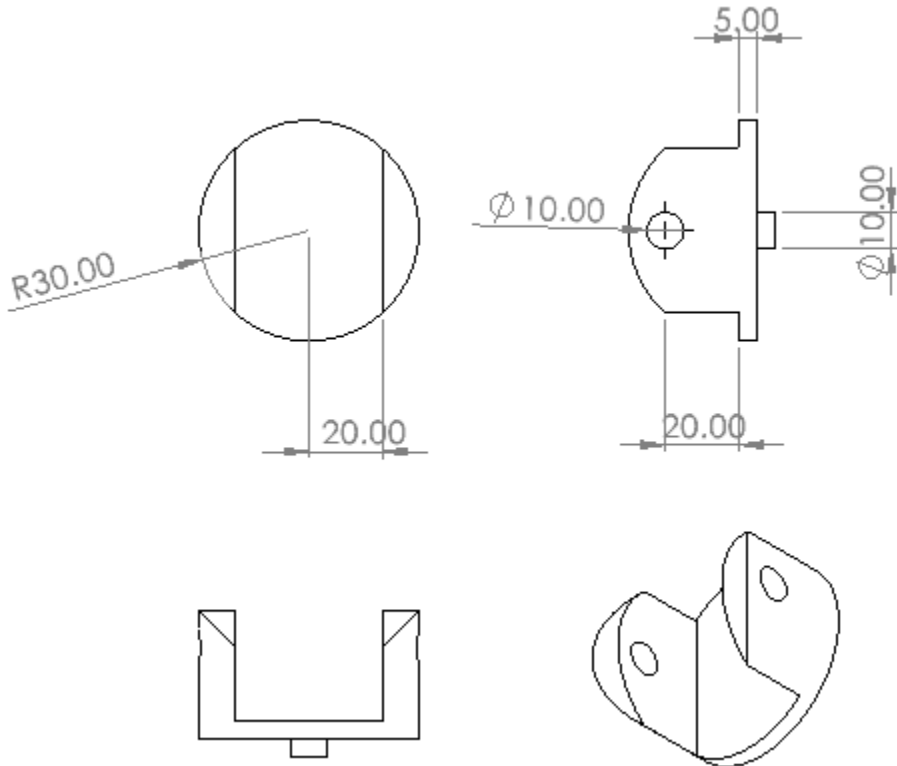
Full Assembly Exploded



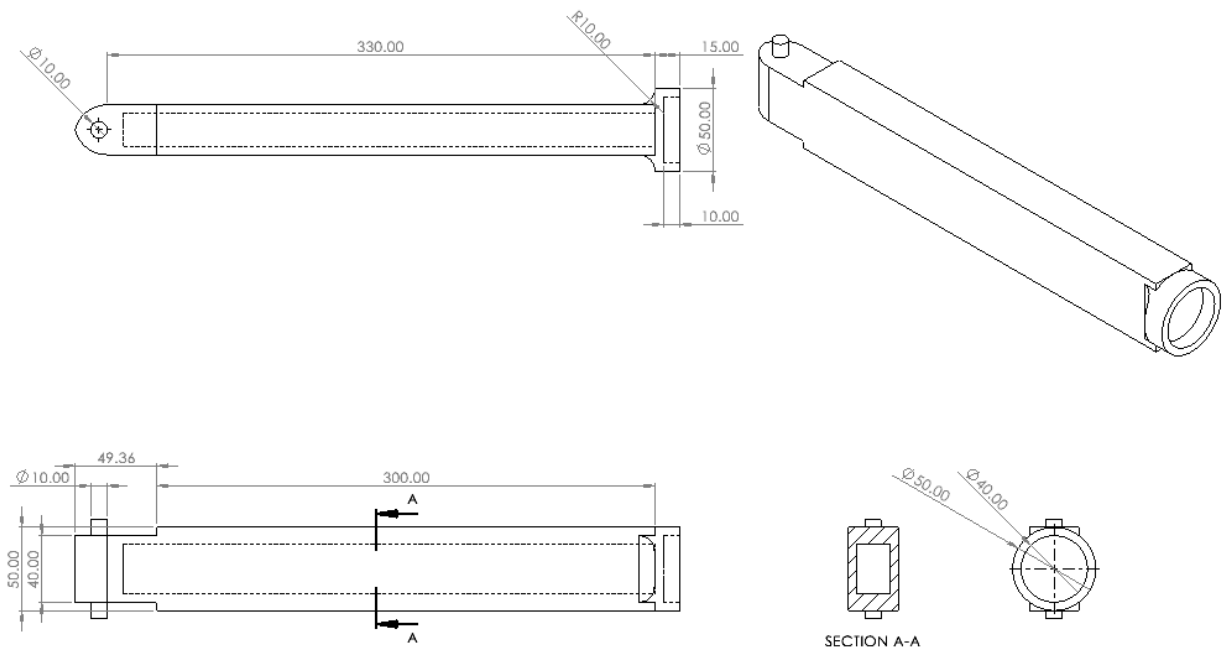
Magnetic End Effector (1)



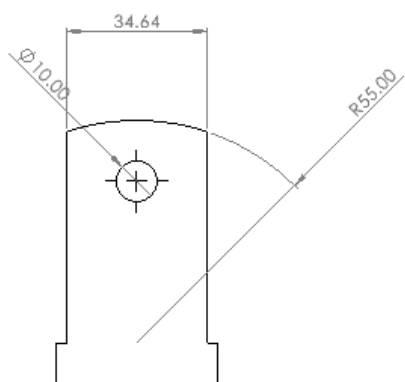
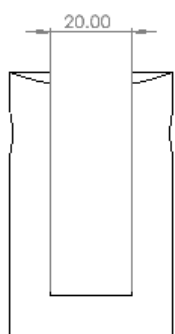
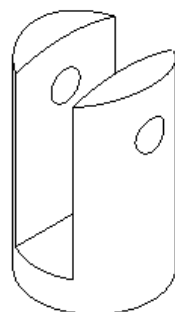
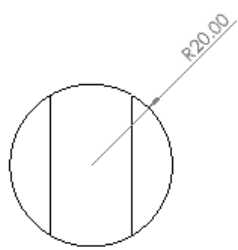
Wrist Turntable (2)



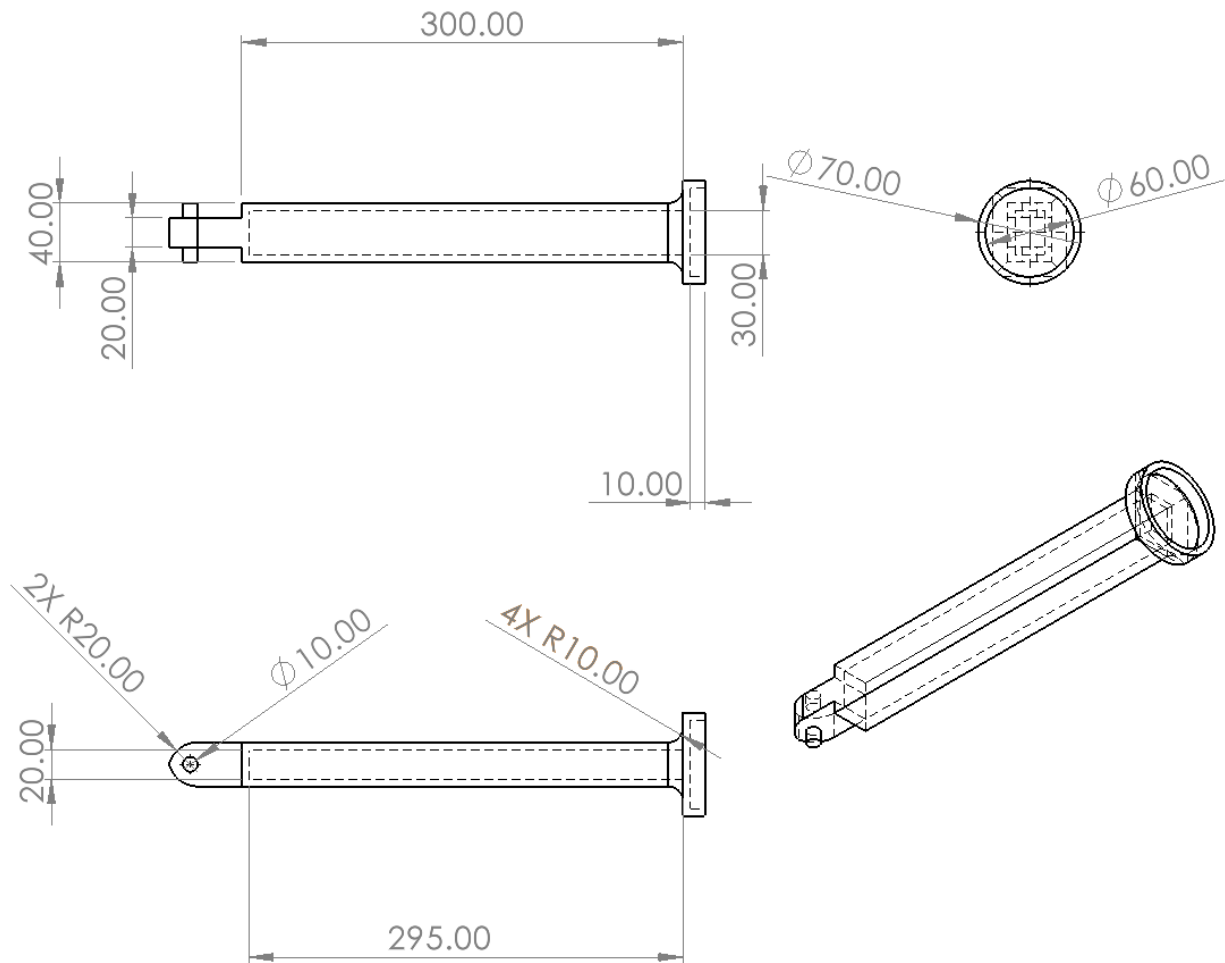
Forearm (3)



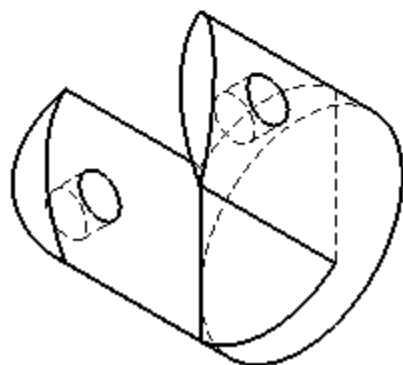
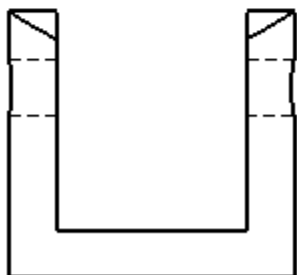
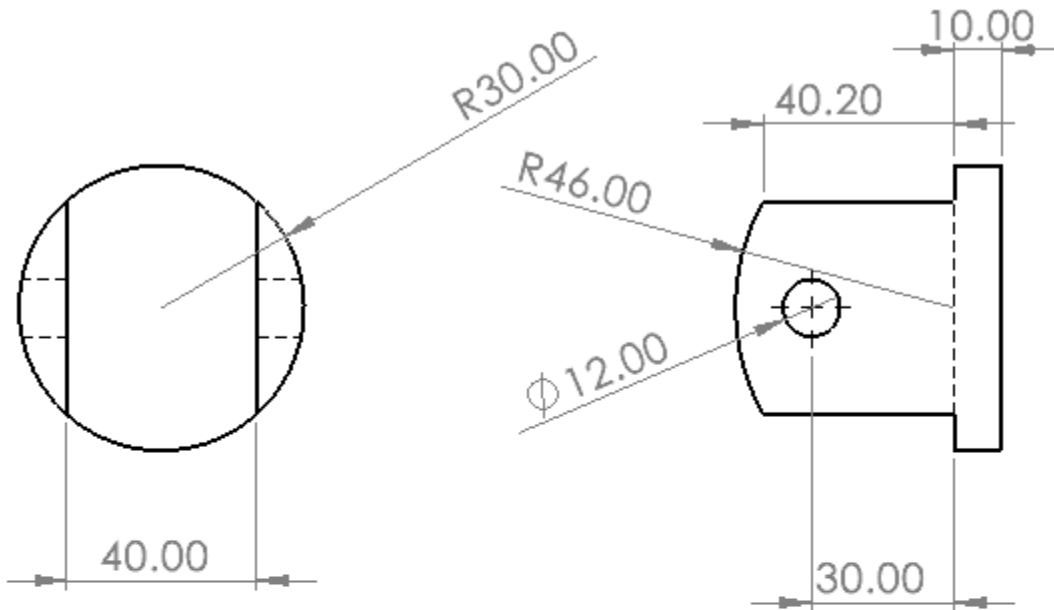
Elbow Turntable (4)



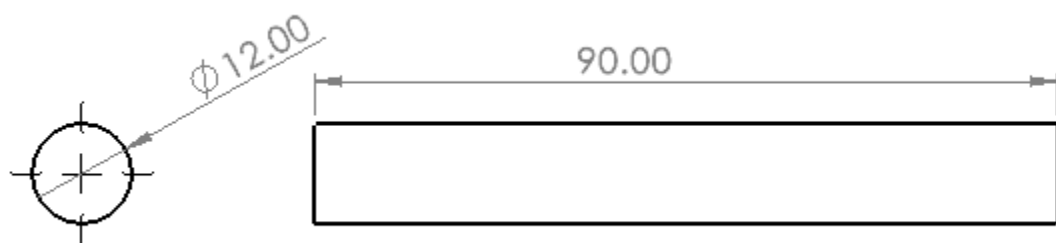
Upper Arm (5)



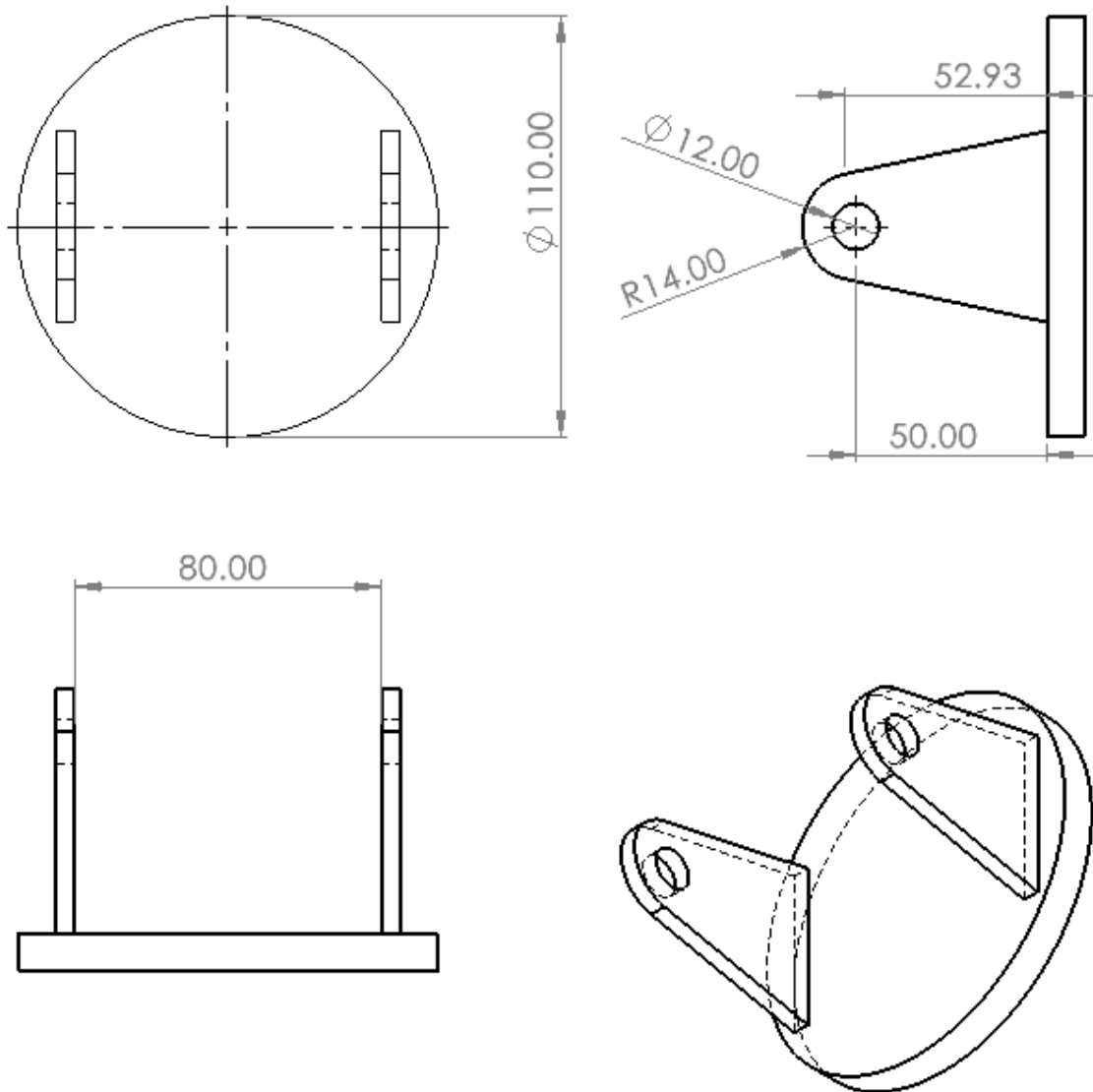
Upper Arm Turntable (6)



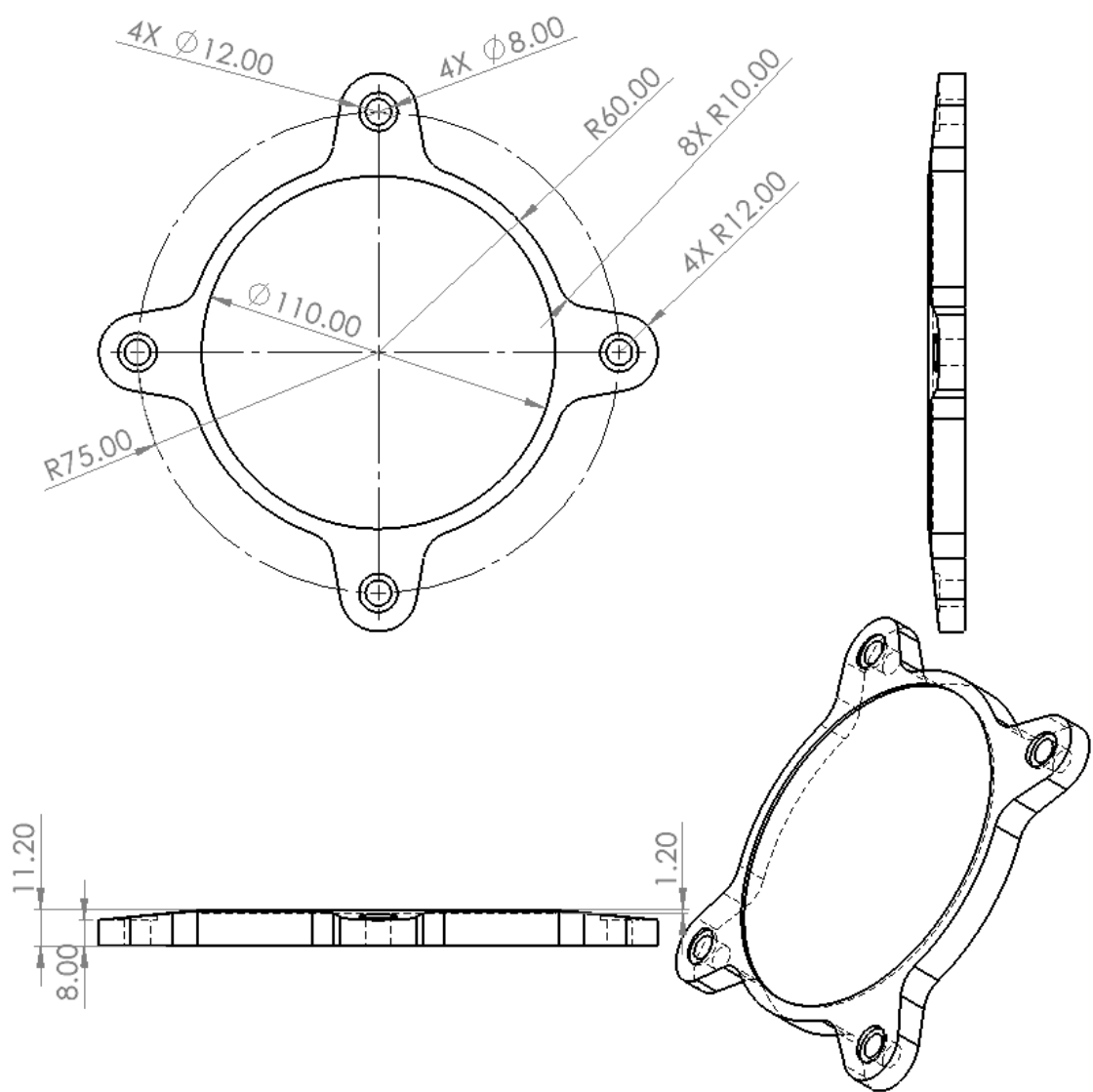
Shoulder Pin (7)



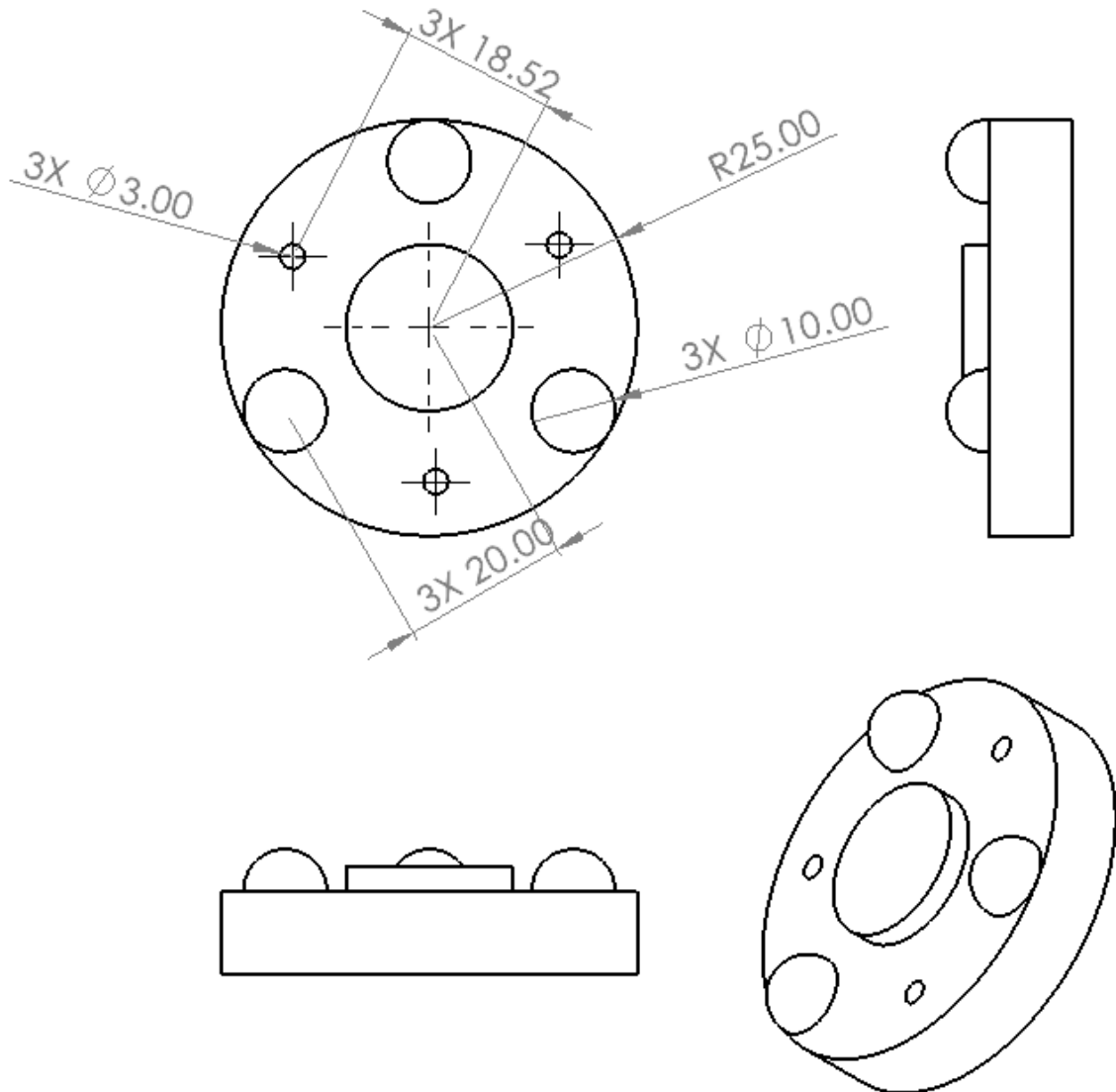
Shoulder Hinge (8)



Shoulder Turntable (9)



Sample Module Kinematic Coupler (10)



Module Holder Tray (11)

